AN ACTIVELY COOLED FLOATING ELEMENT SKIN FRICTION BALANCE FOR DIRECT MEASUREMENT IN HIGH ENTHALPY SUPERSONIC FLOWS

by

Kenneth Michael Chadwick

Dissertation Submitted to the Faculty of the
Virginia Polytechnic Institute and State University
in partial fulfillment of the requirements for the degree of

DOCTOR OF PHILOSOPHY
in
Aerospace Engineering

APPROVED:

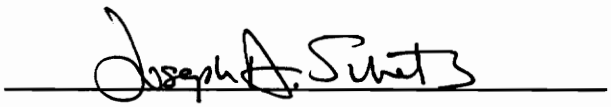

Joseph A. Schetz, Chairman

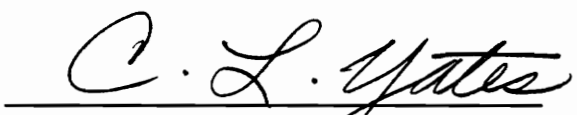

Charlie L. Yates

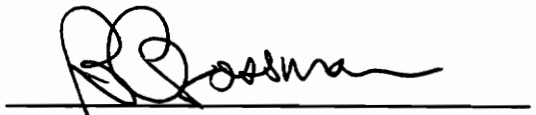

Bernard Grossman

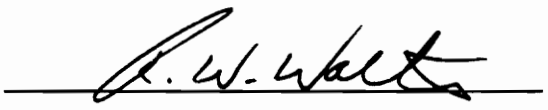

Robert W. Walters

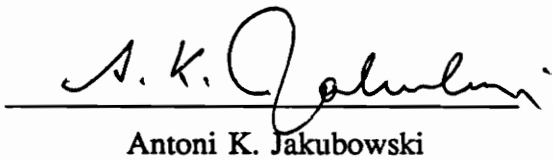

Antoni K. Jakubowski

December, 1992

Blacksburg, Virginia

AN ACTIVELY COOLED FLOATING ELEMENT SKIN FRICTION BALANCE FOR DIRECT MEASUREMENT IN HIGH ENTHALPY SUPERSONIC FLOWS

by

Kenneth Michael Chadwick

Joseph A. Schetz, Chairman

Aerospace Engineering

(ABSTRACT)

An investigation was conducted to design instruments to directly measure skin friction along the chamber walls of supersonic combustor models. Measurements were made in a combustor at the General Applied Science Laboratory (GASL) and in the Direct Connect Arcjet Facility (DCAF) supersonic combustor at the NASA AMES Research Center. Flow conditions in the high enthalpy combustor models ranged from total pressures of 275-800 psia (1900-5550 kPa) and total temperatures from 5800-8400 R (3222-4667 K). This gives enthalpies in the range of 1700-3300 BTU/lb_m (3950-7660 KJ/kg) and simulated flight Mach number from 9 to 13. A direct force measurement device was used to measure the small tangential shear force resulting from the flow passing over a non-intrusive floating element. The floating head is mounted to a stiff cantilever beam arrangement with deflection due to the shear force on the order of 0.0005 in (0.0125 mm). This small deflection allows the balance to be a non-nulling type. Several measurements were conducted in cold supersonic flows to verify the concept and establish accuracy and repeatability. This balance design includes actively controlled cooling of the floating sensor head temperature through an internal cooling system to eliminate non-uniform temperature effects between the head and the surrounding chamber wall. This

enabled the device to be suitable for shear force measurement in very hot flows. The key to this device is the use of a quartz tube cantilever with strain gages bonded at orthogonal positions directly on the surface at the base. A symmetric fluid flow was developed inside the quartz tube to provide cooling to the backside of the floating head. Bench tests showed that this did not influence the force measurement. Numerical heat transfer calculations were conducted for design feasibility and analysis, and to determine the effectiveness of the active cooling of the floating head. Analysis of the measurement uncertainty in cold supersonic flow tests show that uncertainty under 8% is achievable, but variations in the balance cooling during a particular test raised uncertainty up to 20% in these very hot flows during the early tests. Improvements to the strain gages and balance cooling reduced uncertainty for the later tests to under 15%.

ACKNOWLEDGEMENTS

First, I have to express my sincerest thanks and gratitude to Dr. Joseph A. Schetz for giving a young man with big dreams and little resources a chance for success like no other in my life has offered. There have been good times and there have been bad times over the last several years, but there would have been no times without his support and guidance.

Second, I must thank all my fellow graduate students for there help, support and friendship over the past several years. Also, thanks to the members of the Aerospace Engineering machine shop, including Frank Shelor, Robert Frazier, and Kent Morris.

I wish to express my appreciation to the members of my examining committee, including Dr. Charlie L. Yates, Dr. Bernard Grossman, Dr. Robert W. Walters, and Dr. Antoni K. Jakubowski for their instruction and advice.

During the course of this study I was fortunate to have the opportunity to travel to several testing facilities. I wish to thank the efforts of all the involved employees of the General Applied Science Lab., Pratt & Whitney, and Rocketdyne. The efforts of P. Pandolfini, M. Thompson, G. Sullins, M. Lasita, and C. Walton of the Applied Physics Lab. are greatly appreciated. Also, thanks are due to the NASA Ames Research Center DCAF personnel and contractors.

In my life I have seen much success, but none is or will ever be as fulfilling to my life as my young family is to me. It is to them, my wife, Kathryn, and my sons, Ryan and Michael, that I dedicate not only the efforts of my education and of this manuscript, but all that I do ...

TABLE OF CONTENTS

LIST OF SYMBOLS

ARABIC SYMBOLS

A . . . . . .Area

C . . . . . .Specific Heat

C_f . . . . . .Skin Friction Coefficient

C_B . . . . . .Thermal Expansion Coefficient of Substrate

C_S . . . . . Thermal Expansion Coefficient of Silicon

d . . . . . .Diameter of Cantilever Beam

$D_{[\,]}$ . . . . . Diameter of Floating Head

D_c . . . . . .Conductance Coefficient

e . . . . . Electronic Charge

E . . . . . Modulus of Elasticity

G . . . . . .Gap Size

GF . . . . . .Gage Factor

GF_o . . . . . .Initial Gage Factor

GF_T . . . . . .Gage Factor due to Temperature Sensitivity

h . . . . . .Film Coefficient

H_T . . . . . Total Enthalpy

H_2 . . . . . .Hydrogen

i . . . . . .Current in Semiconductor

I . . . . . .Moment of Inertia

I.D. . . . . .Inner Cantilever Diameter

J . . . . . .Diffusion Flux

k . . . . . Thermal Conductivity

L . . . . . Cantilever Length

L_p . . . . . Lip Size of Floating Head

M . . . . . Mach Number

M_∞ . . . . . Equivalent Free Stream Mach Number

n . . . . . Denotes Negative Gage Factor

N_i . . . . . Number of Charge Carriers

N_2 . . . . . Nitrogen

O.D. . . . . Cantilever Outer Diameter

p . . . . . Denotes Positive Gage Factor

P . . . . . Cantilever Load

P_s . . . . . Static Pressure

P_T . . . . . Total Pressure

q_B . . . . . Heat Flux

q . . . . . Heat Generation per unit Volume

q . . . . . Dynamic Pressure

R . . . . . Resistance

R_o . . . . . Initial Resistance

R_T . . . . . Resistance Change due to Temperature

Re_δ . . . . . Reynolds Number based on Boundary Layer Thickness

S . . . . . Average Source Term over Control Volume

T . . . . . Temperature

T_T . . . . . Total Temperature

TCR . . . . . Thermal Coefficient of Resistance

TCGF . . . . . Thermal Coefficient of Gage Factor

U_∞ . . . . . Free Stream Velocity

V . . . . . Velocity

y . . . . . Cantilever Beam Deflection

Y . . . . . Youngs Modulus

GREEK SYMBOLS

α . . . . . Thermal Coefficient of Resistance

α_B . . . . . Total Thermal Coefficient of Resistance

β . . . . . Thermal Coefficient of Gage Factor

Δ . . . . . Incremental Change

$d\tau$ . . . . . Differential Control Volume

$d\sigma$ . . . . . Differential Control Surface

δ . . . . . Differential Length

ε . . . . . Mechanical Strain

ε_a . . . . . Apparent Strain due to Thermal Effects

γ . . . . . Ratio of Specific Heats

μ_{ave} . . . . . Average Mobility of Charge Carriers

ν . . . . . Poissons Ratio

π_L . . . . . Longitudinal Piezoresistive Coefficient

LIST OF FIGURES

CHAPTER ONE

INTRODUCTION

1.1 BACKGROUND

Knowledge of drag resulting from skin friction is important for numerous engineering applications. Before a complete understanding of many internal and external flows can be obtained, an accurate measurement or calculation of skin friction is required. In many supersonic flow combustor testing programs, accurate measurement of skin friction is necessary to correctly determine combustion efficiency from wall pressure measurements. In addition, relatively small amounts of skin friction in a combustor can seriously limit the available thrust from an engine.

Recent interest in supersonic combustion ramjet (SCRAMjet) performance, primarily due to the National Aerospace Plane project (NASP), has renewed an effort to obtain accurate skin friction measurements in the combustors for this type engine. The flows in these combustors are supersonic, chemically-reacting, high-enthalpy flows with a compressible, 3-dimensional, turbulent boundary layer which, at this point, are very difficult to calculate. In this study, instruments are designed and implemented to directly measure the skin friction in various locations along supersonic combustor walls. A schematic of a typical SCRAMjet geometry is included in Fig. 1.1.

The current techniques employed in the measurement of skin friction fit into two

general categories, those being either an indirect or direct methods. Indirect methods involve measurement of the velocity gradient or heat transfer at the combustor wall. Reference 1 contains a review of many strategies adopted in these methods. One of these types of indirect techniques includes heated wires or films located along the combustor wall to measure the heat transfer. References [2 - 8] illustrate the technique. The goal with these types of instruments is to align a thin wire or film along a wall to be sensitive to the heat transfer resulting from a wall shear stress. The wire or film elements are typically configured in a constant temperature hot-wire anemometer system. Reference 5 also includes a discussion of some of the difficulties with these techniques. The conductivity of the material to which the wire or film is bonded is very important to the accuracy of these devices, since this can effect the heat transfer to the wire or film. Flow unsteadiness and turbulence can also have significant effect on the output of these devices if they are not carefully aligned with the wall. Uncertainties with these methods can be quite large, especially in a compressible, 3-D, turbulent boundary layer, because a relation between the momentum and heat transfer mechanisms is required to deduce the skin friction and that is not reliably known for these flows. Another indirect technique commonly used to measure skin friction involves resting a small tube on the wall surface to measure Pitot pressure. This technique was first introduced by Preston[9], and these tubes are commonly called Preston tubes. The tube is placed on the wall with the centerline falling in the logarithmic part of the boundary layer. This type of device would then be insensitive to wall imperfections. In order to calibrate these devices, a logarithmic law is required. For these reasons and considering that the flow types of interest in these studies are very high-heat-flux and combusting, these types of devices would not be suitable for the flows of concern in this study, therefore a direct shear force measurement technique was adopted.

Direct force measuring techniques generally include two types of force balances. The first is a self-nulling type meaning that the shear sensing element is not deflected

under load, but is held fixed in the initial position by a restoring force that is, in theory, equal to the shearing force. The second is a non-nulling type which is just the opposite of the nulling type. The sensing element is allowed to deflect under the shearing load. This latter type of balance design introduces some concern from tilting of the sensing element into the flow while it is exposed to shear, as well as other geometric concerns. These items are discussed in detail in Chapter 3. An interesting type of skin friction balance which utilizes the direct force measurement technique in a non-conventional manner is described in Ref. 10. This balance design employs a tightly wrapped belt around two parallel cylinders. This device is positioned so that only a small portion of the belt between the cylinders is exposed along the line of a wall. Shear is measured by measuring the strain in some flexure panels at the pivot points of the cylinders. The other, and most common type of non-nulling direct force measurement technique involves measuring strain at the base of a cantilever with the beam end (floating head) exposed to the shearing force.

The basic configuration of the skin friction balances of this study consist of a cantilevered floating element. A history of early direct measurement designs which includes floating element designs is presented by Winter[11]. Skin Friction balances that have been developed for supersonic flows include the efforts of Roensch and Cadwell[12], Allen[13,14], and Voisinet[15]. The balances of these studies were primarily subject to supersonic flows with only moderate total temperatures. Reference 16 presents some limited measurements in a scramjet combustor at the Applied Physics Laboratory. DeTurris, Schetz, and Hellbaum[17] present skin friction measurements in scramjet combustors from several test programs. Chadwick, DeTurris and Schetz[18] present more recent data with direct force measuring devices.

The frictional forces that are a result of the supersonic combusting flow passing tangent to the combustion chamber walls are of a small magnitude. The shearing force

must also be measured over a small area, therefore it is necessary for the skin friction balance to be very sensitive. The present designs have the ability to measure forces from 1 psf to over 50 psf accurately (7.0 kPa - 350 kPa). The designs of this study are similar in concept to the design first used by Schetz and Nerney[16] and recently by DeTurris et al[17]. This device employs piezoresistive crystal semi-conductor strain gages in a commercially available cartridge. This type of strain gage is exceedingly sensitive with gage factors in the area of 150, compared to a gage factor of near 2 for common foil strain gages. This kind of sensitivity enabled the adoption of a non-nulling type design. Several benefits are obtained with a non-nulling design over a self-nulling design. First, the non-nulling design is less complex in that it does not require a series of mechanical linkages which can introduce substantial error in the measurement. Second, the time response of the non-nulling device is superior to that of the nulling device. Since the piezoresistive strain gages have a high gage factor, the cantilevered floating element of the current designs undergo extremely small deflections during a measurement. This renders insignificant any misalignment effects due to tilting that could cause an errant measurement. One difficulty that is introduced by these crystal strain gages is that they are sensitive to temperature. An active cooling system near the gages was developed to minimize any error introduced by temperature gradients in the strain sensing elements.

It was determined that a temperature mismatch between the actual floating head of the skin friction balance and the surrounding wall of the combustion chamber can introduce significant error in the shearing force measurement. Only a few studies have been conducted to determine the magnitude of this error. These are illustrated by the studies of Refs. [18,19]. The study by Voisinet[18] showed that in a cold supersonic flow at Mach 2.9 as much as 15% error in the shear measurement can be achieved for an increase of 180°R (100 K) in the floating head temperature over the surrounding wall temperature. The tests conducted by Chadwick, et al[19] showed as much as a 360°R (200 K) difference in temperature between the skin friction balance floating head and the near

wall in SCRAMjet combustors with an uncooled floating head skin friction balance design. In an effort to eliminate the possible error from this temperature mismatch, an optimized design has been developed that actively cools the floating head of the skin friction balance and retains the benefits of the uncooled head design. The design is capable of measuring skin friction in both axial and transverse directions. It is felt that this actively cooled floating head design is needed for skin friction measurements in high-enthalpy, high-heat-flux flows.

1.2 SCOPE OF THE INVESTIGATION

The skin friction balances developed in this study were implemented into two combustor testing programs. The flow in these combustors is supersonic, and heat addition is achieved through spontaneous combustion of hydrogen in high enthalpy air. The wall heat fluxes encountered in these combustors is 0.5-4.0 BTU/in^2/sec (8.7×10^5 - 6.3×10^6 W/m^2). The skin friction balances were also tested in cold supersonic flows. These tests were conducted at Virginia Tech and were primarily used for skin friction balance repeatability and uncertainty analysis as well as testing of the design concept.

The supersonic combustor tests were conducted at the General Applied Science Laboratory (GASL) with Pratt-Whitney and the Rocketdyne Corps. as the principle combustor investigators. The second set of skin friction measurement tests were conducted at the NASA Ames Research Center Direct Connect Arcjet Facility (DCAF) in a Johns Hopkins University/Applied Physics Laboratory (JHU/APL) built supersonic combustor. The first set of tests at the GASL were conducted as an extension of the cold flow tests, meaning that they were used primarily as a test of the concept.

The major effort of this study was concentrated on the test series conducted at the

NASA AMES Research Center. Skin friction balance heat transfer studies were conducted on the NASA ARC design as were other balance optimization efforts, including strain gage selection and temperature compensation. Two separate entries were made in the DCAF combustor. In the first entry, a single skin friction balance was designed, constructed, and implemented. For the second entry, two additional improved balances were designed and constructed along with the balance for the first entry being rebuilt to bring the total to three balances for these tests. Measurements were made in various positions of the combustors, including the divergent and constant area sections. Also, a number of different fuel injector configurations were encountered. Those included were tangential slot injection, transverse injection (normal and inclined), as well as others.

The following Chapters present the process for the design of the actively cooled floating head skin friction balance and a discussion of the results obtained for hot and cold flow tests. In Chapter 2, the design of the cantilever beam and floating elements are discussed along with misalignment considerations regarding the floating head and the surrounding wall. Also, a detailed discussion of strain gage theory and instrumentation is presented in Chapter 2. Chapter 3 presents the details of a heat transfer study conducted to determine the feasibility of an actively cooled floating head design. The overall skin friction balance design and configuration is given in Chapter 4 for the skin friction balances constructed for this study. Chapter 5 contains a description of the test facilities and Chapter 6 presents the results obtained for both the hot and cold flow tests conducted during this study. Conclusions and recommendations for future designs are given in Chapter 7.

CHAPTER TWO

CANTILEVER BEAM AND INSTRUMENTATION DESIGN

PART I - BEAM ELEMENT DESIGN

2.1 GENERAL DESIGN ATTRIBUTES AND MOTIVATION

The general design of the balances of this study consist of a non-nulling cantilevered tube with a attached floating head (Fig. 2.1). The principle behind this technique is to measure the wall shear force from a passing flow with a non-intrusive element. This element must be aligned with the plane of the wall (non-intrusive) to insure exposure to only a shear force. The method of this study is to use a floating head attached to the free end of a cantilever and allow it to deflect under a load due to a shearing force. This arrangement is fit into a housing which in turn is fit into the wall of a the specific testing facility model. The gap between the floating head and the housing is kept to a small fraction of the diameter of the floating head. Although all the skin friction balances of this study have circular floating heads and are designed to measure the shear force along flat surfaces, neither of these conditions are requirements for this type design. A shear produced by a flow over the top of the floating head will lead to a measurable strain on the surface of the beam at the base. In order to sense this strain, strain gages are cemented in orthogonal positions around the circumference of the base. The primary flows of interest of this study are those inside supersonic combustors. Wall temperatures in the combustors can be in excess of 1000 degrees Rankine. Since heat transfer through the skin friction balance would in general not be as high as that of a combustor wall, the temperature of the floating head could be much greater than that of the surrounding

combustor wall. An example of this temperature difference is evident in the results presented in Fig. 2.2. The skin friction balance used to obtain these results is a non-nulling cantilever with attached floating head. It has a 0.25 inch (0.64 cm) floating head and was fit into the wall of a supersonic combustor. This figure shows the floating head temperature and the combustor wall temperature at a point approximately 1.0 in (25.4 mm) upstream of the floating head. Reference [20] contains a summary of other results from these supersonic combustor skin friction measurements. A net change in floating head to combustor wall temperature of 150°C (270 °R) was observed because heat transfer through the cantilever and floating head is not as high as through the surrounding combustor wall. This result could in fact lead to significant error in the skin friction measurement. The study by Voisinet[18] showed as much as a 0.45% increase in the shear measurement for every degree Kelvin increase in floating head temperature over the surrounding wall temperature. If this is true, the above described test could have over-predicted the wall shear by nearly 70%. Therefore, the balances of this study were designed with an active floating head cooling system which can control the temperature of the floating head. The specific goal is to match the floating head temperature to the temperature of the surrounding wall, which would eliminate over prediction of the shear force. Although these balances are designed specifically for high temperature supersonic flows, they can readily operate in other flow conditions as well. The cooling system involves an axis-symmetric co-axial flow pattern established inside the cantilever requiring that the cantilever be tubular. Extensive heat transfer calculations were conducted to design the active floating head cooling system and is discussed in Chapter 3. The remainder of this chapter is dedicated to the design of the cantilever beam, floating head, and strain gage elements.

2.2 CANTILEVER BEAM AND FLOATING HEAD

The skin friction balance is essentially a cantilever beam with forces applied to

the end which will create a measurable strain on the surface at the base. There are three types of forces which can be applied at the beam end to produce stress and hence strain in the beam. These forces are illustrated in Fig. 2.3 and are a lip force that can be produced by protrusion of the beam end into the flow, a normal force which could come from a pressure gradient acting on the beam end and a shear force which is from the skin friction. In the design of the balance, steps must be taken to eliminate both a lip and normal force or at least make them insignificant when compared to the shearing force.

The design of the beam element is of primary importance to the design of the skin friction balance, since it governs the performance of the instrument, including time response and output level. The small shear force due to the flow passing over the beam end or floating head requires that the balance must be very sensitive. Static and dynamic response as well as sensitivity to the shear force are all related to the beam geometry and material. These performance characteristics can be controlled by several aspects of the beam and floating head.

Material of the floating head is determined by the material of the specific test facility. In the tests of this study, the combustor material is either copper or zirconium-copper (Amzirc). Therefore, to be consistent and since copper conducts heat very well making it a good choice for the cooling system, the floating head on these balances are constructed of either copper or zirconium-copper to match the specific test facility. Since the beam is tubular to accommodate internal cooling, the floating head is constructed to fit over the end. A circular geometry was chosen for its symmetry and ease of manufacture. In all the balances of this study, it was required that the maximum diameter of the balance housing be set at 0.5 inches (.127 cm) to accommodate the testing facilities. Both the housing enclosing the beam element and floating head must fit within this diameter. The floating elements for this study are circular with a diameter of 0.323 in (8.13 mm). This size was chosen to accommodate a 0.328 inch bore (.833 cm) for the

housing, which is a standard machine size and still leaves enough material for the housing wall. A 0.025 in (0.35 mm) lip around the top circumference of the head tapers to 0.28 in (7.11 mm) resulting with an overall length of 0.5 in (12.7 mm). An internal diameter of 0.238 in (6.05 mm) is the bore to a depth that leaves a head thickness of 0.033 in (0.838 mm). This geometry (Fig. 2.4) yields a $L_p/D = 0.078$ (lip to diameter ratio) and a $G/D = 0.013$ (gap to diameter ratio) which are within the constraints described in a study by Allen[13,14] which will be discussed in the next section (2.3).

Beam material and geometry also control the strain in the beam for a given shear force. The facilities that these balances are designed to fit into are inherently crowded on the exterior, which leaves relatively little room for the balance. This requires that the balance be small. As a general rule of thumb, at least 10 microstrain should be produced at the beam base for any realistic chance to measure it with strain gages. The small size puts limitations on the length and diameter of the beam. Since the beam must be stiff, the material choices are limited as well. Experience and measurements in the past give an indication of the order of magnitude of the shearing force. Given this, a parametric study can be undertaken to choose the cantilever beam material and geometry using simple mechanics of materials. The strain in a cantilever beam is given in Eqn. 2.1 as :

$$\varepsilon = \frac{\sigma}{E} \tag{2.1}$$

where E is the modulus of elasticity and σ is the applied stress. The stress in the beam, σ, is given by :

$$\sigma = \frac{PLd}{2I} \tag{2.2}$$

with

$$I = \frac{\pi}{64} (O.D.^4 - I.D.^4) \tag{2.3}$$

for a tubular beam. P is the applied load at the beam end and L is the beam length of outer diameter d. The resulting strain at the base of the cantilever beam is :

$$\varepsilon = \frac{PLd}{2EI} \tag{2.4}$$

With Eqn. 2.4 and the equation for the beam end deflection,

$$\Delta y = \frac{PL^3}{3EI} \tag{2.5}$$

beam geometry and material can be determined to produce a measurable strain at the base while remaining stiff enough to keep the deflection of the beam end small. The beams in the balances of this study are constructed of fused quartz. This material was chosen because the required deflection of the beam must be small in order to prevent protrusion and/or recession errors of the floating head from a tilt angle. Also, since strain gages are very temperature sensitive, the selection of quartz, which has small thermal conductivity (1.5 $W/m^2/°C$), will act as a heat barrier between the flow and the strain gages. Straightness of the tube is also an alignment concern. The quartz tubes used in this study have straightness tolerance to under 0.001 inches per inch (0.0025 cm/cm) which is

adequate for alignment of the beam within the housing. The maximum deflection of the beam end for these balances is only 0.0005 in (0.0125 mm) which translates to a protrusion of the floating head of only 5 microinches into the flow. By itself, this protrusion should be insignificant, but the floating head geometry is designed to help eliminate any effect from this type of misalignment through gap size.

The selection of quartz as the cantilever beam presented a difficult problem of fastening the copper or zirconium-copper floating head to the quartz. A high temperature ceramic-like cement was used for the earlier designs. This cement has a tensile strength of 425 psi (3000 kPa) and can take temperatures up to 2500 °F. Some bench tests were conducted to determine the bonding strength of the cement to the copper and quartz. It was found that the cantilever could take internal cooling fluid working pressure up to 400 psi for a short duration. However, in some of the later tests, the balance was subject to an impulsive load as a series of pumps would boost the pressure of the cooling fluid reservoir. This resulted in what was felt to be a weakening of the bond and was a factor in the detachment of the parts during a high temperature test. For this reason, a technique was developed to solder the copper head to the quartz for the later balances. This was accomplished by applying a thin silver film to the quartz tube. A silver paint was applied to a very clean tube and then fired in a kiln to insure a firm bond. A silver solder paste was then used to solder the copper floating head to the quartz. This was done by heating the floating head on a hot plate and inserting the quartz tube with the silver-solder paste into it in a similar manner as sweating a copper pipe joint.

2.3 FLOATING HEAD GEOMETRIC CONCERNS

The floating element skin friction balance is a non-intrusive instrument, meaning that it does not alter the flow from which the measurement is being taken. Any intrusion

of the floating element into the flow has the potential to introduce significant error in the measurement. Ideally, the floating element would be aligned perfectly with the wall from which the measurement is being taken (Fig. 2.5). This would effectively eliminate resultant forces from protrusion or recession of the floating head. It is desirable to understand the magnitude of misalignment forces if only for design considerations. Further, the effect of the gap between the floating element and the surrounding wall is important, since this gap is unavoidable in the design. The small size of the balances in this study prohibits ones ability to do a systematic investigation of these potential error forces, because the magnitudes are very small. A relevant investigation was conducted by Allen[13,14] with a large version of a non-intrusive, direct force measuring balance in unheated supersonic flow at NASA Langley Research Center. In that parametric study, the effects of each individual misalignment was investigated as well as the effect of the gap size on each. Figure 2.6 illustrates these potential sources of error. The balance of Allen's study was of the nulling type and the flows that were studied were cold supersonic flows without the high heat flux rates as in this study. In order to use Allen's study as a design criteria for the skin friction balances of this study in a rigorous sense, one must assume that the protrusion from a slightly tilted floating head of a non-nulling device will produce the same effect as simple protrusion or recession from a nulled floating head. Also, Allen bases his criteria for minimizing the effects of misalignment on knowledge of the boundary layer thickness in which the measurements are being made. For instance, specific ratios of lip-to-diameter and gap-to-diameter will produce negligible effects on the shear measurement for a given boundary layer thickness to diameter ratio at a specified amount of protrusion or recession of the floating head. In this study, the boundary layer thickness is an unknown quantity, therefore an attempt to accurately quantify the error from these effects is not possible. What can be done though, is to use this study to understand these misalignment effects and give insight to the design process. The best procedure to follow is one where the skin friction balance will not either protrude or be recessed from the combustor wall within reasonable limits (on the order

of 0.0005 inches). Given this, the following is a discussion on the possible effects of floating head misalignment.

Floating head protrusion has a strong effect on the force measurement. Small ratios of protrusion to the floating head diameter may result in forces larger than the shear force[12]. Intuitively, it would seem that this error would be dependent on the characteristics of the boundary layer, and it would possibly be more significant the thinner the boundary layer. One common assumption about gap size is that having as small a gap size as possible is beneficial. In fact, Allen observed that as gap size is increased, protrusion errors become less significant. Also, a common misconception is that a small amount of floating head recession relative to the wall is preferable to protrusion. Allen showed that either protrusion or recession is equally damaging to the measurement. All of the balances in this study have insignificant amounts of protrusion or recession misalignment. The magnitude of any possible misalignment is smaller than the capability of conventional machinists measuring devices used to determine this misalignment. This would put the magnitude at less than 5 ten-thousands of an inch (< 0.013 mm).

The general conclusion drawn from Allen's study is that for small protrusion or recession of the floating head, lip and normal forces can be large enough to thwart any attempt to determine the shear force. Therefore, in the construction of the balances of this study, great care is taken to insure that the floating head will be aligned perfectly with the surrounding wall as stated above. Allen found that a small gap size is not necessarily preferable to a relatively large gap size. However, the balances of this study are liquid filled and the capillary forces between the floating head and the surrounding wall are important to keep the liquid inside the balance. Therefore, these balances are designed with minimal gap, which magnifies the importance of proper alignment.

Another consideration to the design is the effect of a pressure gradient on the

floating head, either uniform or non-uniform. One of the principle reasons for filling the balance with an incompressible liquid is to make the balance appear in the view of a pressure gradient as a wall thus eliminating any effect it could have. This technique was shown to be effective in the study of Refs. [21, 22]. A non-uniform pressure gradient would tend to put a moment on the cantilever. This type of applied force is also canceled in the configuration of the Wheatstone bridge, with one active strain gage in tension and another in compression on opposing sides of the cantilever.

PART II -- STRAIN GAGE THEORY AND APPLICATION

2.4 BACKGROUND

Strain is defined as the ratio of change in length of a specimen to an initially unstressed reference length. A strain gage is an element that senses this change and can convert it to an electrical output. Typically, the strain gage is firmly bonded to a substrate from which the strain is to be measured. As the substrate undergoes a strain, it is directly transmitted to the strain gage by elongating or compressing it. When a strain gage is stretched or compressed, it will result in a change in its electrical resistance since its cross-sectional area is changed. Strain gages are readily available and the user must chose to accommodate the particular test environment. In order to record a change in resistance of a strain gage, they are configured in a Wheatstone bridge circuit. Figure 2.7 illustrates a typical circuit. It should be noted that in the bridge arrangement 1, 2, or all 4 elements may be active, with the others providing bridge completion. An active gage is one that directly senses the desired strain to be measured. In this study, all electrical circuits in the skin friction balances are either a full bridge (4 active strain gages) or a half bridge (2 active strain gages and 2 completion resistors). Total strain is always the sum of the strain

measured by all four elements of the bridge in the following manner :

$$\varepsilon_T = \varepsilon_1 - \varepsilon_2 + \varepsilon_3 - \varepsilon_4 \tag{2.6}$$

When a strain gage is subjected to a tensile stress, it will produce a positive voltage, and, in compression, it will produce a negative voltage assuming a positive excitation voltage. If the gages are mounted to a specimen in such a way as to produce a compression force in elements 2 and 4, and a tensile force in elements 1 and 3, the resulting output voltage from the bridge circuit will be the sum of the absolute value of all the elements. In the cantilever beam arrangement of the skin friction balance designs of this study, this is easily accomplished by placing strain gages on opposite sides of the beam in either a full or half bridge circuit (Fig 2.8). When constructing a Wheatstone bridge circuit, lead wire resistance can be of some concern. It is good practice to use the same type and the same *length* wires for each strain gage. Lead wires are also best to be as short as possible to decrease the potential of contaminating noise from external sources. Shielding of all wiring harnesses is good practice as well.

A Wheatstone bridge circuit is in a null state, that is, it will not produce an output voltage for a given excitation voltage, when the product of R_1R_3 is equal to the product R_2R_4. When one or all of the strain gages in a bridge circuit is subject to a stress resulting in a resistance change in any of the strain gages, the previously stated null equality will not be true. The result is that the bridge circuit will produce an output voltage proportional to this resistance change. Strain is related to this resistance change by Eqn. 2.7 :

$$\varepsilon = \frac{\Delta R}{R_o\,(GF)} \tag{2.7}$$

The gage factor (GF) in the above equation is effectively a measure of the sensitivity of a particular strain gage. These values range from 2 to 200 and will be discussed in the next sections. The output voltage for a bridge circuit with two active gages with equal and opposite strains (typical of the cantilever beam arrangement) follows directly as :

$$E_{output} = \frac{E_{input}\, GF\, \varepsilon}{2} \tag{2.8}$$

By substituting the expression for the strain in a cantilever beam from Chapter 3 (3.3), the final expression for output voltage of the bridge circuit for a cantilever beam with a half-bridge arrangement is as follows :

$$E_{output} = E_{input}\, \frac{(GF)}{2}\, \frac{PLd}{2EI} \tag{2.9}$$

The output for a full-bridge arrangement (two pairs of gages with equal and opposite strains) would simply be double the above expression.

2.5 SEMI-CONDUCTOR STRAIN GAGES

In the early skin friction balance designs of this study (GASL Test Series and the first DCAF entry), semi-conductor strain gages were used to sense the beam strain (shearing force at the end). The large benefit of these type of strain gages is that they exhibit very high sensitivity to strain as compared with standard (foil) strain gages. These gages operate on the principle of piezoresistivity. Piezoresistivity is defined as a change in electrical resistivity with applied stress. This is the basic principle applied to silicon based semi-conductor strain gages. For a semi-conductor :

$$i = \frac{1}{e\ N_i\ \mu_{ave}} \tag{2.10}$$

where :

N_i = number of charge carriers

μ_{ave} = the average mobility of N_i

e = electronic charge

i = current

When a stress is applied to a semi-conductor, both N_i and μ_{ave} change depending on the carrier concentration and the crystallographic orientation to stress. A particular manufacturer has control over both the number of charge carriers and the orientation enabling the strain gage design for various requirements, including gages with both positive and negative gage factor. Change in current along a particular stress axis is then given by :

$$\frac{\Delta i}{i_o} = \pi_L \sigma \tag{2.11}$$

where :

π_L = Longitudinal Piezoresistance Coefficient

σ = Applied Stress

This leads directly to the definition of the gage factor for semi-conductor strain gages as the fractional change in the resistance of a gage with applied strain :

$$GF = \frac{\Delta R}{R_o \varepsilon} = 1 + 2\nu + \pi_L Y \tag{2.12}$$

where :

υ = Poisson's Ratio

Y = Young's Modulus

The first two terms in the above expression represent change in resistance due to dimensional changes and the last term represents change in resistance due to strain. Reference 23 presents the detailed theory of semi-conductor strain gages.

2.6 STRAIN GAGE SELECTION

The semi-conductor strain gages used in most of the skin friction balances of this study are silicon based gages. Gage factors for these types can range from a low of +55 to a high of +140. The strain gages are encapsulated in a glass/epoxy matrix with solder tab terminals provided by the manufacturer (Kulite Semi-Conductor). Nominal dimensions of the glass gage/solder tab matrix is 0.30 in (0.76 cm) by 0.15 in (0.38 cm). Figure 2.9 illustrates the typical geometry. The strain gages are cemented onto the quartz tube at the base which has been ground square, as previously discussed, with standard strain gage mounting adhesive (Micro Measurements Type AE-10 or M-Bond 610). Lead wires are attached to the solder tab terminals with silver solder to insure proper electrical contact. Figures 2.10 and 2.11 show how temperature effects resistance and sensitivity for these semiconductor strain gages. Figure 2.12 shows some data obtained during a hot flow test where a thermal gradient at the strain gage position was present without a shearing load on the floating head. This data was used in the uncertainty analysis in Appendix A.

In the later skin friction balance designs, foil strain gages were used. These strain gages (Micro Measurements, Type 062P) have a matched thermal expansion coefficient to quartz and are fully encapsulated in a high temperature epoxy resin and are constructed of a K-alloy (constantan). M-Bond 610 (Micro Measurements) strain gage cement was

used to attach the gages to the quartz tube. The resistance of the strain gages is 350 ohms with a gage factor of 2.0. The uncompensated temperature sensitivity of these gages is plotted in Fig. 2.13.

2.7 GENERAL STRAIN GAGE THERMAL EFFECTS

Under ideal conditions, a strain gage that is bonded to a test part would respond only to an applied strain in the part. In practice, ideal conditions are not usually observed. The electrical resistance of a strain gage varies not only with the applied strain but with temperature change as well. Also, the sensitivity of a strain gage, the relation between strain and resistance change (gage factor), varies with temperature. In order to insure accuracy of the strain measurement, these phenomena must be understood so that they can be either compensated for or corrected.

Apparent strain due to thermal effects is the most serious error source in the strain measurement. In this investigation, the relatively small shear force being measured translates to a small strain at the gage location (50 - 100 microstrain). Given this fact, an uncompensated bridge circuit can easily result in larger output from thermal effects than from actual strain due to the shearing force.

The thermal output of a strain gage is caused by two algebraically additive effects. The first is simply that the electrical resistivity of the material of the strain sensing element is temperature dependent. The second contribution to thermal output arises from a differential in thermal expansion between the strain gage and the substrate to which it is bonded. With a temperature change, the substrate expands or contracts depending on the thermal gradient. Since the strain gage is firmly bonded to the substrate, it has to undergo the same expansion or contraction. If the thermal expansion coefficient of the substrate and the strain gage material are not the same, then a residual strain in the gage

will result.

All strain gages to some extent exhibit sensitivity to temperature. The nature of the semi-conductor strain gages tends to amplify these effects over those of common (foil) strain gages. Concerning resistive temperature effects, two items contribute to the apparent strain measured from thermal inconsistency. First, there is an inherent change in resistance due to temperature change expressed through a temperature coefficient of resistance (TCR) that can be determined experimentally and is usually supplied by the manufacturer. A 10% to 20% change in resistance per 100 °F (310 K) is typical for these types of strain gages. Second, the differential thermal expansion between semi-conductor (silicon) and the substrate to which the gages are bonded leads to an apparent strain as well. These two effects combine to give:

$$\varepsilon_a = \left[(C_b - C_s) + \frac{TCR}{GF} \right] \tag{2.13}$$

where:

TCR = thermal coefficient of resistance, α

C_B = thermal expansion coefficient of substrate

C_S = thermal expansion coefficient of silicon

GF = gage factor

ε_a = apparent strain due to thermal effects

Overall, the temperature effect on the strain gage resistance is as follows :

$$R_T = R_o \, (1 + \alpha_B \Delta T) \tag{2.14}$$

with

$$\alpha_B = \alpha + (C_B - C_S)GF \tag{2.15}$$

Equation 2.14 shows change in resistance to be linear with change in temperature, although very high resistance strain gages (750 Ω - 1000 Ω) may exhibit some non-linear characteristics for large changes in temperature. The parameter, α_B, accounts for both the inherent thermal effect and the differential expansion effect.

The second major thermal characteristic that these gages exhibit is a change in sensitivity or gage factor to temperature. The basic rule is :

$$GF_T = GF_o\ (1 + \beta\Delta T) \tag{2.16}$$

where β is the temperature coefficient of gage factor, TCGF, which is the inherent sensitivity to temperature coefficient. Depending on the strain gage selection this parameter can range from 2% to 20% per 100 °F (310 K).

2.8 COMPENSATION FOR THERMAL OUTPUT

There are basically two techniques to compensate for thermal output. In theory, either of these two methods will completely eliminate temperature effects. The first is to use a "dummy" strain gage in an adjacent arm of the Wheatstone bridge circuit. This "dummy" strain gage must be subjected to identical thermal conditions (therein lies the difficulty) as the active strain gage but on an unstrained specimen. By arranging these strain gages in a half-bridge, the thermal effects will subtract resulting, in output from the bridge due to only the actual mechanical strain in the substrate. The difficulty with this technique is obtaining an unstrained substrate under identical thermal conditions as the active strain gage substrate. In this investigation, the required small size of the balance

prohibited the implementation of a "dummy" strain gage.

The second technique, which has several benefits over the first, was employed in all of the balances of this study, with improvements being made with each successive design iteration. If identical thermal conditions can be maintained around the beam at the strain gage location, the two strain gages can be installed on opposite sides of the beam in the plane normal to the plane of bending. In this case, the strain gages are installed on opposite sides of the cantilever (see Fig 2.8). The active half-bridge that is formed will result in temperature compensation over a small range of temperature change. In the half-bridge configuration, the outputs from each strain gage are effectively subtracted. In the cantilever beam configuration, one arm of the bridge is in tension and the other is in compression. This results in a doubling of the bridge output. The temperature compensation is achieved, since the thermal output from each strain gage is of the same sense and is effectively subtracted out of the circuit output. Ideally, this technique will exactly cancel the thermal output effect, but as will be discussed in the following sections, the effectiveness of this technique varies with type of strain gage and even from pair to pair of strain gages.

In the harsh test environments of this study and given the potential for large error from temperature effects, an analysis was performed to try to determine how best to implement temperature compensation. In addition to actively cooling the strain gages through cooling channels and the combustor spray cooling of the NASA ARC DCAF combustor tests, design equations were developed to aid in gage selection to best alleviate temperature effects. It is possible to manufacture semi-conductor strain gages with both positive and negative gage factors. This result can be used, in theory, to compensate for resistance temperature effects. If both a positive gage factor strain gage and a negative gage factor strain gage are used in adjacent arms of the Wheatstone bridge, the output due to thermal effects can be written:

$$\left[\frac{\Delta V}{V}\right]_{thermal} = \left[\frac{\Delta R}{R}\right]_p - \left[\frac{\Delta R}{R}\right]_n \tag{2.17}$$

By substituting Eqns. 2.14 and 2.15 into Eqn. 2.17 and setting the thermal output equal to zero, a design equation is obtained which depends on gage factor, temperature coefficient of resistance, and thermal expansion coefficients.

$$(C_B - C_S) - \frac{\alpha_n - \alpha_p}{|G_n| + G_p} = 0 \tag{2.18}$$

Since C_S, the thermal expansion of silicon, is fixed and C_B is that of the quartz beam, the semi-conductor strain gages must be selected so that the second term of the above expression be set equal to the first term.

A shortcoming of the above technique for semi-conductor strain gages is that the gage factor is also a variable with temperature. A common technique to compensate for this effect is called span compensation. This method employs a series resistor in the case of a constant voltage bridge circuit or a shunt resistor in the case of constant current excitation to compensate for an increase or decrease in sensitivity due to gage factor temperature properties. A design equation can easily be obtained through Thevenin equivalent circuit (Ref. [23]) analysis as :

$$R_c = \frac{R_o \beta}{\alpha + (C_B - C_S)G - \beta} \tag{2.19}$$

where :

β = Temperature coefficient of Gage Factor

R_c = compensation resistance

G = equivalent Gage Factor for multiple arms of a bridge

This equation along with Eqn. 2.18 can be used to select a set of semiconductor strain gages that will help to compensate for temperature effects.

2.9 PRACTICAL ASPECTS OF TEMPERATURE COMPENSATION

The above techniques were utilized to try to select an optimum set of semi-conductor strain gages for the skin friction balances of this study. Some success was achieved with the implementation of semi-conductor strain gages in two separate balance designs. Although great care was taken to optimize the gage selection for temperature compensation, in practice the techniques do not work as well as predicted. This is due simply to the nature of semi-conductor strain gages. These gages are manufactured by doping essentially a non-conductor with an impurity to make them semi-conductors. On the microscale, this is done by filling in the holes of the structure with the impurity. It may be that it is not possible to identically match the microstructure of each individual gage or even a pair of gages. For this reason, the temperature compensation techniques described above do not perform as well as predicted, because they do not behave equally for a given temperature change.

The later skin friction balance designs use more common foil type strain gages. The microstructure of these type strain gages are more uniform from gage to gage, making the temperature compensation techniques more effective. A big price is paid in sensitivity with these gages though; gage factors of two are common, as compared to 140 for the semi-conductor gages used in this study. Since gage factor directly scales the output of the bridge circuit, resolution of the data acquisition equipment, amplifier stability, and noise levels and filtering all become more critical to the accuracy of the measurement. There is some benefit to standard foil strain gages. The sensitivity to

temperature for these types of strain gages is much smaller than the semi-conductor strain gages. In fact, it is possible to have the gages manufactured with an alloy that has an expansion coefficient which can match that of the substrate and effectively eliminate that part of the resistive temperature effects. This is the major reason that these types of strain gages were utilized in the later skin friction balance designs.

CHAPTER THREE

HEAT TRANSFER ANALYSIS

3.1 BALANCE COOLING AND HEAT TRANSFER

The heat transfer through the skin friction balance plays a very important role in determining the accuracy of the measurement and survivability of the balance under the harsh conditions to which it is exposed. While designing a balance of the types in this study, it is important to choose materials to direct heat in beneficial directions. It is essential to use good engineering judgement in the selection of materials, but with the complicated geometry of the design, this may not necessarily be sufficient. Therefore, a numerical analysis was performed to better understand the heat transfer characteristics of these instruments. The most important aspect of the design to understand is the feasibility and effectiveness of the floating head cooling. Early in the design process, various bench tests were conducted in an attempt to determine just this. It is virtually impossible to try to duplicate the harsh conditions of supersonic combustion on a bench. By using devices such as an oxygen-acetylene torch, heat loads similar to those faced in a combusting flow can be produced and some practical knowledge of the survivability of the balance was gained. These tests were not sufficient to determine the effectiveness of the internal floating head cooling. The numerical analysis then becomes very important to determine the floating head cooling effectiveness. A parametric study was conducted to determine how best to configure the floating head cooling system.

The cooling system consists of a co-axial flow arrangement internal to the cantilever beam. A flow pattern to cool the backside (internal) of the floating head is developed along the internal walls of the cantilever beam with cooling fluid entering through a manifold at the base of the beam. Fluid is exhausted through a smaller stainless steel tube (0.062 inch diameter) along the centerline of the cantilever, which extends to within 0.062 inches (0.157 cm) of the backside of the floating head. Figure 3.1 illustrates the flow path. The technique is essentially the same for all the skin friction balances constructed during this study. The details of each individual skin friction balance are included in the design discussion of Chapter 4. The primary goals of the numerical analysis were to determine the feasibility and effectiveness of such a system. Also, the calculations aided in choosing the thickness of the floating head between the shear sensing exterior and the backside (interior).

3.2 THE HEAT EQUATION

A simple derivation of the heat equation can be obtained by considering a control volume fixed in space and applying the first law of thermodynamics. For a solid material, there will be no mass passing through the surface. The energy statement with no work being done on the volume is:

The rate of energy stored within the control volume equals the net flux of energy through the control surfaces plus the rate of energy generated by internal heat sources.

For a solid with heat capacity, C, mass density, ρ, and temperature, T, the energy stored (internal energy) in an infinitesimal control volume, $d\tau$, is $\rho CTd\tau$. Heat transferred by conduction through the surface is $-k(\partial T/\partial n)d\sigma$ where $d\sigma$ is the infinitesimal surface. This is the empirical law of heat conduction which states that the rate of heat flow by conduction in a given direction is proportional to the area normal to the direction of the

heat flow and to the gradient of temperature in that direction. The rate of energy generated by internal sources is q the heat added per unit volume. For a finite control volume, V, and control surface, S, integrating the above expressions yield the governing equation for heat conduction in a solid as :

$$\frac{d}{dt}\iiint_V \rho c T d\tau = \iint_S k\frac{\partial T}{\partial n}d\sigma + \iiint_V q\, d\tau \tag{3.1}$$

In order to obtain the differential form of the above, the divergence theorem is applied:

$$\iint_S k\frac{\partial T}{\partial n}d\sigma = \iint k\nabla T \circ n\, d\sigma = \iiint_V \nabla \circ k\nabla T\, d\tau \tag{3.2}$$

with continuous derivatives, Eqn. (3.1) can be rewritten as:

$$\iiint_V \left[\rho c\frac{\partial T}{\partial t} - \nabla\circ(k\nabla T) - q\right] d\tau = 0 \tag{3.3}$$

Since the above integral is equal to zero, the integrand must equal zero as well. The result is the differential form of the heat equation. Expanding to cartesian coordinates yields :

$$\frac{\partial^2 T}{\partial x^2} + \frac{\partial^2 T}{\partial y^2} + \frac{\partial^2 T}{\partial z^2} + \frac{1}{k}q = \frac{\rho c}{k}\frac{\partial T}{\partial t} \tag{3.4}$$

This result is a first order in time and second order in space partial differential equation. This is classified as a parabolic equation and must be solved as an initial/boundary value problem. Either T or $\partial T/\partial n$ must be specified on the boundaries and T at time equal zero must be specified everywhere in the domain.

3.3 THE HEAT CONDUCTION CODE

A computer program, CONDUCT[24], was used to calculate the heat conduction through the skin friction balance and the near combustor wall. This code is designed for the solution of partial differential equations of the heat conduction type. The code is structured to include an invariant part and provisions for the user to set-up the framework for a specific problem. In this later part, the details of material properties, heat sources, boundary conditions,output format, and grid generation are included. In addition, an input deck was added to eliminate the need to recompile the code for a parametric study, and a convergence criteria on the L2-NORM of the solution, a routine to use external grid generation packages, and an output format for several popular contouring routines were added.

The numerical scheme of the code is a finite volume, fully implicit scheme with block correction[24,25,26]. The governing heat equation (3.4) is discretized in the following manner for a typical computational cell (Fig. 3.2) :

$$(\rho c)_P \left[\frac{\Delta V}{\Delta t}\right] (\phi_P - \phi_P^{\circ}) = J_w A_w - J_e A_e + J_s A_s - J_n A_n + S\Delta V \qquad (3.5)$$

For this heat transfer case, the dependent variable, ϕ, is temperature. The superscript, o, denotes the value of ϕ at the beginning of a time step. The J's are diffusion fluxes across control volume faces. ΔV is the volume of the control volume and A is the area of the control volume faces. S is the average source term over the control volume. The diffusion flux across a control volume face (e for instance) is calculated as:

$$J_e A_e = D_e (\phi_P - \phi_E) \qquad (3.6)$$

where D_e is the conductance coefficient and is calculated from the thermal conductivity at P and E.

$$D_e = A_e \left[\frac{\delta_{x_{e^-}}}{k_P} + \frac{\delta_{x_{e^+}}}{k_E} \right]^{-1} \tag{3.7}$$

The increments δ_{xe} are defined in Fig. 3.2. The definitions for the other faces are constructed in a similar manner. The source terms are linearized by constructing S as :

$$S = S_c + S_P \phi_P \tag{3.8}$$

with S_c as S_P as constants. For constant source terms S_P is set to zero. Substituting 3.7 and 3.8 into 3.6, the final discretized equation is obtained :

$$a_P \phi_P = a_E \phi_E + a_W \phi_W + a_N \phi_N + a_S \phi_S + b \tag{3.9}$$

where the a_i terms are given by the corresponding D_i terms from Eqn. 3.7 and

$$b = S_c \Delta V + a_P^{\bullet} \phi_P^{\bullet} \tag{3.10}$$

with

$$a_P^{\bullet} = \frac{\rho c \Delta V}{\Delta t} \tag{3.11}$$

and

$$a_P = a_E + a_W + a_N + a_S + a_P^{\bullet} - S_P \Delta V \tag{3.12}$$

A more elaborate formulation of the discretization technique, from which this is summarized, is given in Ref. [24].

3.4 BOUNDARY CONDITIONS

The skin friction balance installed into the combustor will experience a heat flux from the combustor flow for which experimental data is available. The combustor spray cooling provides cooling to the backside of the combustor wall and to all exterior surfaces of the skin friction balance. Internal to the skin friction balance, the floating head cooling system will convect heat from the backside of the floating head and along internal surfaces of the cantilever beam. These conditions were all modeled in the calculations.

A diffusion flux at a boundary is handled in the code in the following manner. A diffusion flux on a boundary is defined as :

$$J_B = f_C + f_P \phi_B \tag{3.13}$$

where J_B is defined as the boundary flux and f_C and f_P are constant flux coefficients. In this study, a constant boundary heat flux to simulate the heat flux obtained during an actual fueled combustor test is specified for the inner combustor wall boundary. Since the heat flux is fully known, f_P is set equal to zero. Although, if the heat flux is a linear function of ϕ_P then f_P is not zero. If a non-linear heat flux is specified, f_C and f_P must be iteratively updated. Sign convention is such that J_B is positive for heat added to the domain.

If the boundary flux is given as a convection coefficient, then :

$$J_B = h(\phi_\infty - \phi_B) \tag{3.14}$$

where ϕ_B stands for the temperature of the boundary and ϕ_∞ is the temperature of the surrounding fluid. To express the above in a similar manner as Eqn. 3.6 then $f_C = h\,\phi_\infty$ and $f_P = -h$ where h is a film coefficient.

In order to bring a convective heat flux into a boundary control volume, extra source terms are used. For the convective boundary, the heat flux can be written as (see Fig. 3.3) :

$$q_B = h(\phi_\infty - \phi_B) \tag{3.15}$$

and the heat conduction from B to P is :

$$q_B = \frac{k}{\delta}(\phi_B - \phi_P) \tag{3.16}$$

By eliminating ϕ_B from the above relations, the expression for q_B is obtained as :

$$q_B = \left[\frac{1}{h} + \frac{\delta}{k}\right]^{-1}(\phi_\infty - \phi_P) \tag{3.17}$$

For area, A, and volume, V, the extra source term becomes :

$$S_{extra} = \frac{A}{\Delta V}\left[\frac{1}{h} + \frac{\delta}{k}\right]^{-1}(\phi_\infty - \phi_P) \tag{3.18}$$

If this is separated into a constant and ϕ_P coefficient terms as was done with the other flux formulations, then the result is :

$$S_{c,extra} = \frac{A}{\Delta V}\left[\frac{1}{h} + \frac{\delta}{k}\right]^{-1}\phi_\infty \tag{3.19}$$

and

$$S_{P,extra} = -\frac{A}{\Delta V}\left[\frac{1}{h} + \frac{\delta}{k}\right]^{-1} \tag{3.20}$$

Since only a section of the combustor wall is modeled, a symmetry boundary condition is set at the wall ends. This essentially fixes the diffusion flux in those boundary cells as zero.

3.5 SOLUTION TECHNIQUE

For each control volume, a discretized equation from the discussed formulation is constructed. This results in a set of linear algebraic equations with as many equations as unknowns. For the two dimensional (axisymmetric) problem solved in this study, a pentadiagonal coefficient matrix is obtained. The solution technique is a line-by line method with a block correction scheme. The principle behind the block correction technique is that for an unconverged $\phi_{i,j}$ from a prior iterations is corrected by adding uniform corrections ϕ_i along lines of constant i. The corrections are chosen so that integral conservation over the control volume blocks defined by each constant i line is exactly satisfied.

For a given computational cell, in the y-direction, the ϕ_N and ϕ_S are considered to be known. If this is done for the entire system of equations, the result is a tri-diagonal system which can easily be solved with an algorithm like the Thomas Algorithm[27]. The line-by-line method in this code uses this technique. First, the tri-diagonal matrix

algorithm is applied to all the lines in the x-direction, followed by all the lines in the y-direction. As the values of ϕ along a line are calculated, they are used as estimates for the next line. The solution procedure is iterative. The solution algorithm consists of block corrections in i and j followed by four sweeps of the line-by-line method. This set of operations is repeated a specified number of times or until the local relative error is found to be less than a specified value. The error is defined by the absolute value of the residual divided by the largest of the terms in the discretized equation. The residual is given from the discretized equation (Eqn. 5.9) for the interior of the domain as:

$$RESIDUAL = a_E\phi_E + a_W\phi_W + a_N\phi_N + a_S\phi_S + b - a_P\phi_P \qquad (3.21)$$

3.6 THE COMPUTATIONAL GRID AND BALANCE MODELING

In the initial phase of the numerical study, three computational grids were constructed. All three were rectangular Cartesian grids with either 101 by 51, 151 by 51, or 201 by 51 nodes. Figure 3.4 illustrates the finest mesh. The fineness of the mesh is not resolvable on this figure, therefore, Figure 3.5 shows enlarged view of the area indicated by the box on Figure 3.4. The solution to an initial baseline test case showed that either grid was sufficient to obtain a grid converged solution. Since the calculation is relatively inexpensive and quick on the computer used (Silicon Graphics 340), the finest mesh was employed for all calculations. The grid dimensionally represents a six inch (15.25 cm) by 3 inch (7.62 cm) rectangle. A centerline slice of the skin friction balance was modeled. The result is a T-shaped domain of solid material including the balance and the combustor wall (see Fig. 3.5). A six inch (15.25 cm) length of the 0.25 inch (0.64 cm) combustor wall was modeled with the skin friction balance screwed into the center. The geometry of the skin friction balance was modeled to scale with separate zones set up for each different material (i.e. different thermal conductivity, mass density, and specific heat). The

grid was stretched appropriately to capture areas of large temperature gradients.

3.7 RESULTS

A parametric study was conducted with a specified heat flux on the internal wall of the combustor varying from 0.5-4.0 BTU/in^2/sec. Typically, heat fluxes on the order of 1.0 BTU/in^2/sec were observed during the actual test series. Pre-test estimates of the wall heat flux obtained from JHU/APL were much higher (5.0-7.0 BTU/in^2/sec), consequently the balance was designed to withstand higher heat flux, as well. A film coefficient was prescribed on the outer surfaces of the wall (0.0154 BTU/in^2/sec/°R, 14000 W/m^2/°C, from JHU/APL) and the skin friction balance (from 0.0022 - 0.050 BTU/in^2/sec/°R, 2000 - 45000 W/m^2/°C). The value of the film coefficient was set initially with estimates and later updated with data from the first test series. Figure 3.5 shows a schematic of the modeled geometry. The internal floating head cooling film coefficient was varied to determine what was required to match the floating head temperature with the neighboring combustor wall. It was determined that a single internal cooling film coefficient was sufficient to maintain the floating head temperature at the inner combustor wall temperature independent of the wall heat flux. This is illustrated in Fig. 3.6. In this figure, the floating head temperature is plotted against the range of internal cooling flow film coefficients for four values of inner combustor wall heat flux (1.0-4.0 BTU/in^2/sec, 1.635x10^6 - 6.54x10^6 W/m^2). The temperature of the inner combustor wall is plotted on the curve for each individual inner wall heat flux as the black dot. It is evident that a single internal flow film coefficient of approximately 17500 W/m^2/C is required to match the floating head temperature to the inner combustor wall temperature. The combustor wall and floating head temperature both increase with an increase in heat flux from the flow, but the cooling to the floating head is such that convection from a single convection coefficient applied to the backside of the floating head is sufficient to maintain the wall and floating head temperature at an equivalent

level.

Figures 3.8 through 3.19 show predicted temperature contours for heat flux to the combustor wall varying from 0.5 - 4.0 BTU/in^2/sec. The internal floating head cooling film coefficient was set at 17500 W/m^2/°C. There are two figures for each combustor inner wall heat flux. The first set shows about 4 inches (10.16 cm) of the combustor wall and the skin friction balance (Figs. 3.8 - 3.13). The second set (Figs. 3.14 - 3.19) show an enlarged area surrounding the floating head of the skin friction balance. The temperature scale in all the figures is in °C. Regarding Figs. 3.8 through 3.13, a few interesting features are evident. First, in the area of the strain gages (Fig. 3.5 shows the schematic), it can be seen that as the combustor wall heat flux increases so does the temperature at that location. This is significant because the uncertainty of the measurement is dependent on the temperature change of the strain gage bridge. For the lower combustor wall heat flux values (0.5 - 1.5 BTU/in^2/sec) the temperature change at the gage location ranges from 3°C to 8°C (T_o = 15°C). Also, in these figures the effectiveness of the floating head cooling is apparent. This is especially true in the next set of figures which are enlargements of Figs. 3.8 - 3.13. Figures 3.14 through 3.19 show that the combustor wall and the floating head temperatures scale with the combustor wall heat flux. There are small noticeable hot spots in the oil filled gap on either side of the floating head near the inner wall surface due to the fact that the silicon oil is a thermal barrier when compared to the copper combustor wall. This and the fact that the flange of the skin friction balance increases the wall thickness leads to a slight increase in inner wall temperature (less than 5% in any test case). The major significance of these calculations is that the concept of internal floating head cooling appears to be feasible and that only a single fluid flow rate inside the balance should be sufficient, independent of the combustor flow conditions within an inner combustor wall heat flux range from 0.5 - 4.0 BTU/in^2/sec (8.65×10^5 - 6.35×10^5 W/m^2).

A few other test cases are presented here as well. The first was to determine the effect on the heat transfer characteristics of the balance if there was no silicon oil (assuming stagnant air). The result is illustrated in Figs. 3.20 and 3.21. The combustor wall heat flux was set at 1.0 BTU/in^2/sec and the internal film coefficient was maintained at 0.020 BTU/in^2/sec/°R (17500 W/m^2/°C). Comparing these figures to Figs. 3.9 and 3.15 shows that there is relatively no change in the heat transfer near the combustor wall and floating head. The temperature in the area of the strain gages is, however, lower for the case with no oil. Unfortunately this cannot directly be taken advantage of, since the effects of a pressure gradient on the head could become significant without the presence of the oil. The other test case is shown in Figs. 3.22 and 3.23. Again, the combustor wall heat flux was set at 1 Btu/in^2/sec (1.635×10^6 W/m^2). In this case, however, the internal cooling film coefficient was set to zero to determine the effects of no cooling. The figures show the disastrous result. Without the floating head cooling, the head temperature approaches 3000°C even at this moderate combustor heat flux. This would result in structural failure of the balance since the methods used to attach the floating head to the balance will not withstand temperatures above 300°C.

CHAPTER FOUR

SKIN FRICTION BALANCE DESIGNS

4.1 GASL COMBUSTOR BALANCE DESIGN

The basic balance configuration is shown in Fig. 4.1. The shear sensing floating head is supported by a quartz cantilevered tube with an outside diameter of 0.062 cm (0.238 in) and an inside diameter of 0.40 cm (0.157 in). The balance is enclosed by an outer housing constructed of copper as is the floating head and the cantilever beam base. The balance is mounted into the GASL test facility with small (#6-32) screws through a flange on the outer housing. The GASL facility is constructed of copper, therefore the majority of the parts for this balance are constructed of the same material for consistency.

In order to measure the sensor head deflection, piezoresistive semiconductor strain gages are mounted directly to the cantilevered quartz tube. At the location of the strain gages, the tube is machined square with an abrasive diamond wheel cutter to provide a secure smooth base to mount the strain gages and insure orthogonality of the measurement axes. The sensor head is mounted to the tube which is then mounted into the base with the ceramic-like high temperature cement.

The strain gages are piezoresistive semiconductor type gages. These gages provide several advantages over conventional foil gages including higher sensitivity, resistance, and fatigue life, as well as small size. Kulite 750 ohm semiconductor strain gages are

used in this instrument. These are ruggedized gages encapsulated into an epoxy/glass matrix with large solder tab terminals. Overall dimensions of each gage are 0.11 cm (0.28 in) by 0.06 cm (0.14 in). These strain gages as well as the others used in this study are discussed in detail in Part II of Chapter 2. Four gages are mounted to the quartz cantilevered beam with a thin layer of a high temperature strain gage cement and coated with several layers of both polyurethane and an acrylic for protection from the environment. The gages are arranged in a half Wheatstone bridge, one gage in tension and one in compression for each axis of measurement while the sensor head is displaced. This provides compensation for any axially imposed strain which may arise from an axial force on the sensor head. Bridge completion is accomplished externally with precision resistors and a potentiometer for pretest output balance. The strain gages are powered by a +5 volt regulated DC power supply.

A flow pattern for sensor head cooling is developed through a co-axial tube arrangement. A stainless steel 0.160 cm (0.063 in) tube is mounted along the centerline of the instrument to provide an inflow passage for the cooling fluid to the back side of the sensor head. The geometry of this system is shown in Fig. 4.1. Heat transfer calculations were made with a computer code to determine the optimum thickness of the sensor head. In this calculation, the sensor head thickness was varied to determine the thickness that would closely match the sensor head temperature with the surrounding combustion chamber wall. A heat flux that is expected from a supersonic combustor and a convection coefficient which is obtainable with water as the cooling fluid were prescribed as boundary conditions. A sensor head thickness of 0.083 cm (0.0325 in) was found to be sufficient to match the floating head temperature to the inner combustor wall temperature over a range of inner combustor wall heat flux. The cooling fluid is exhausted from the instrument by flowing back along the outside of the stainless steel tube and inside of the quartz tube. At the base of the quartz beam, the exiting liquid passes through a manifold and out through a 0.317 cm (0.125 in) copper line. A variable

convection coefficient at the sensor head is obtainable by regulating the pressure of the incoming cooling liquid. Tests were conducted, and it was determined that the sensor head cooling system is able to withstand pressures up to 400 psi (3450 kPa). Calibration tests were conducted with the water flow on and off. These tests showed that the flowing water did not influence the tangential force measurement.

The balance is enclosed by an outer housing constructed of copper as is the floating element sensor head and the cantilever beam base. The cantilever beam is supported into a base which fits into the main housing. These parts are shown in Fig. 4.2. The floating head is aligned within the housing by a series of small (#0-80) set screws around the circumference of the end of the housing into which the beam support fits. By adjusting the torque on these screws, the floating head can be moved a small amount in any direction to center it within the housing. A cooling channel is also located at this end of the housing around the circumference. It can be seen in Fig. 4.1. The purpose of this cooling channel is to provide temperature stabilization of the strain gages. A 0.062 inch copper tube (1.58 mm) is wrapped around the circumference of the housing and then soldered to it. Brass fittings (Swagelok) at the tube ends mate the channel with a closed-circuit high-pressure water cooling supply at the GASL test facility. The balance is mounted into the test facility with screws through a flange on the outer housing, with a high temperature O-ring providing the seal. As with all of the designs in this study, the cavity between the beam and the housing is filled with a silicon based heat transfer fluid, primarily in this case for vibration damping and pressure gradient effect minimization. A calculation was performed to estimate the time response of the instrument and was found to be 1.5 kHz. This was done with a Rayleigh Integral Method, which is an energy method requiring an estimated beam deflection curve for vibrating beams. The details of this technique are contained in Ref. [30]. The damping effect of the silicon oil was not included in this calculation which would tend to lower the time response. Overall length of the balance is 8.89 cm (3.5 in). The sensor head was designed as described in Chapter

2 with a diameter of 0.812 cm (.320 in) and a 0.013 cm (0.005 in) gap. Lip size was set at 0.051 cm (0.020 in).

4.2 NASA ARC DCAF COMBUSTOR SKIN FRICTION BALANCE DESIGNS

The tests at the NASA Ames Research Center were conducted in two separate series. For the first entry, one skin friction balance was constructed. Two more balances were constructed for the second test series. One of these balances was configured with a longer beam than the other (2.5 inches versus 3.5 inches). This was done to increase the sensitivity of the balance which was located in an area of low shear in the combustor. These balances operate on the same principle as the balance design for the GASL tests, although they appear quite dissimilar on the exterior. The combustor for these tests is cooled on the exterior by a spray cooling system as discussed in Chapter 5. This cooling system enables the walls of the combustor to be only 0.25 inches (6.35 mm) thick. There was some uncertainty as to the effectiveness of the cooling system prior to the conducting of tests. Estimates by JHU/APL showed possible inner combustor wall heat flux spikes from 5.0 - 7.0 BTU/in^2/sec. This caused some concern about the use of hardened steel machine screws to secure the skin friction balance into the combustor. Since the screws would not conduct heat as well as copper, it was feared that the hot spots caused by this could be severe enough to cause overheating of the combustor walls in the area of the screws. The resulting solution to this potential problem was to design the copper skin friction balance housing to be screwed directly into threaded holes in the combustor wall.

The head for this balance is circular with a diameter of 0.320 in (8.13 mm). A 0.025 in (0.35 mm) lip around the top circumference of the head tapers to 0.28 in (7.11 mm) resulting with an overall length of 0.5 in (12.7 mm). An internal diameter of 0.238 in (6.05 mm) is bore to a depth that leaves a head thickness of 0.033 in (0.838 mm). This

geometry yields $L_p/D = 0.078$ and $G/D = 0.013$ which are within the constraints prescribed by Allen. The alignment of the floating head with the surrounding wall must still be carefully set to eliminate misalignment effects.

The basic design consists of a non-nulling cantilevered tube with a floating head (Fig. 4.3 and 4.4) similar to the GASL design. This design is possible since the deflection of the floating head is very small (0.0005 in) due to the high stiffness of the cantilever beam. Lip and normal forces on the floating head are eliminated through careful alignment with the combustor wall and filling the balance with an incompressible liquid as before. The resulting force due only to the wall shear, will lead to a measurable strain at the base of the beam. This arrangement is fit into a housing which in turn is incorporated into the test facility wall. The cantilevered tubes for these balances are constructed of quartz with a floating head of zirconium copper, which matches that of the supersonic combustor model walls. In order to sense the deflection of the floating head, the strain gages are cemented in four orthogonal positions around the circumference of the tube base. In the first test series, semiconductor strain gages were selected due to their high sensitivity. Along with high output due to actual strain, semiconductor strain gages also have high sensitivity to temperature. It was determined that this sensitivity can produce an unacceptable level of uncertainty in the shear measurement. Therefore, standard foil strain gages were selected for the second test series. These gages were chosen to provide self-compensation for thermal expansion effects of the quartz by a matched expansion coefficient. The strain gages are electrically configured in a half-bridge arrangement with one active gage in tension and the other in compression on opposing sides of the quartz beam. This is accomplished by grinding the beam square with an abrasive diamond wheel at the gage location (Fig. 4.5). In theory, this type of geometry will provide both moment and temperature compensation. The result of having four strain gages is two pairs which can sense shear in two orthogonal directions by carefully aligning the balance with the combustor, both a streamwise and cross-stream

component of the shear force is obtained.

An internal co-axial tube arrangement was developed and implemented which actively cools the floating head to eliminate any errors arising from a temperature mismatch between the floating head and the surrounding combustor model wall (Fig. 4.6). The design of the cooling system is essentially equivalent to the GASL balance design. The one major difference is that the flow path is opposite to the GASL balance because it provides better thermal stability in the strain gages. For the second test series, one of the balances was fitted with a small stainless steel sheathed Type-K thermocouple through the inside of the quartz beam and soldered into the floating head providing a floating head temperature measurement to verify the effectiveness of the cooling system. All of the balances are fitted with Type-K thermocouples cemented to the quartz cantilever at the strain gage position. Extensive numerical heat transfer analysis using estimates and later updated with actual data for heat flux from the first test series as boundary conditions were conducted. These numerical results are discussed in detail in Chapter 3.

The balance housing consists of two pieces, an upper and lower part. The upper housing is constructed of zirconium copper and is threaded to screw into the supersonic combustor model wall. Fig. 4.7 illustrates the upper housing geometry. Note that since one of the skin friction balances was fitted with a longer beam, this extra length was made up in the length of this housing. It is basically cylindrical with a 0.5 inch diameter (12.7 mm). Threads are cut (1/2"-20) into the combustor end of the housing to screw it into the combustor wall. A custom copper washer is required to make the seal between the wall and the housing flange. This was accomplished by precisely measuring the wall thickness in the hole that the balance would fit into and sizing an annealed copper washer to make up the difference between that thickness and the distance between the housing flange and end. The smoothness of the this fit on the inner combustor wall was verified by inspection from inside the combustor. The lower housing supports the quartz beam and

exchanges cooling fluid to and from the floating head. It is constructed of stainless steel for strength and desirable heat transfer properties. The balance for the first set of tests was constructed of a one piece lower housing (Fig. 4.8). This design required precise sizing of the balance elements to insure proper alignment of the floating head and upper housing upon assembly. The other two balance housings constructed for the second entry tests were constructed in two pieces. These pieces are illustrated in Fig. 4.9. The beam was fit into a threaded cylinder that fit into the other housing part. This design enabled height adjustment of the floating head inside the upper housing. The two parts were securely fastened with a locking nut. The upper and lower housings are mated by using a brass ferrule between them. The ferrule is seated into the stainless steel beam support centered around the internal bore of the part. In turn, the inside diameter of the copper upper housing is countersunk to meet the flare of the ferrule. This arrangement serves two primary purposes. First, it provides a seal to prevent internal fluid leakage. Second, and more importantly, the ferrule provides a pivot to center the floating head within the bore of the upper housing. This geometry proved to be very effective in accomplishing both functions while providing a very rugged enclosure for the fragile and sensitive internal workings of the balance.

The path of heat transfer through the instrument is of primary importance to the design, therefore material selection for the balance was chosen to optimize design requirements. Since cooling of the combustor walls is essential during the tests to prevent catastrophic failure, it is necessary to match the materials of the skin friction balance to the combustor walls, in this case, zirconium copper. Additionally, the accuracy of the measurement requires that the wall temperature be constant. From the point of view of the balance, a high heat transfer rate through the balance is undesirable because thermal consistency at the strain gage location is necessary to maintain accuracy of the skin friction measurement, especially for the semiconductor strain gages used during the first test series. For this reason, stainless steel was chosen for the lower housing, since it has

a relatively low thermal conductivity. Also, by using a ferrule to mate the two housings, the total area of solid-to solid contact between the two is reduced. It should be noted that the spray cooling of the combustor also provides a significant amount of cooling to the outside of the skin friction balance and this was relied upon to maintain the strain gages at or near a constant temperature. At one point, one of the balances was fitted with a cooling channel around the lower housing to determine if this could provide better control over the strain gage temperature. Even though high pressure water was circulated through this channel, it did not prove as effective as the spray cooling alone.

As mentioned above, thermal protection of the strain gages is necessary to reduce uncertainty in the skin friction measurement. In addition to the conduction of heat through the solid housings of the balance, heat transfer through the internal beam damping fluid and through the beam itself can lead to an increase in strain gages temperature. A high viscosity silicon based oil was chosen as the damping fluid, since its low thermal conductivity will help to minimize this effect. Also, quartz has a very low thermal conductivity which prevents heat from being directly transferred to the strain gage location through the beam. Understanding the effect of temperature on strain gages is of utmost importance since cooling of the balance is provided by the external spray cooling system of the combustor model and the amount of cooling is not completely known until the conducting of the tests. The silicon oil also serves to provide beam damping and to minimize pressure gradient effects.

CHAPTER FIVE

EXPERIMENTAL FACILITIES AND DATA PROCESSING

5.1 VIRGINIA TECH SUPERSONIC WIND TUNNELS

A series of measurements of skin friction were made in the supersonic wind tunnels at Virginia Tech. These facilities are blow-down type wind tunnels, which means high pressure air is stored in holding tanks and then blown-down through the supersonic tunnel after which it is exhausted to the atmosphere. There are currently two high pressure air storage tanks with a holding capacity of 23 cubic meters. These tanks are charged with a four-stage reciprocating air compressor (Ingersoll-Rand Type HHE) driven by a 480 volt, 500 horsepower electric motor (Marathon Electric Company). The compressor has the capability of charging the storage tanks to 50 atmospheres.

A schematic of the facility layout is shown in Fig. 5.1. Measurements were made in two of the three illustrated facilities. The first is the large supersonic wind tunnel. This tunnel has a 9 in by 9 in (23 cm by 23 cm) test section and can run at Mach numbers 2.4, 3.0, and 4.0 by the use of interchangeable two-dimensional nozzle blocks. The settling chamber contains a perforated cone and several screens for flow dampening. A pressure probe and transducer and a Type-K thermocouple provide settling chamber information. The tunnel operating and control system includes a fast-actuating butterfly valve and a 12 inch diameter hydraulically actuated servo-valve for the purpose of pressure regulation.

The valve is controlled by a servo-amplifier with feedback from the settling chamber pressure transducer. The test section also has large doors with Schlieren quality glass for good model accessibility.

The second wind tunnel used for this study is also depicted in Figure 5.1. This facility is a free jet blow-down supersonic wind tunnel. Air is exhausted through a supersonic converging-diverging nozzle with a 2 inch by 2 inch exit area (5 cm by 5 cm) at Mach 2.0 and atmospheric pressure. Total pressure of the flow is regulated with a high pressure dome regulator upstream of the settling chamber. Air from the storage tanks is discharged through the tunnel with a manually operated 3 inch diameter gate valve (Milwaukee Valve Company). A flat plate is mounted to the exit of the nozzle, in which the skin friction balance is mounted at a distance of two inches from the nozzle exit along the centerline.

5.2 GASL Test Facility

Tests were conducted at the General Applied Science Laboratory (GASL). The measurement facility is a vitiated-air supersonic combustor testing facility. Air for the facility is supplied from a bank of high pressure air tanks. The enthalpy of the flow entering the supersonic combustor is raised by burning hydrogen in the airstream upstream of the combustor, adding additional oxygen to replace that consumed in the combustion and then accelerated to approximately Mach 3.0 in a converging-diverging nozzle. The gas stream is exhausted into a vacuum sphere at the exit of the supersonic combustor model. Skin friction measurements were taken in the constant area section of the combustor.

5.3 DIRECT CONNECT ARCJET FACILITY

The Direct Connect Arcjet Facility (DCAF), located at the NASA Ames Research Center, is an Arcjet Facility for assessing hypersonic engine combustor performance. The combustor for a supersonic combustion ramjet (SCRAMjet) will experience high enthalpy air at the inlet during high Mach number flight conditions. In order to simulate these conditions, an electric arc heater is used to raise the energy of high pressure air upstream of the combustor. Before entering the combustor, this high-enthalpy high-pressure air is accelerated to a supersonic speed in a Mach 3.3 nozzle. Hydrogen fuel is added in the combustor to mix and react with the airstream. Upon exiting the combustor, the reacting mixture is quenched and slowed to subsonic speeds.

A high voltage arc (up to 100 Megawatts of power) is confined inside a water jacketed copper channel to increase the energy of the high pressure air passing through. The basic elements of the arc heater are two co-axial tubular electrodes separated by a large cylindrical swirl chamber. The upstream anode ends at the swirl chamber and the downstream cathode exits into the supersonic converging-diverging nozzle. Both electrodes are constructed of six inch diameter copper pipes. A magnetic field coil is located at the end of the heater to confine and spin the arc to prevent burning of the electrode ends. Current to the arc and airflow are increased after the arc is started at low pressure during a test run. Air is introduced into the swirl chamber through tangential injectors which produce a vortical flow in the electrodes to prevent the arc from burning through the walls. The electrodes are cooled by a jacket with high pressure deionized water supplied through non-conductive hoses.

A supersonic nozzle is connected to the arc heater through a transition section. This nozzle accelerates the heated air from the heater to approximately Mach 3.3 conditions. The nozzle has a rectangular exit of 2.5 inches by 15.25 inches. A schematic

of the combustor duct is shown in Figure 5.2. The 0.25 inch (0.64 cm) combustor ducts are constructed of zirconium-copper plate and are directly connected to the supersonic supply nozzle. Also, illustrated in Figure 5.2 are the locations of the skin friction balances which will be discussed further in the Results section. This combustor is cooled by an external water spray cooling system. A series of spray nozzles are configured around the combustor ducts to keep the combustor from overheating. Wall heat flux values on the order of 1 BTU/in^2/sec are typical. These spray nozzles also provide cooling of the skin friction balances during the conducting of a test. This spray cooling is a closed system with the ambient temperature water being pumped from a reservoir to the nozzles and collected in a basin below the combustor which routes the water back to the reservoir. After the first set of tests were conducted in this facility, it was determined that the cooling provided by spray nozzles was insufficient. Essentially, there was not enough cooling provided to the exterior of the balance which resulted in elevated strain gage temperature. Therefore, the combustor spray pattern geometry in the area of the skin friction balances were specifically configured to optimize the balance cooling efficiency during the second set of tests. This included the addition of extra nozzles around the balances. Descriptions of this facility in more detail are presented in Refs. [31 - 33].

5.4 SIGNAL CONDITIONING - GASL TESTS

The balance design for the GASL test series was accompanied by a custom set of amplifiers and bridge completion circuits. A set of four amplifiers were constructed at Virginia Tech. The key to these instruments are the use of Burr-Brown Model INA101P instrumentation amplifier integrated circuits. In addition, precision resistors were added to the circuit to complete the Wheatstone bridge. Figure 5.3 shows the circuit diagram for these amplifiers. Variable gain from 1 to 1000 is possible with these instruments. The amplifiers were assembled into a sheet metal container with a regulated +5 Vdc power supply to provide excitation to the bridge circuit. Filtering of the data was done by post-

processing the obtained signal through a digital filter. The algorithm for this filter was obtained from Ref. 34. The data was processed with a 10 point running average for smoothing as well.

5.5 DATA ACQUISITION - GASL TESTS and COLD FLOW TESTS

Data was acquired using a PC equipped with an 80286 micro-processor. In addition, this computer was fitted with a Metrabyte DAS-16F A/D D/A expansion card. This card is capable of sampling 16 single ended or 8 differential channels. Two analog and two digital output signals are included as well. Temperature measurements were taken with a Metrabyte EXP16 multiplexing expansion card. This board requires one channel from the DAS-16F card. It has 16 multiplexed channels with an electronic ice point and instrumentation amplifier on the card.

A commercially available software package was used to control the DAS16-F/EXP16 data acquisition cards. This software, LABTECH NOTEBOOK, has selectable channel gains and curve fits for thermocouple data. Calibrations can be directly entered to obtain engineering units in the output data files. This data acquisition system was used for the tests at the General Applied Science Labs and for the cold flow tests in the Virginia Tech Mach 2 free jet wind tunnel. A triggering system was enabled at the GASL tests so that the acquisition system could be activated during a specific event of a particular test. Data was recorded for 15 seconds at 100 Hz. For the cold supersonic flow tests, the data acquisition system was manually triggered with an acquisition period of 10 seconds at 100 Hz.

5.6 SIGNAL CONDITIONING - NASA ARC DCAF COMBUSTOR TESTS

Powerful signal conditioning amplifiers (Micro Measurements, Model 2310 and

2210) which are specifically designed for strain gage use were obtained for the tests at the NASA ARC DCAF combustor tests. These signal conditioners have some significant features including: adjustable calibrated gain (1 to 11000, Model 2310, and 1 to 3300, Model 2210), selectable bridge excitation from a few millivolts to 14 Vdc, high input impedance (over 100 megohms), a four cut-off frequency active filter (Butterworth, 2-pole), and automatic bridge completion and balancing. The use of these signal conditioners allowed optimization of the excitation voltage and on-line filtering so that digital filtering was not required as with the GASL and cold supersonic flow tests.

5.7 DATA ACQUISITION - NASA ARC DCAF COMBUSTOR TESTS

For the combustor tests conducted at the NASA Ames Research Center Direct Connect ArcJet Facility, the signal output from the skin friction balances was recorded by the main data acquisition system of the facility. The raw data are recorded by a PDP 11/34 computer. The data is compressed with a 10 point running average and then sent through a Micro VAX via data link to a PC environment. JHU/APL developed software reconfigures the data into time histories and provides a separate data group for the relevant skin friction data and temperatures. This data is then processed to produce skin friction coefficients. Typically, a test period is less than 120 seconds. Data are taken in what is called a "burst" mode for the entire run. This results in an acquisition rate of about 17 Hz.

5.8 SKIN FRICTION BALANCE CALIBRATION

The skin friction balances are calibrated by directly applying a force in the desired measurement axis. The balance is fixed in a vertical position which yields the desired calibration axis to be vertical. Weight standards are attached to the center of the floating head via a thin line and allowed to hang vertical (Fig. 5.4), insuring that the force is

applied in the desired direction. The balances are filled with the silicon oil and the floating head cooling system is operating while calibrating the instruments, although, it was found that if the cooling system was not on the calibration was not effected. The balance output was recorded with either the A/D expansion card in the PC or recorded manually with a digital voltmeter. For calibration data taken with the PC, samples were recorded at 100 Hz for one second and then averaged. Sample calibrations for the skin friction balances are shown in Figs. 5.5 through 5.8. Any error in the orthogonality of the axes is accounted for in the calibration by recording both the axial and transverse signals from each bridge. Transverse axis output was less than 5% of the axial output for all the balances of this study. A least squares regression was performed on the calibration data to obtain the linear calibration curves. Variance is on the order of 10^{-4}. Calibration of the transverse axis is obtained by simply rotating the entire skin friction balance 90° and repeating the above procedure.

An exception to the above procedure was encountered for the tests conducted during the first entry of the DCAF combustor series. Since it was required that the balances be screwed into the combustor wall, the orientation of the balance orthogonal axes in relation to the streamwise and cross-stream directions of the combustor flow is not known until the conducting of the tests because of the way in which threads are cut in the balance and the combustor. For this reason, the skin friction balance was configured in a full bridge which eliminates the possibility of a dual axis measurement, but at the same time increases the effectiveness of the temperature compensation by having the full bridge at one temperature. Calibrations for this balance were performed every 10°, thus resulting in 36 separate calibrated axes. This limited misalignment to a maximum of 5% between the streamwise direction of the combustor flow and a calibrated axis. An analysis to determine the error associated with this possible misalignment was conducted and is detailed in Appendix A. For the second DCAF combustor series entry, the lower housing (beam support piece) was redesigned so that the orthogonal axes of the

skin friction balances could be aligned with the streamwise and cross-stream directions of the combustor flow.

5.9 DATA REDUCTION

The parameter that is actually measured by the skin friction balance is a shear force over the area of the exposed part of the floating head. In order to normalize the shear force, a value of dynamic pressure at some point in the flow is required. For the tests conducted at the General Applied Science Lab., this value was provided by the major contractor for the tests, it is an estimate calculated with deduced combustor inlet flow variables.

For the tests conducted at Virginia Tech, the dynamic pressure at the boundary layer edge at the skin friction balance location was calculated in the following manner with measured free stream flow variables. The definition of the dynamic pressure of the free stream flow is defined as:

$$q = \frac{1}{2}\rho_\infty U_\infty^2 \tag{5.1}$$

Extending this to variables measured in the compressible flow, the following relation for a perfect gas is obtained :

$$q = \frac{\gamma}{2}P_\infty M_\infty^2 \tag{5.2}$$

In the above equation, the Mach number and gamma (1.4) are known and the static pressure is calculated from the measured total pressure with the following simple relation:

$$\frac{P_T}{P} = \left[1 + \frac{\gamma - 1}{2} M^2\right]^{\frac{\gamma}{\gamma-1}} \tag{5.3}$$

In order to obtain C_f, the measured shear values are normalized with the dynamic pressure. The result is :

$$C_f = \frac{\tau_w}{\frac{1}{2}\rho_\infty U_\infty^2} \tag{5.4}$$

For the tests conducted in the DCAF combustor, the value of dynamic pressure used to calculate the skin friction coefficient was calculated in a slightly more involved manner. Because the facility nozzle flow chemistry is in equilibrium up to the nozzle throat, and equilibrium calculations can be performed to deduce the conditions at the throat. This was done using an equilibrium cycle analysis code called RJPA (Ref. 35) which uses JANNAF data to calculate conditions. Using a deduced total enthalpy supplied by JHU/APL, the stagnation pressure iterated on in the code and the resulting set of properties for the settling chamber (arc heater) are expanded to Mach 1 (the nozzle throat) until the calculated mass flow at the throat reaches the measured value. The stagnation properties from this analysis are then supplied to a finite rate chemistry quasi-1D nozzle analysis code (MIX1D, Ref. 36) to calculate properties throughout the combustor supply nozzle for the known geometric area distribution. This calculation provides a nozzle exit (combustor inlet) density and velocity to calculate a reference dynamic pressure to normalize measured shear values.

CHAPTER SIX

RESULTS AND DISCUSSION

6.1 COLD SUPERSONIC FLOW RESULTS

The first tests for this type of skin friction balance were conducted in a cold Mach 3.0 flow in the large Virginia Tech supersonic wind tunnel. These tests were conducted at Mach 3.0 with total pressure of 95 psia and total temperature of 285 K and Reynolds number per meter of $5x10^7$. Output from this test is shown in Fig. 6.1. This result indicates that this type of skin friction balance has excellent time response, apparent by its following of the start of the supersonic tunnel on the left of the figure and unstart of the supersonic tunnel on the right of the figure. Output reached a steady constant value which translates into a skin friction coefficient by way of the calibration and dynamic pressure of the flow to $C_f = 0.0015$. A calculation of the skin friction coefficient based on the boundary layer thickness at this balance location from a nanoshadowgraph indicates a skin friction coefficient of $C_f = 0.0014$. This analytical result was obtained by first measuring the boundary layer thickness at the measurement location from a shadowgraph[37]. Then the empirical Schultz-Grunow[38] (Eqn. 6-1) relation for the skin friction coefficient in wall-bounded incompressible turbulent boundary layers is used to get an initial estimate of the skin friction coefficient. This is valid up to approximately $Re_x = 10^7$.

$$C_f = 0.0456(Re_\delta)^{-0.25} \quad (6\text{-}1)$$

The flow of interest is of course a compressible flow, therefore this incompressible C_f estimate is improved with a C_f incompressible to compressible relation. This comparison for a given Reynolds number is based on experimental data and calculations (see Ref 37).

A series of cold supersonic flow (Mach 2) tests were conducted with the skin friction balance designed for the first set of tests conducted at NASA Ames Research Center Direct Connect Arcjet Facility combustor. In this test series, a total of twenty test runs were conducted in as near identical flow conditions as possible in the Virginia Tech Mach 2.0 Free Jet Tunnel to establish the repeatability of the balance. Total pressure of the airflow for these tests is 108 psia (745 kPa) and total temperature is ambient (approximately 285 K). Pressure at the nozzle exit is atmospheric which gives a dynamic pressure of 2.43 atm (250 kPa) and Reynolds number per meter is $1x10^7$. This value was used to normalize all the test data. Also, even though there is not a high heat flux to the wall (actually the wall is cooled by the flow) for these tests, the floating head cooling system is operating during all test runs with a flow rate obtained from tap water (100 psi, 690 kPa). The temperature of the strain gages in the skin friction balance was monitored for all test runs as well. The strain gage temperature was not affected by the airflow for these tests. Temperature change of less than 0.5 Kelvin was typical and is within the accuracy of the thermocouple. Figure 6.2 shows a typical output from the balance for these cold flow tests. Table 6-1 summarizes these results. Regarding Fig. 6.2, the tunnel valve is opened manually at about 2.5 seconds. Response to the starting shock and vibration is evident at the test start. A nearly constant output is recorded from 3 seconds until the tunnel is shut down at 9 seconds. As with the test in the Mach 3.0 cold supersonic flow, the skin friction balance has no trouble following the starting and stopping of the wind tunnel. The skin friction balance also returns to a null output after

the tunnel valve is shut-off, indicating for these tests at least that there are insignificant thermal effects on the strain gages in the measurement. A mean skin friction coefficient of 0.0020 was measured for all the test runs with maximum deviation from the mean of 8%. This compares to analytical estimates of the skin friction at 0.0019 based on the boundary layer thickness at these flow conditions. It is believed that results of this accuracy can be obtained with this design in high-speed high-heat-flux flows.

Run No.	τ_w	C_{fx}	C_{fy}
001	503.3	0.0019	0.0005
002	506.7	0.0020	0.0005
003	500.0	0.0019	0.0005
004	476.1	0.0019	0.0005
005	557.7	0.0022	0.0006
006	511.3	0.0020	0.0005
007	588.4	0.0023	0.0006
008	564.5	0.0022	0.0006
009	547.5	0.0022	0.0005
010	499.9	0.0019	0.0005
011	561.1	0.0022	0.0006
012	509.5	0.0020	0.0005
013	514.7	0.0020	0.0005
014	557.7	0.0022	0.0006
015	490.2	0.0019	0.0005
016	503.3	0.0019	0.0005
017	548.4	0.0022	0.0006
018	506.4	0.0020	0.0005
019	487.8	0.0019	0.0005
020	540.1	0.0022	0.0006

TABLE 6-1 -- Summary of Virginia Tech Mach 2.0 Free Jet Tunnel Tests

6.2 GASL TEST RESULTS

The skin friction balance designed for the tests conducted at the General Applied Science Lab. was installed into the constant area section of the combustion chamber with some success achieved for this first hot flow test of this actively cooled head design. Combustor entrance Mach number is 3.3 for these tests with total pressure of 800 psia (5500 kPa) and total temperature of 4000 °R (2222 K). The dynamic pressure used to normalize these results was based on the combustor inlet properties as is typical for these tests since it is not trivial to obtain local flow conditions. This value was set at 7800 psf (7.7 GPa). Figure 6.3 illustrates the output from GASL test run 602. An average voltage output was taken over the range during which fuel was being injected (approximately 9-11 seconds on the plot) and a skin friction coefficient was calculated to be C_f = 0.0033. Table 6-2 contains the results from another test run as well as relevant flow conditions. The mean flow conditions for these fueled tests are essentially equivalent, but the specific fuel condition (i.e. injection geometry and fuel equivalence ratio) are not. This may or may not account for the 12% difference in the two values. The uncertainty in the measurement approaches this 12% value as well.

Test Run Number	GASL Test 601	GASL Test 602
Mach No.	3.3	3.3
P_t (psia)	800	800
T_t (R)	4000	4000
V (ft/sec)	6300	6300
q (psf)	7800	7800
τ_w (psf)	23.0	26.1
C_f	0.0029	0.0033

TABLE 6-2 -- Summary of the GASL Test Results

6.3 NASA AMES RESEARCH CENTER DCAF RESULTS

Skin Friction during the first test series conducted at the NASA ARC DCAF combustor was measured at the location indicated on Fig. 6.4 as position 5. Fuel was injected through a tangential slot with the injectant type being indicated as being either hydrogen or nitrogen. The balance was located 60 inches downstream of the combustor model entrance on the side (bottom) wall. This places the balance 6 inches downstream of the entrance to the first of two diverging sections, this one being three degrees. Skin friction coefficients were obtained by normalizing the measured shear values with a calculated dynamic pressure at the fuel injector plane as was described in Chapter 4. This calculation was done with a finite-rate chemistry quasi-1D nozzle calculation with equilibrium composition at the nozzle entrance. Figures 6.5 - 6.12 contain actual output of the skin friction balance for all the tests conducted during the first entry. Since flow conditions are dependent on the power supplied to the arc heater, it would be expected to see skin friction balance output related to it. Figure 6.12 shows balance output for DCAF Run 1031, and Figure 6.13 shows arc heater power data for the same run. At an elapsed time of 20 seconds, arc power begins to ramp up as does the wall shear indicated by the balance. At 40 seconds when arc power (and flow conditions) is constant, a constant shear force is indicated, as well. Shear force rises sharply at 60 seconds when hydrogen fuel is injected and returns to a null value when the tunnel is shut down at 70 seconds as indicated by the arc heater power plot. This general trend is evident in all the data presented here. Average shear values were calculated over the range where flow conditions were constant. This was determined from arc power data.

Table 6-3 presents a summary of the data collected from a total of nine test runs during the first test series. Relevant flow conditions including total pressure, total temperature, enthalpy, and equivalent flight Mach number are listed. Shear values were normalized by the indicated flow dynamic pressure.

DCAF Run No.	1018	1022	1023	1026 -3	1026 -4	1028	1030	1031
P_t (psia)	276	192	383	365	365	344	391	324
T_t (°R)	5881	5767	6163	7812	7721	8073	8103	8387
H_t (BTU/lb_m)	1710	1670	1835	2890	2825	3091	3082	3327
M_∞	9.3	9.1	9.5	12.0	11.9	12.0	12.0	12.5
Fuel	-	N_2	H_2	-	-	-	-	H_2
q (psf)	4050	2805	5613	5356	5371	5059	5745	4750
τ_w (psf)	17.8	8.8	18.5	21.5	28.6	14.7	31.3	16.0
C_f	.0044	.0031	.0033	.0040	.0053	.0029	.0054	.0034

TABLE 6-3 -- Results from NASA ARC DCAF Combustor Tests, 1st entry

Since the semiconductor strain gages used in the balance for the first test series are very temperature sensitive, the effectiveness of the spray cooling to maintain the strain gages at a constant temperature is important to the uncertainty of the measurement. Although some temperature compensation techniques were implemented, uncertainty levels were elevated as a result of marginal cooling. Figure 6.14 shows the local temperature of the strain gages for DCAF1031. Figures 6.15 through 6.19 show the strain gage temperature for the remainder of the test runs. It should be noted that the cooling of the strain gages is quite good considering that the wall temperature of the combustor only 2 to 3 inches away is at or above 800 °R, but this small temperature change is

enough to raise uncertainty in the measurement to about 20%.

A total of three skin friction balances were available for the second test series with improved self-temperature compensating strain gages in each. Measurements were made in the DCAF combustor in positions 1, 2, or 4 as indicated in Fig. 6.3. This places the balances either 5, 10, or 20 inches downstream of the tangential injector location. For test runs DCAF2010 and DCAF2011, fuel was injected through an array of circular normal injectors located a few inches upstream of the tangential injector location. The tangential injectors were blocked off for these tests resulting in approximately a 0.187 inch step. For test runs 2027 and 2028, fuel was injected through ramped injectors at or about the same position as the normal injectors. Figures 6.20 through 6.29 present the results for these tests, and Table 6-4 summarizes the tests with shear values, skin friction coefficients, and other relevant flow parameters. These results indicate low values of shear relative to those taken at position 5 (Fig. 6.3, Table 6-3). This may be due, in part, to the presence of the upstream step from the tangential slot injector.

Figures 6.30 and 6.31 illustrate the effectiveness of the internal floating head cooling system. Figure 6.31 shows temperatures for the floating head, inner combustor wall, and outer combustor wall near the skin friction balance. When fuel is injected between 90 and 100 seconds of elapsed run time, the inner combustor wall and the floating head differ by only 15°R which is less than 5%. The predicted combustor wall temperature value in the heat transfer analysis (775°R) agrees with the measured value (785°R) very well. Figures 6.30 and 6.31 also show the temperature at the location of the strain gages on the quartz cantilever beam. The combustor spray cooling and the improvements to the balance cooling helped to keep bridge temperature to within 4°R from start to finish of a test. Given this fact and the improved self-temperature compensation of the strain gages, the uncertainty in these later measurements is under 15%. A more detailed discussion of these uncertainties is presented in Appendix A.

DCAF Run No.	2010	2011	2027	2028
H_t (BTU/lb_m)	2838	2270	*	*
M_∞	12	10	*	*
Fuel	H_2	H_2	N_2	H_2
q (psf)	4050	2805	5000	5000
Balance 1 τ_w (psf)	4.7	2.4	10.2	10.2
Balance 2 τ_w (psf)	7.4	3.0	-	-
Balance 3 τ_w (psf)	-	2.5	17.7	-
Balance 1 C_f	.0009	.0005	.0020	.0020
Balance 2 C_f	.0015	.0060	-	-
Balance 3 C_f	-	-	.0035	-

* unavailable

TABLE 6-4 -- Summary of NASA ARC DCAF Tests, 2^{cd} entry

CHAPTER SEVEN

CONCLUSIONS AND RECOMMENDATIONS

7.1 CONCLUSIONS

The major goal of designing, constructing, and implementing an instrument to accurately measure wall shear (skin friction) in high enthalpy supersonic flows was achieved. A new technique to match the temperature of the shear sensing element to the temperature of the surrounding chamber walls was successfully implemented. This active internal cooling technique was shown to be effective in both numerical calculations and experimental measurement. A key to this design is that a single internal cooling fluid flow rate is required to match these temperatures over the range of wall heat flux tested (0.5 - 4.0 BTU/in^2/sec).

Results of the tests showed accurate measurements can be obtained with a non-nulling cantilever skin friction balance with active cooling of the floating head. Results from both high and low heat flux supersonic flows were obtained. The tests in the cold supersonic flow showed that uncertainty in the shear measurement to under 8% is achievable with this type of skin friction balance. The mean result obtained from the cold flow free jet tests agreed with an analytical estimate of the skin friction based on the measured boundary layer thickness to 5%. Results were obtained in the GASL combustor and in two separate entries in the NASA ARC DCAF combustor. GASL results showed moderate values of skin friction in the constant area section of the combustor. Primary emphasis was placed on obtaining results from the DCAF combustor.

The effectiveness of the combustor model spray cooling in the first DCAF combustor entry in providing a constant temperature at the strain gage location in the balance proved to be marginal. The spray water that hits the combustor wall and then the skin friction balance was not at a constant temperature during a test duration, ultimately resulting in higher uncertainty than was predicted from the cold flow tests (up to 20%). During the second DCAF combustor entry this problem was corrected with improvements to the skin friction balance cooling system and by adding self-temperature compensating strain gages. The combustor model spray cooling nozzles were also redesigned in the area of the skin friction balances to provide more efficient cooling to the balance housing. These improvements reduced the uncertainty in the measurement to under 15% for these later tests.

7.2 RECOMMENDATIONS

In future tests with skin friction balances of this type design, several areas of the design could be improved upon to reduce uncertainty in the measurement and improve the integrity of the balance. First, the addition of a larger floating head area would increase the amount of mechanical strain in the cantilever thus reducing the percentage of the total strain measurement resulting from temperature effects. Second, although the selection of quartz as the beam element provided the proper heat transfer properties, it rendered assembly of the skin friction balance very difficult. At times this difficulty proved to be a hindrance to the structural integrity of the instrument. Selection of a different material may be a good option, possibly a cantilever beam composed of more than one material would be wise. For instance, the beam ends could be constructed of materials which can be fastened to the floating head and beam holder with ease, and then only a portion of the beam would be constructed with a low thermal conductivity material. Third, effort should be spent in the area of the strain gage configuration. The best thermal stability of the bridge circuit is obtained with a full bridge circuit on the

beam. This could be done for multiple axis measurements, possibly even with custom built semi-conductor strain gages designed with the equations developed in Chapter 4. This would help to reduce uncertainty as well as raise the output from the bridge. Also, an effort should be made to better isolate the strain gages from the damping/pressure gradient fluid. This fluid is slightly reactive and over a period of time it contaminates the electrical circuitry of the strain gage leads and solder connections. Fourth, the internal floating head cooling system would be better served if it were a separate self-contained system.

BIBLIOGRAPHY

1. Nitsche, W., Haberland, C., and Thunker, R., "Comparative Investigations of the Friction Drag Measuring Techniques in Experimental Aerodynamics", ICAS-84-2.4.1, 14th ICAS Congress, Sept. 1984.

2. Bruno, J. R., "Balance For Measuring Skin Friction in the Presence of Heat Transfer," NOLTR 69-56, June 1969.

3. Gador, A. Y., and Louis, J. F., "High Temperature Heat Transfer and Skin Friction Measurements in Turbulent Flows Along Highly Cooled Walls," AIAA 86-1235, AIAA/ASME 4th Joint Thermophysics and Heat Transfer Conference, June 1986.

4. Owen, F. K., and Bellhouse, B. J., "Skin Friction Measurements at Supersonic Speeds," *AIAA JOURNAL*, Vol. 8, July 1970, pp. 1358-1360.

5. Owen, F. K., and Johnson, D. A., "Separated Skin Friction Measurement - Source of Error, an Assessment, and Elimination, AIAA 80-1409, AIAA 13th Fluid and Plasma Dynamics Conference, July 1980.

6. Bellhouse, B. J., and Schultz, B. L., "The Measurement of Skin Friction in Supersonic Flow by Means of Heated Thin Film Gages," Aeronautical Research Council, ARC R&M 3490, 1968.

7. Mabey, D. G., and Gaudey, L., "Performance of Small Skin Friction Balances at Supersonic Speeds," *JOURNAL OF AIRCRAFT*, Vol. 12, 1975, pp. 819-825.

8. Seto J., and Hornung H. G.,"Internally Mounted Thin-Liquid-Film Skin Friction Meter-Comparison with Floating Element Method and Without Pressure Gradient," AIAA 91-0060, 29th Aerospace Sciences Meeting, Jan. 1991.

9. Preston, J. H., "The Determination of Turbulent Skin Friction by Means of Pitot Tubes," J. Roy. Aero. Soc., Vol. 58 N0518, pp. 809-831, 1954.

10. Vakili, A. D., and Wu, J. M., "Wall Shear Stress Measurements Using a New Transducer," AIAA 86-1092, AIAA/ASME 4th Fluid Mechanics and Plasma Dynamics and Lasers Conference," May 1986.

11. Winter, K. G., "An Outline of the Techniques Available for the Measurement of Skin Friction in Turbulent Boundary Layers", *Progress in Aerospace Sciences*, Vol. 18, 1977, pp. 1-57.

12. Roensch, R. L., and Cadwell, J. D., "Direct Measurements of Skin Friction in a High Reynolds Number Supersonic Blowdown Wind Tunnel", Douglas Paper 1728, Douglas Aircraft Company.

13. Allen, J. M., "Systematic Study of Error Sources in Supersonic Skin-Friction Balance Measurements", NASA-TN-D-8291, Oct. 1976.

14. Allen, J. M., "Improved Sensing Element for Skin-Friction Balance Measurements", *AIAA Journal*, Vol. 18, Nov. 1980, pp. 1342-1345.

15. Voisinet, L. P., "Combined Influence of Roughness and Mass Transfer on Turbulent Skin Friction at Mach 2.9", AIAA 79-0003, 17th Aerospace Sciences Meeting, Jan. 1979.

16. Schetz, J. A., and Nerney, B., "Turbulent Boundary Layer with Injection and Surface Roughness", *AIAA Journal,* Vol. 15, Sept. 1977, pp. 1268-1274.

17. DeTurris, D. J., Hellbaum, R. F., and Schetz, J. A., "Direct Measurements of Skin Friction in a Scramjet Combustor", AIAA 90-2342, 26th Joint Propulsion Conference, July 1990.

18. Voisinet, L. P., "Temperature Step Effects on Drag Measurement of Skin Friction Drag," AIAA 78-0779, 1978.

19. Westkaemper, J. C., "Step Temperature Effects on Direct Measurement of Drag," AIAA Journal, Vol. 1, No. 7, July 1963, pp. 1708-1710.

20. Chadwick, K. M., DeTurris, D. J., Schetz, J. A., "Direct Measurement of Skin Friction in Supersonic Combustion Flow Fields," ASME 92-GT-320, International Gas Turbine and Aeroengine Congress and Exposition, June 1992.

21. Frei, D., and Thomann, H., "Direct Measurement of Skin Friction in Turbulent Boundary Layers with a Strong Adverse Pressure Gradient," *Journal of Fluid Mechanics*, Vol. 101, 1908, pp. 79-95.

22. Hirt, F., Zurfluh, U., and Thomann, H., "Skin Friction Balances for Large Pressure Gradients," *Experiments in Fluids*, Vol. 4, 1986, pp. 296-300.

23. Kulite Semiconductor Products, "Kulite Semiconductor Strain Gage Manual", Leonia NJ.

24. Pantankar, S. V., *Computation of Conduction and Flow Duct Heat Transfer*, Inovative Research, Inc., Maple Grove MN, 1991.

25. Pantankar, S. V., "A Calculation Procedure for Two-Dimensional Elliptic Situations," Numerical Heat Transfer, Vol. 4, 1981, p. 409.

26. Settari, A. and Azziz, K., "A Generalization of the Additive Correction Methods for Iterative Solution Matrix Equations," SIAM Journal of Numerical Analysis, Vol. 10, p. 506.

27. Anderson, D. A., Tannehill, J. C., Pletcher, R. H., *Computatinal Fluid Mechanics and Heat Transfer,* McGraw-Hill, New York, 1984.

28. Ozisik, M. N., *Heat Transfer : A Basic Approach*, McGraw-Hill, Inc., 1885.

29. Holman, J. P., *Heat Transfer*, Fifth Edition, McGraw-Hill Book Company, New York, 1981.

30. Rao, S. S., *Mechanical Vibrations*, Addison-Wesley Publishing Company, Reading MA, 1986.

31. Applied Physics Laboratory, Staff, "Final Test Plan for ARC Tunnel Direct-Connect Combustor Tests, GWP 50," December 1991.

32. Applied Physics Laboratory, Staff, "Final Report for ARC Tunnel Direct-Connect Combustor Tests, GWP 50," June 1992.

33. Applied Physics Laboratory, Staff, "Final Test Plan for ARC Tunnel Direct Connect Tests, GWP 107a," July 1992.

34. Horowitz, P., Hill, W., *The Art of Electronics*, Cambridge University Press, Cambridge, 1980.

35. Pandolfini, P. P., Freidman, M. A., "Instructions for Using Ramjet Performance Analysis (RJPA),"JHU/APL-AL-92-P175, Johns Hopkins Applied Physics Laboratory, Laurel MD, 1992.

36. Kee, R. J., Miller, J. A., Jefferson, T. H., "CHEMKIN : A General Purpose, Problem Independent, Transportable, Fortran Chemical Kinetics Code Package," SAND80-8003, Sandia, Albuquerque NM, 1980.

37. Mills, J. R., "A Mach 1.95 Free-Jet Facility For Experimental Investigation of Injectant Flow Patterns," MS Thesis, Virginia Tech, October 1991.

38. Schetz, J. A., "Foundations of Boundary Layer Theory for Momentum, Heat, and Mass Transfer," Prentice Hall, Englewood Cliffs NJ, 1984.

39. Measurements Group Tech Note, "Optimizing Strain Gage Excitation Levels", TN - 502, 1979.

40. Measurements Group Tech Note, "Errors Due to Wheatstone Bridge Nonlinearity", TN - 507, 1982.

41. Measurements Group Tech Note, "Strain Gage Thermal Output and Gage Factor Variation with Temperature", TN-504-1, 1992.

APPENDIX A

UNCERTAINTY ANALYSIS

A.1 CALIBRATION UNCERTAINTY

Uncertainty in the skin friction measurement due to calibration has the potential to have a significant effect, but with prudent experimental technique it can be virtually eliminated. A calibration must be performed at a constant temperature to insure an insignificant amount of drift in the bridge from thermal effects is null. Any change in temperature will have an effect on bridge output dependent on the effectiveness of the temperature compensation techniques. Temperature change for calibrations conducted for the balances of this study were smaller than 0.1 K. In the load range that these skin friction balances are tested, calibration curves are linear. Variance on the order of 10^{-5} to 10^{-7} is typical. the repeatability of a given calibration point was observed to be between 0.1% and 0.3%. Current calibrations are always used to reduce data from a test. Calibrations are also conducted with the same instrumentation and cabling that will be used during a particular test to eliminate uncertainty from amplifiers, filters and lead wires. Temperature sensitivity of the amplifiers is published at 1 microvolt per °C.

The skin friction balance design for the first set of DCAF combustor tests presented a unique difficulty with calibration. Since the balance was mounted into the combustor through a tapped hole, the alignment of the bridge axes is dependent on the cut of the threads in the hole. A calibration for every conceivable angle at which the balance axes could be aligned with the streamwise direction is not practical, therefore calibrations were performed

every 10° around the circumference of the balance. An analysis was performed to calculate the possible error from the balance being aligned between calibrated axes. By comparing two adjacent calibrations (i.e. 0° and 10°) an overall uncertainty from balance alignment between curves can easily be calculated by associating the predicted output from each at a single alignment angle. For example, assume that a constant force measurement was made with the bridge aligned at 5° from the 0° calibrated axis. Through trigonometric manipulation the calibration from either 0° or 10° can be used to reduce the data. Each calibration does not necessarily predict the same shear force. This indicates some uncertainty in the measurement. Since 5° is the largest possible misalignment from any calibrated axis, this uncertainty would represent the largest possible assuming a continuous linear distribution. An analysis for the balance designed for the DCAF tests showed this uncertainty to be 0.15% per degree of misalignment from a calibrated axis with the maximum being .75% at 5°.

A.2 REPEATABILITY

Repeatability represents the largest source of uncertainty in the measurement of skin friction next to thermal effects of the strain gages. Although static force measurement of these balances indicate repeatability to less than 0.5%, these instruments are required to take data in dynamic flows. A series of tests were conducted in the Virginia Tech Mach 2 free jet tunnel. The results of which were discussed in Chapter 6. The results of this test showed a spread of 8% from the mean shear value. Several things should be noted here, though. An attempt to keep airstream conditions at a constant was made but small variations in the flow properties most likely are represented by some part of this 8%. Also, there may be some actual unsteadiness in the wall shear even at steady flow conditions. This uncertainty would be reflected in the 8% as well.

A.3 STRAIN GAGE TEMPERATURE UNCERTAINTY

The error in the measurement that can be caused by temperature gradients at the strain gage location have potential to produce larger bridge output than the shear force itself. As was stated in Chapter 2, the temperature compensation techniques do not completely eliminate the effects of temperature on the bridge output, especially for the semi-conductor strain gage balances. Fortunately, some data was obtained from the DCAF test series with the semi-conductor strain gage based balance installed in the combustor with temperature changing in the strain gage location without a shear force on the floating head. This data is shown in Fig. 2.12. This showed a linear dependence on temperature, as was predicted in the analysis, of 6.5 millivolts of bridge output per degree Rankine. For DCAF test Run 1031, which is a hydrogen fueled test, the strain gages experienced an 8°R change from constant fuel on to pre-test tare value. This would result in an uncertainty in this particular test of 13%. The highest recorded change in temperature at the strain gage location was 12°R for DCAF test 1023. This would result in a maximum uncertainty of 15% based on the overall output of the bridge for that particular test.

A.4 OVERALL SUMMARY

Floating head geometric error sources were discussed in detail in Chapter 3. Significant error in the shear measurement is obtainable if the floating head is improperly aligned. In all the skin friction balances constructed for this study, great care was taken to insure proper alignment of the floating head. Maximum protrusion or recession is on the order of 0.0000 to 0.0002 inches. This result is an order of magnitude lower than what was measured by Allen to have any effect on the measurement independent of the boundary layer thickness on the floating head. The only source that can not be determined that could have an effect is that of a pressure gradient on the head. It has been shown though that these effects can be minimized by filling the balance with the incompressible liquid. It is the authors opinion that putting and uncertainty of 1% on these geometric concerns would be quite sufficient and most likely very conservative. Noise and vibration are dynamic sources

and would result in only fluctuation from the static response due to shear and not add any significant uncertainty to the measurement since these effects were filtered and averaged out in the processing of the data. In summing up the maximums of all the possible uncertainty sources a total uncertainty of approximately 22% is obtained. Two things should be noted here. First, with the exception of the DCAF 1023 test, uncertainty would be reduced to under 20% for the remainder of the tests. Second, the later skin friction balance designs utilized self-temperature compensating strain gages. Given that all other uncertainty concerns except the temperature effect are equivalent, this would lower the uncertainty of the measurement. Also, a maximum change in strain gage temperature of only 4°R was observed in these later tests because of improved cooling in the area of the strain gages. Given these facts, it is felt that uncertainty would be reduced to under 15% with a good possibility of actually being closer to 10%.

FIGURES

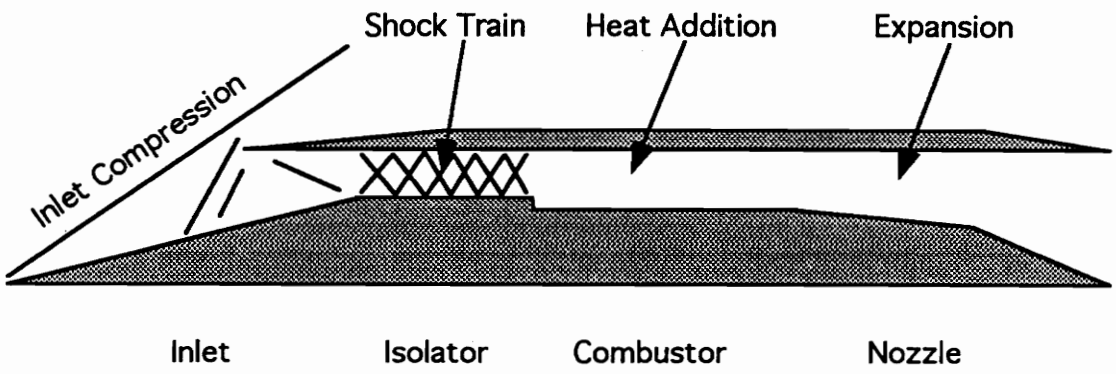

Figure 1.1 : SCRAMjet Schematic

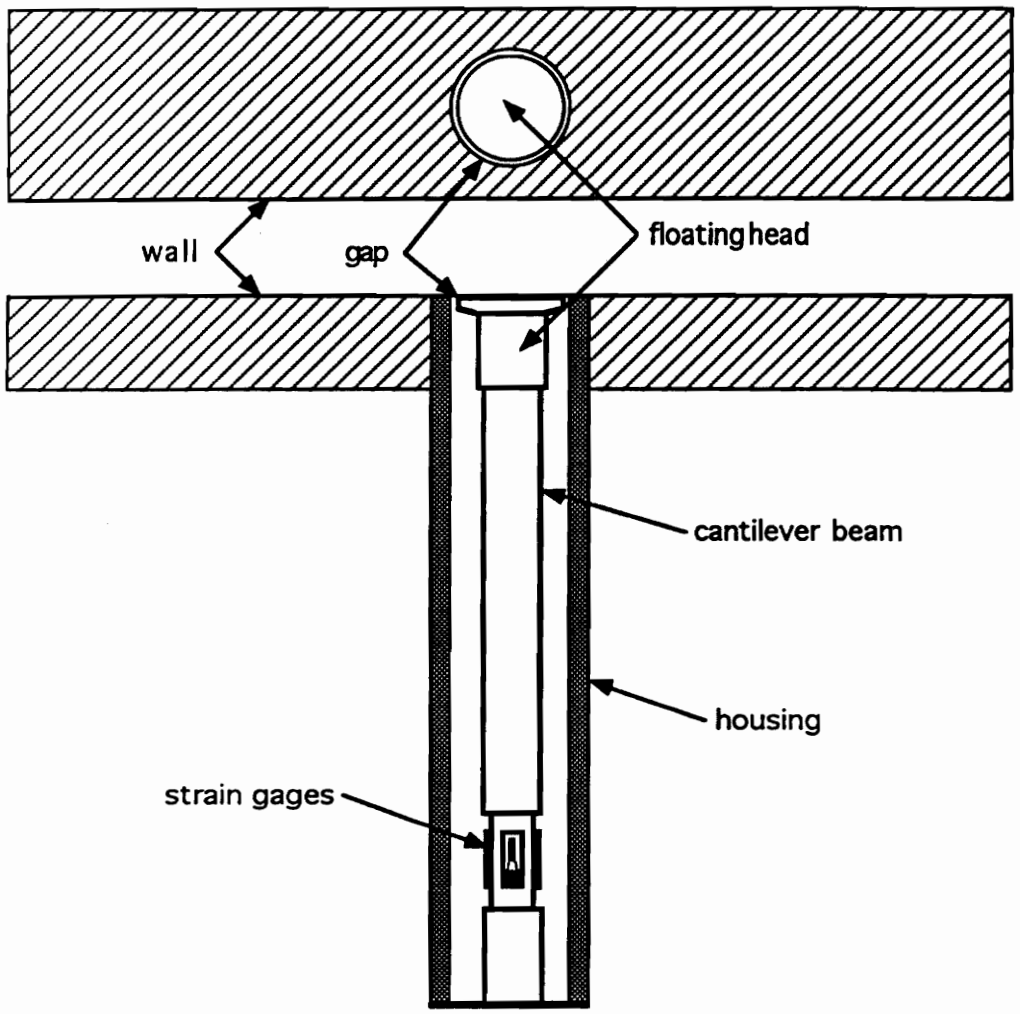

Figure 2.1 : Skin Friction Balance Schematic

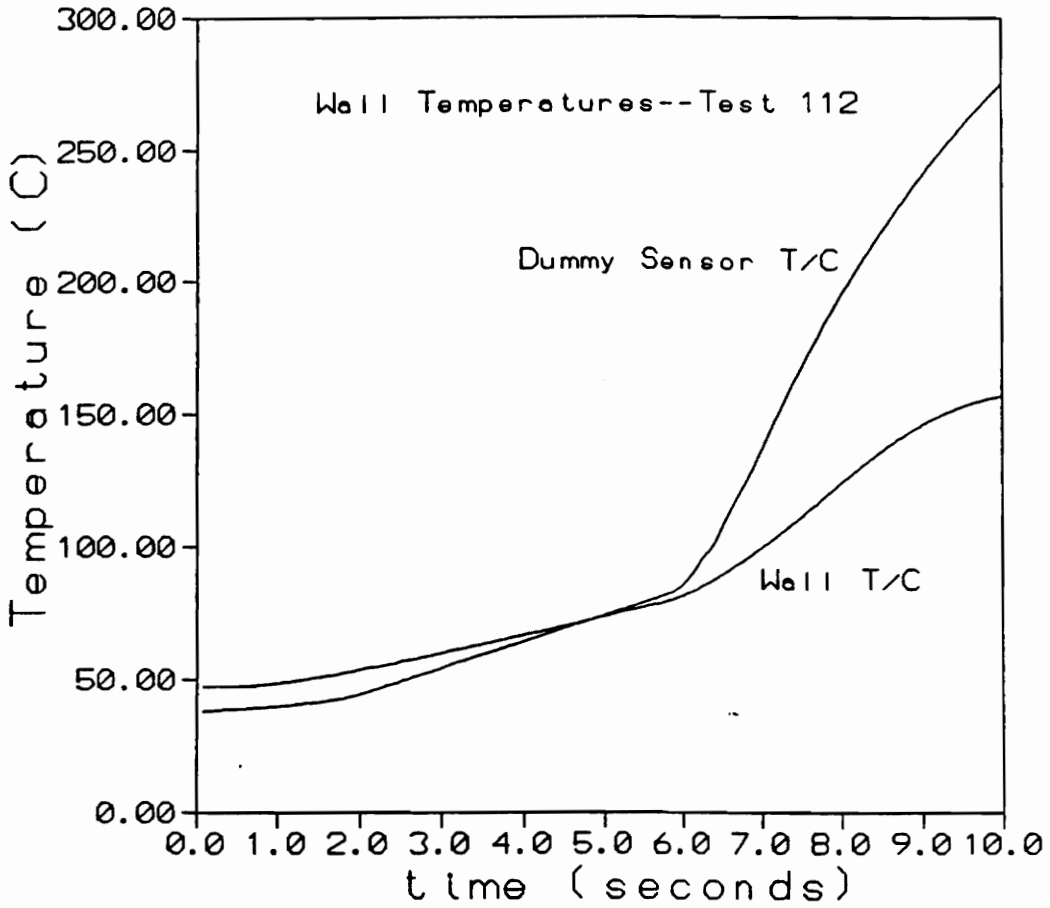

Figure 2.2 : Temperature Mismatch Between Floating Head and Near Wall

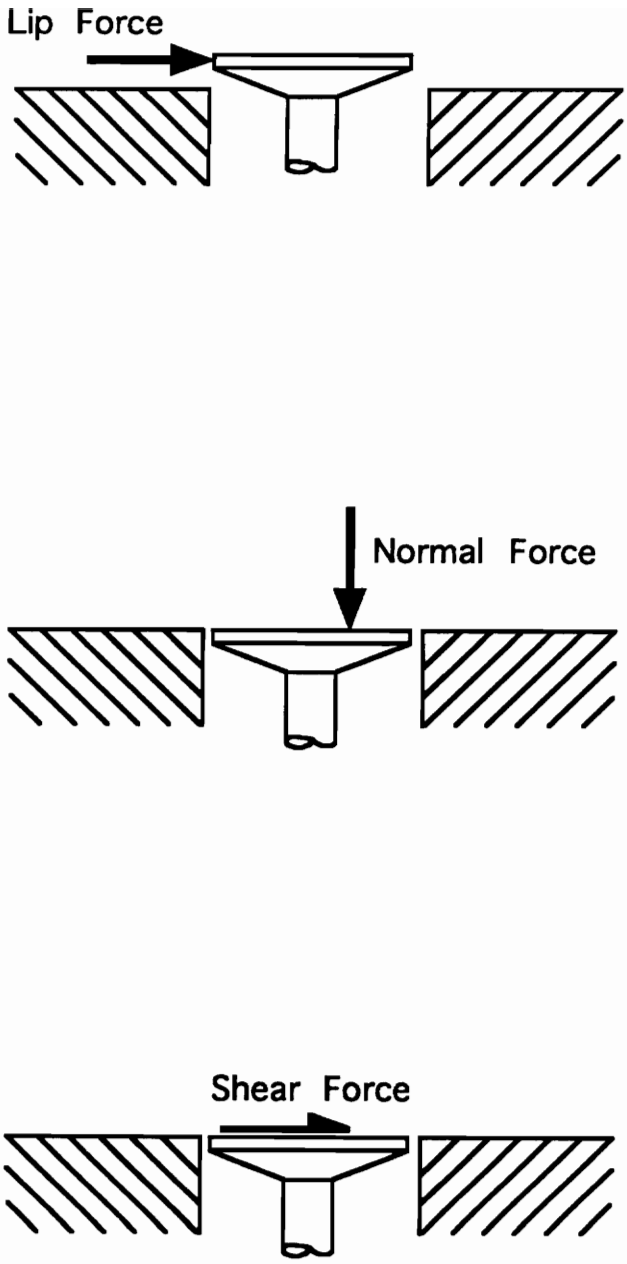

Figure 2.3 : Forces on a Skin Friction Balance Floating Head

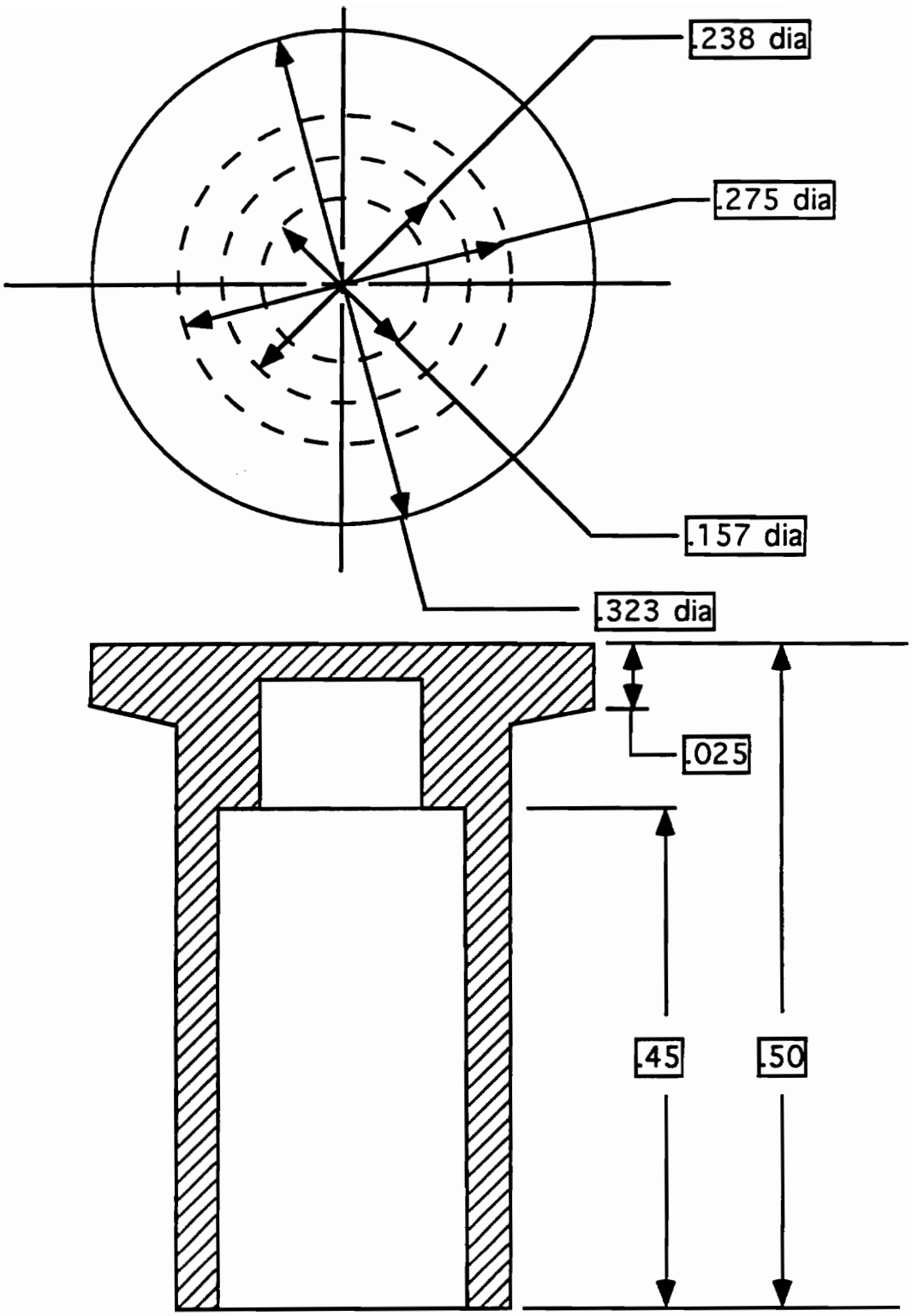

Figure 2.4 : Skin Friction Balance Floating Head Geometry

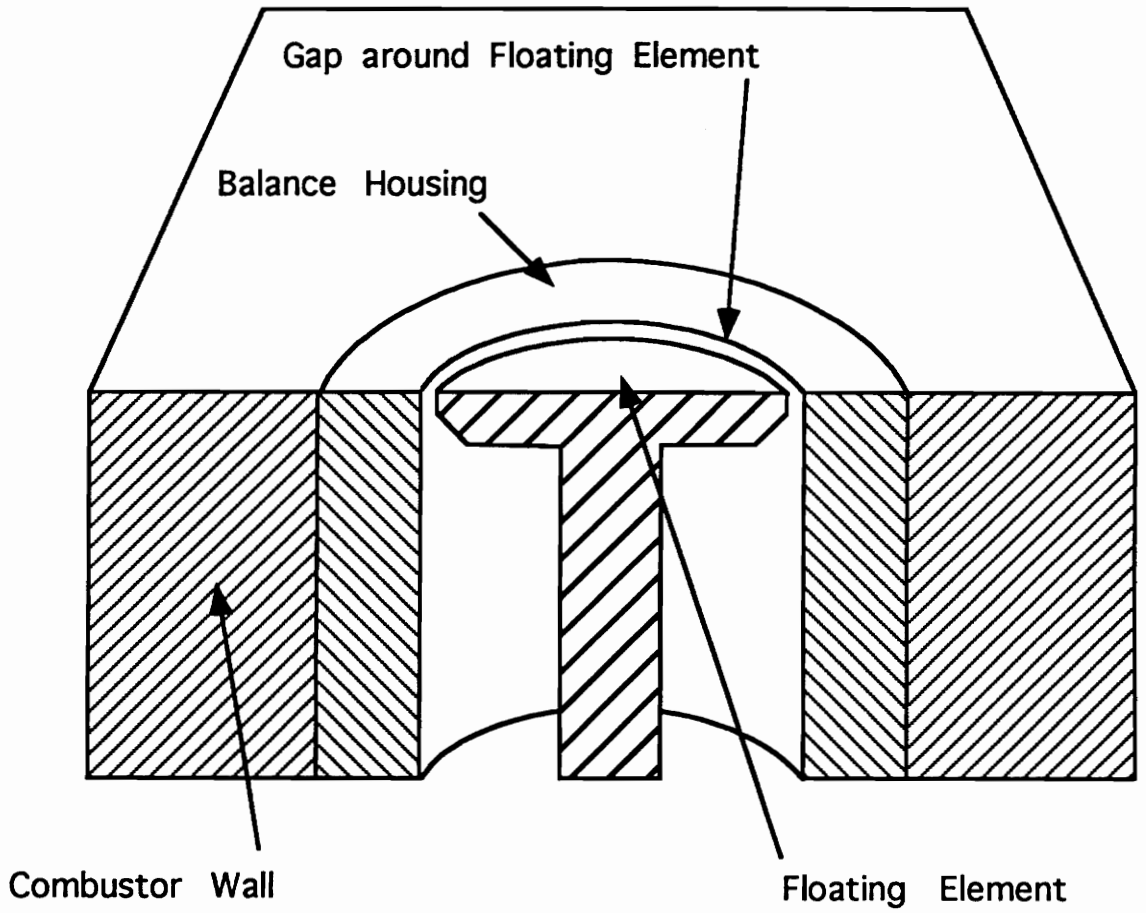

Figure 2.5 : Floating Head and Combustor Wall Schematic

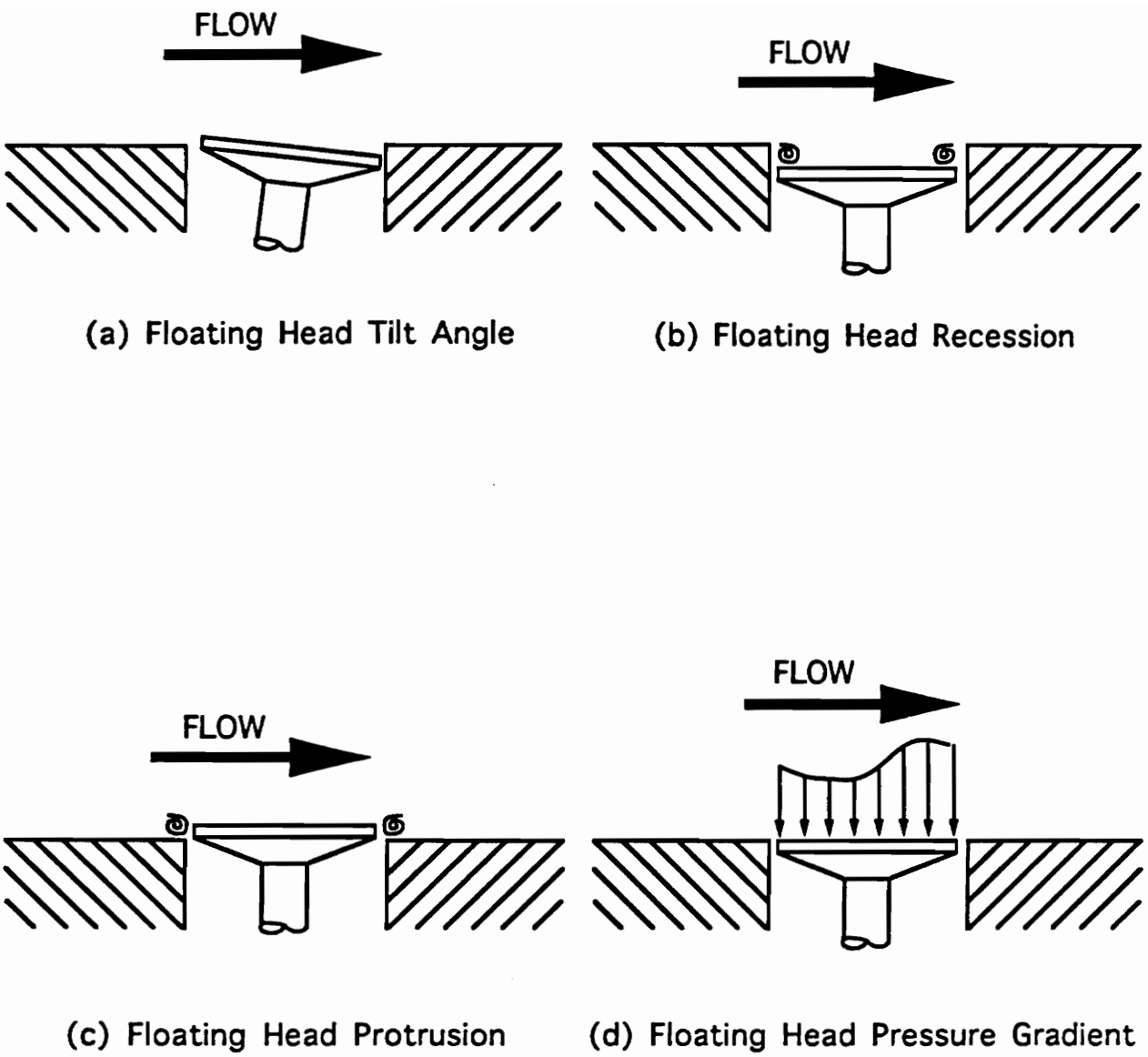

Figure 2.6 : Potential Error Sources of Floating Head Misalignment

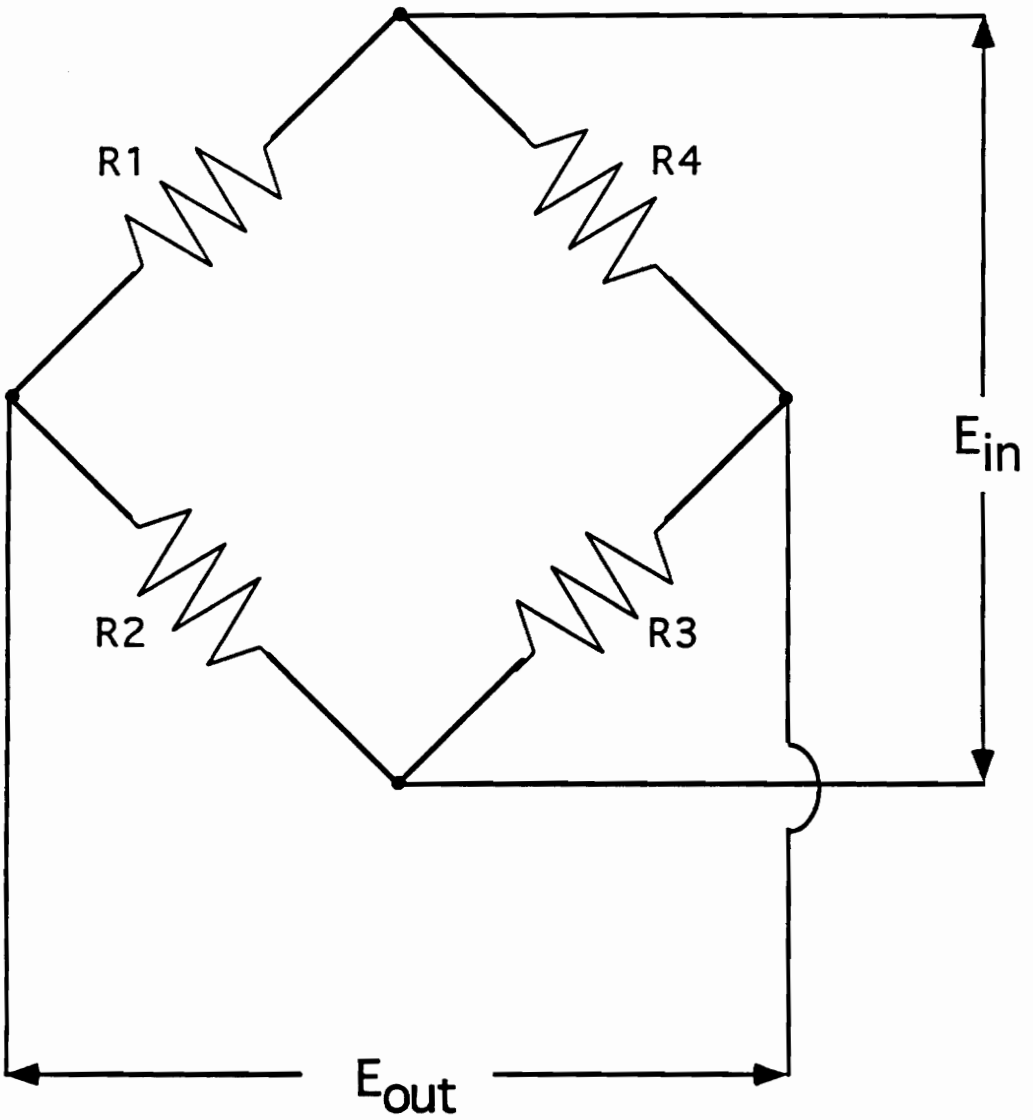

Figure 2.7 : Typical Wheatstone Bridge Circuit

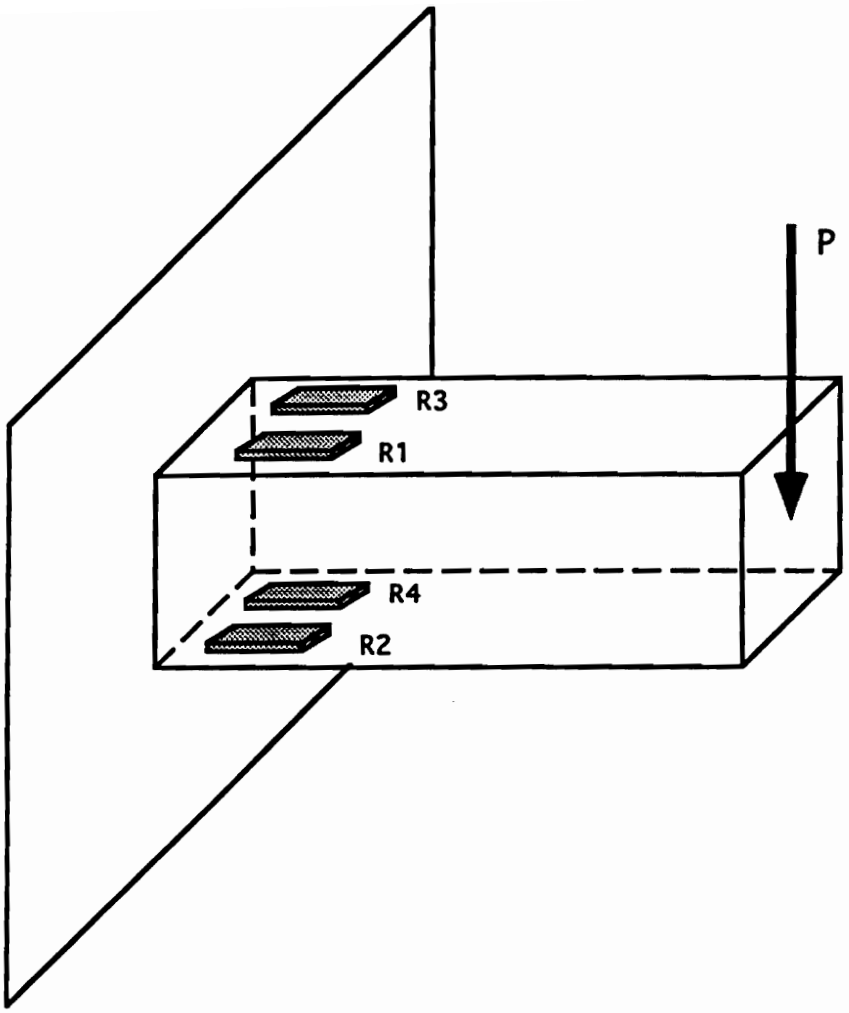

Figure 2.8 : Cantilever Beam Strain Gage Arrangement

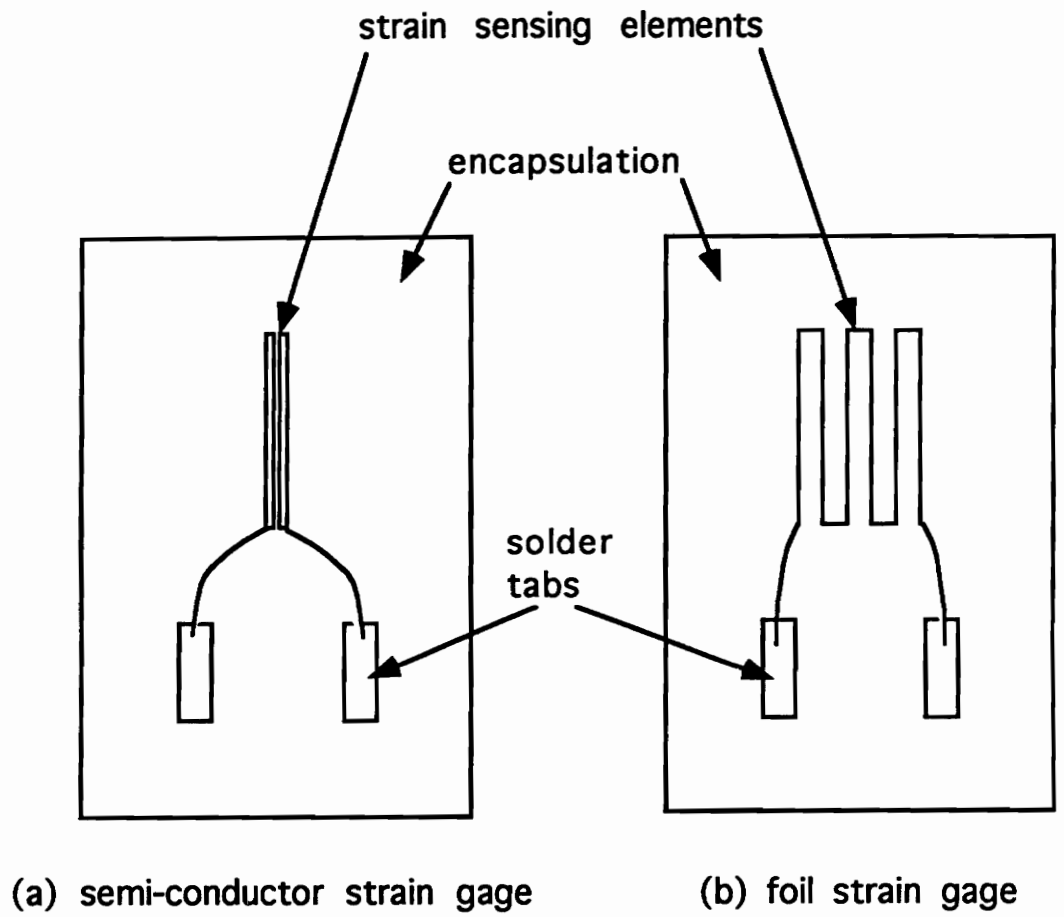

Figure 2.9 : Strain Gage Geometries

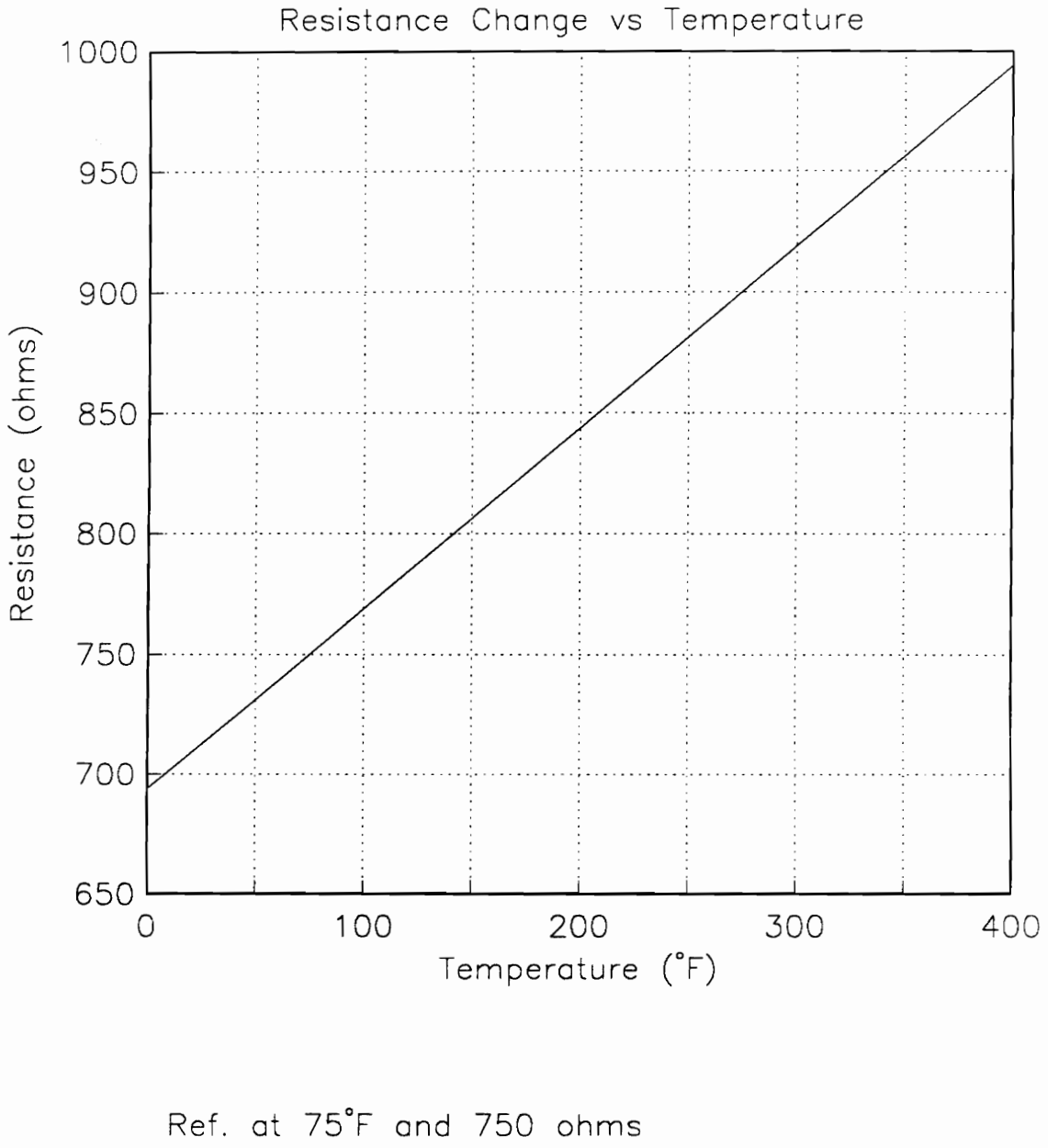

Figure 2.10 : Semi-conductor Strain Gage Resistance Temperature Effect

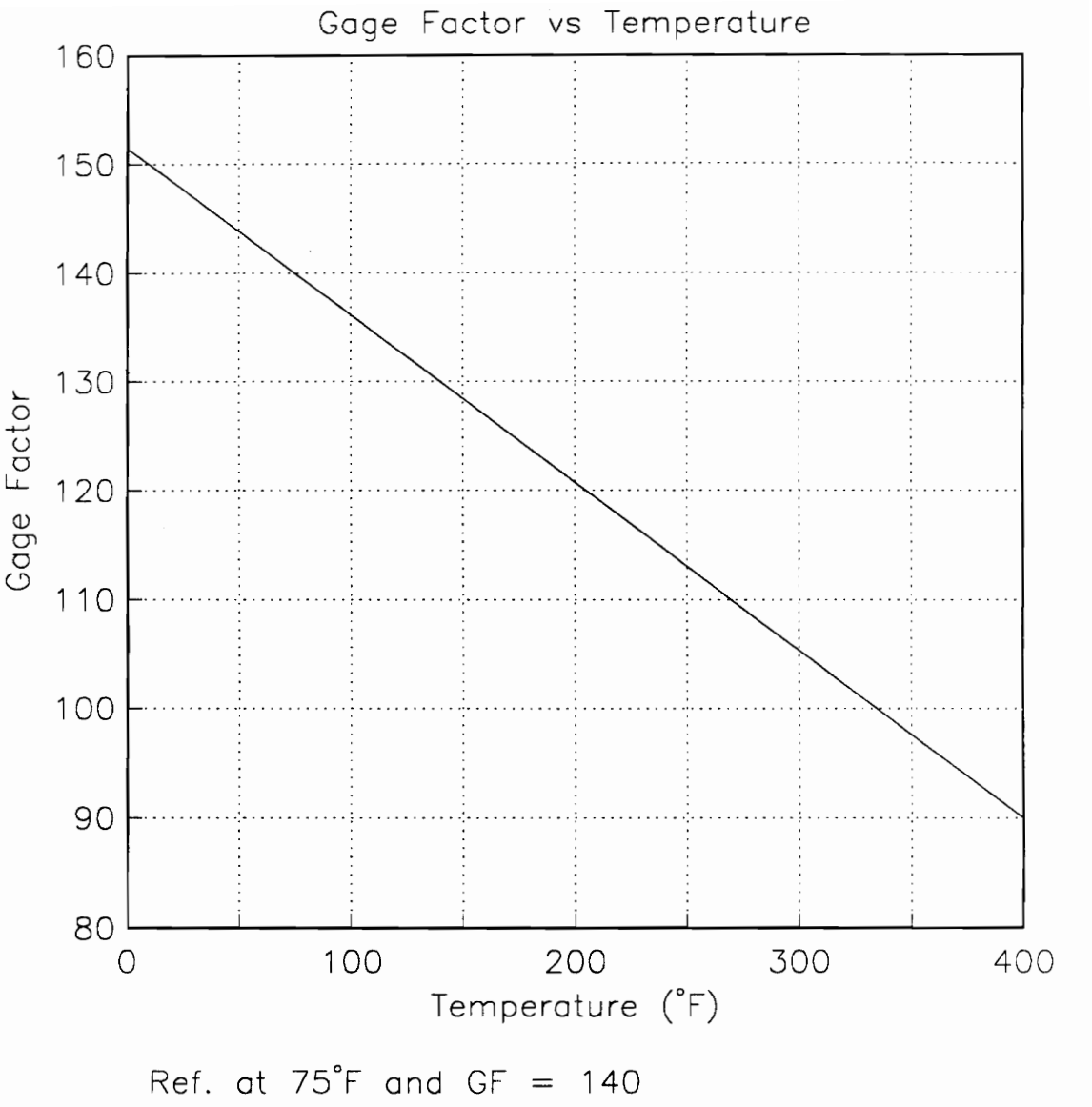

Figure 2.11 : Semi-conductor Strain Gage Sensitivity Temperature Effect

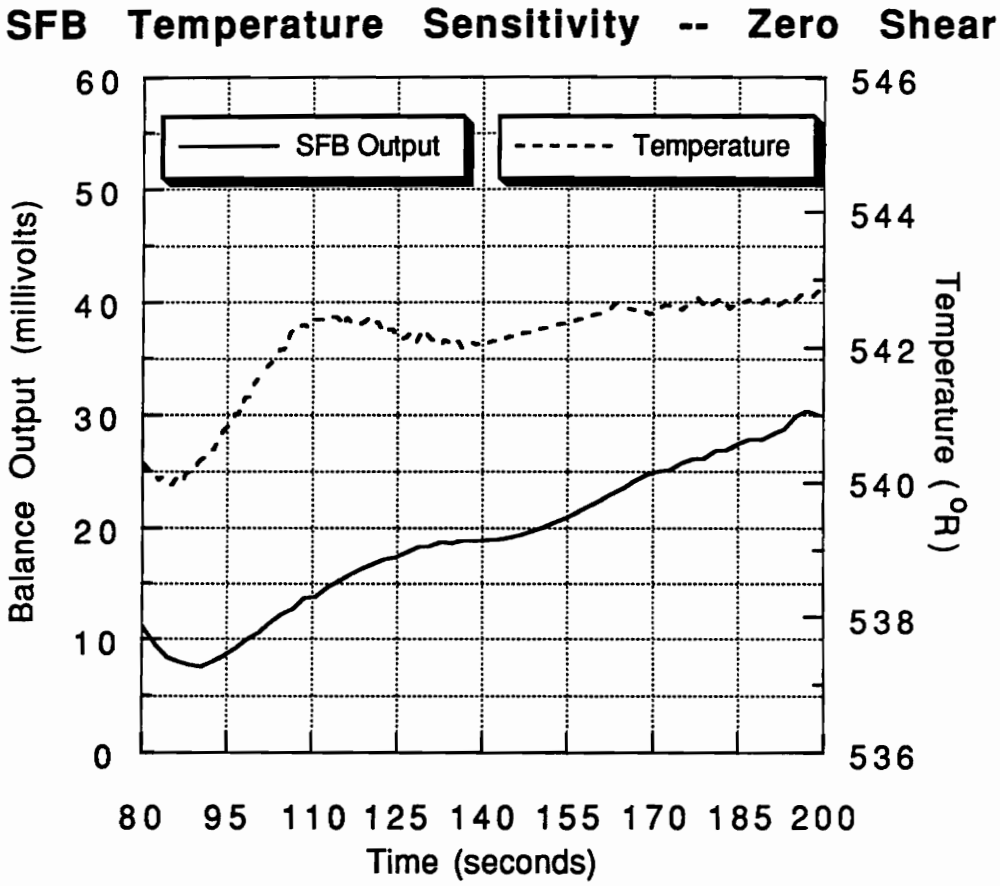

Figure 2.12 : Skin Friction Balance Temperature Sensitivity, DCAF 1st Entry

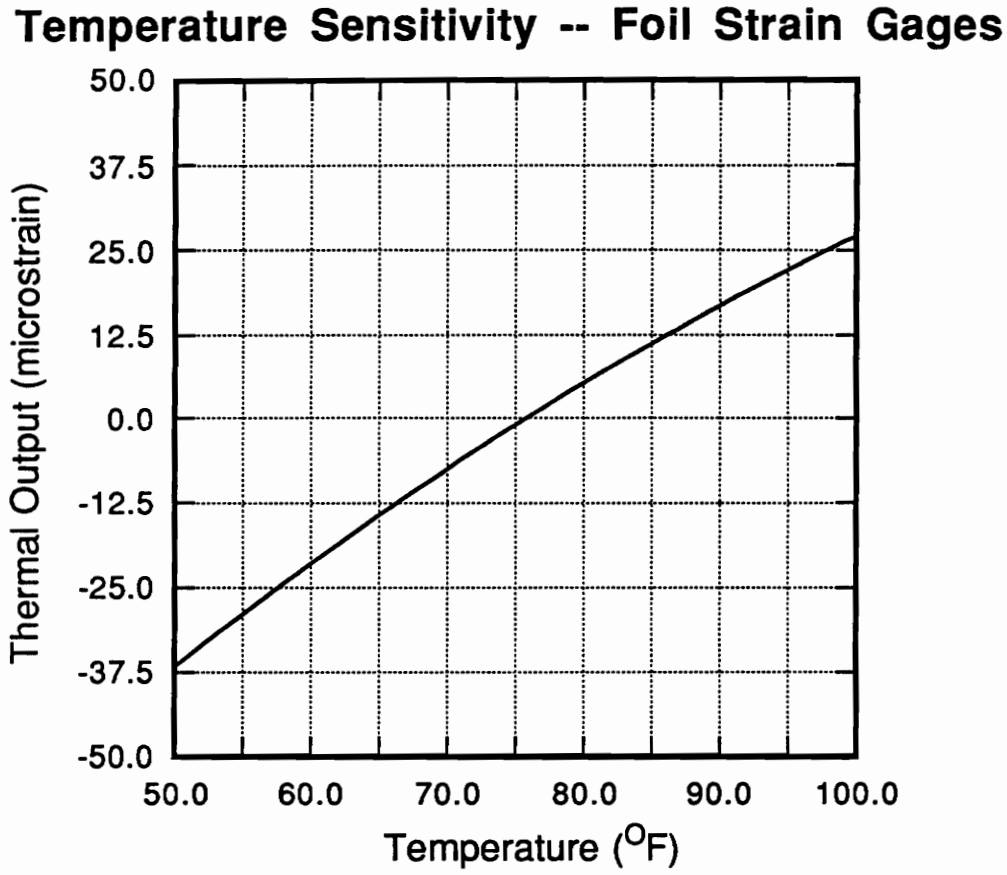

Figure 2.13 : Foil Strain Gage Resistance Temperature Effect

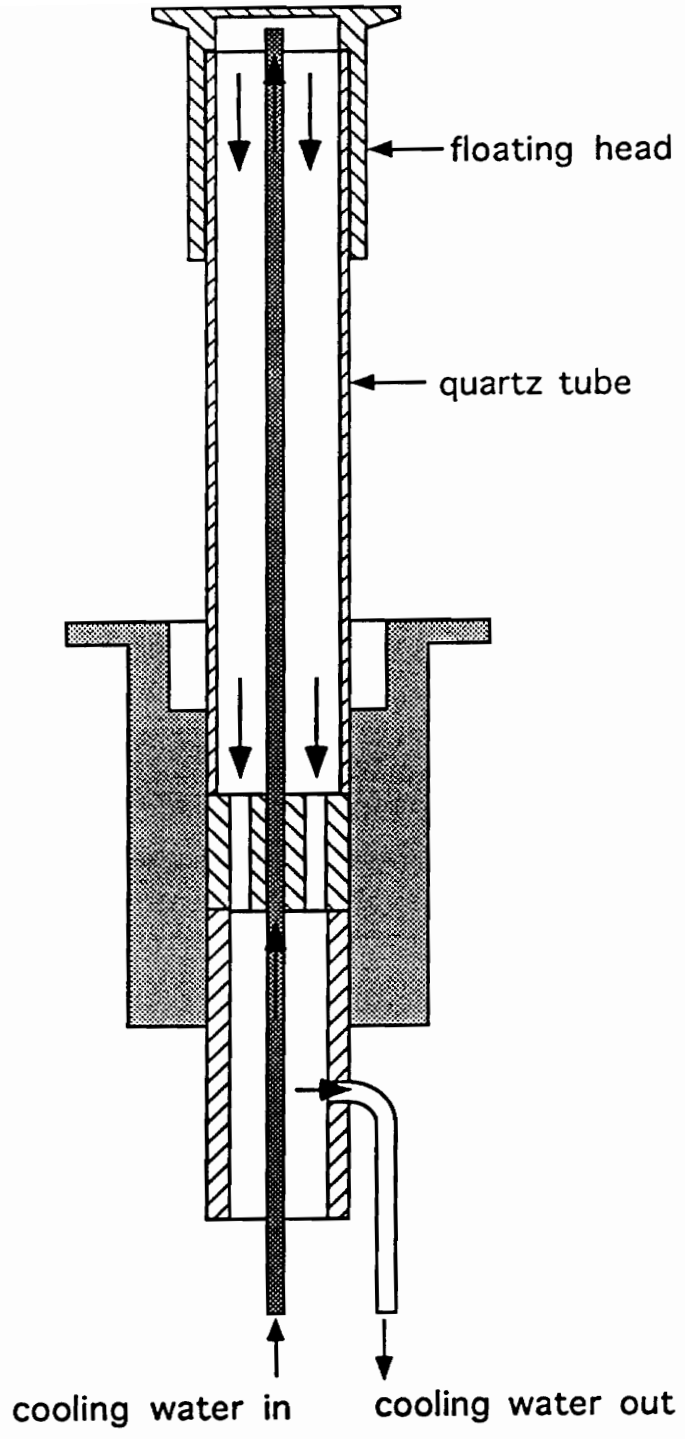

Figure 3.1 : Internal Floating Head Cooling Path, GASL Design

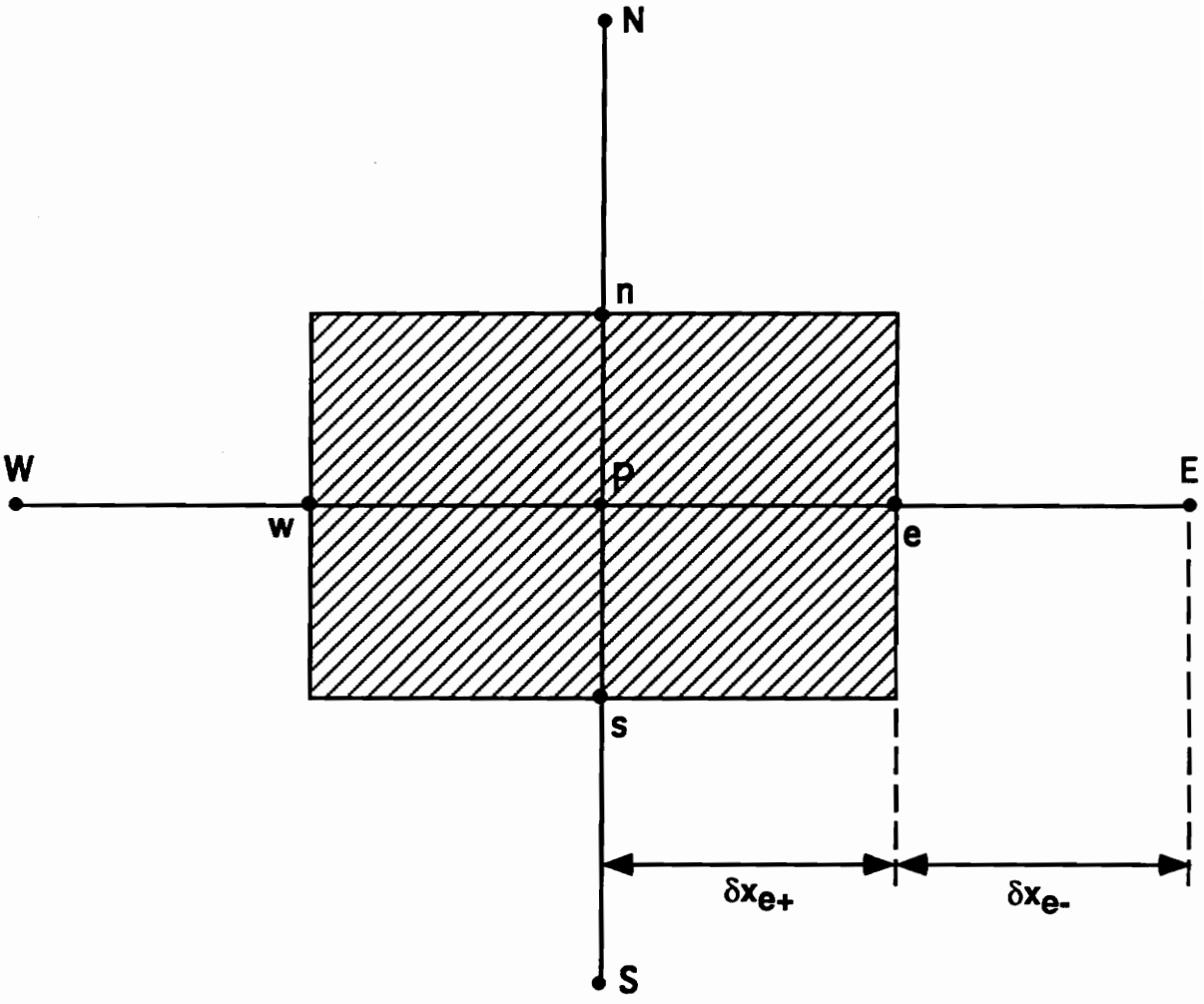

Figure 3.2 : Typical Computational Control Volume

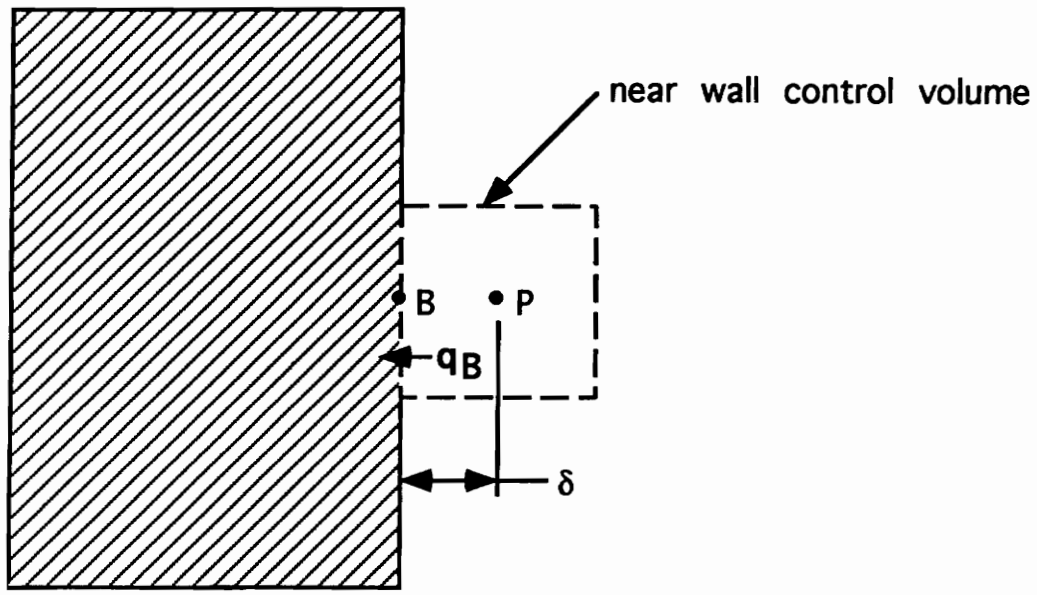

Figure 3.3 : Convective Boundary Control Volume

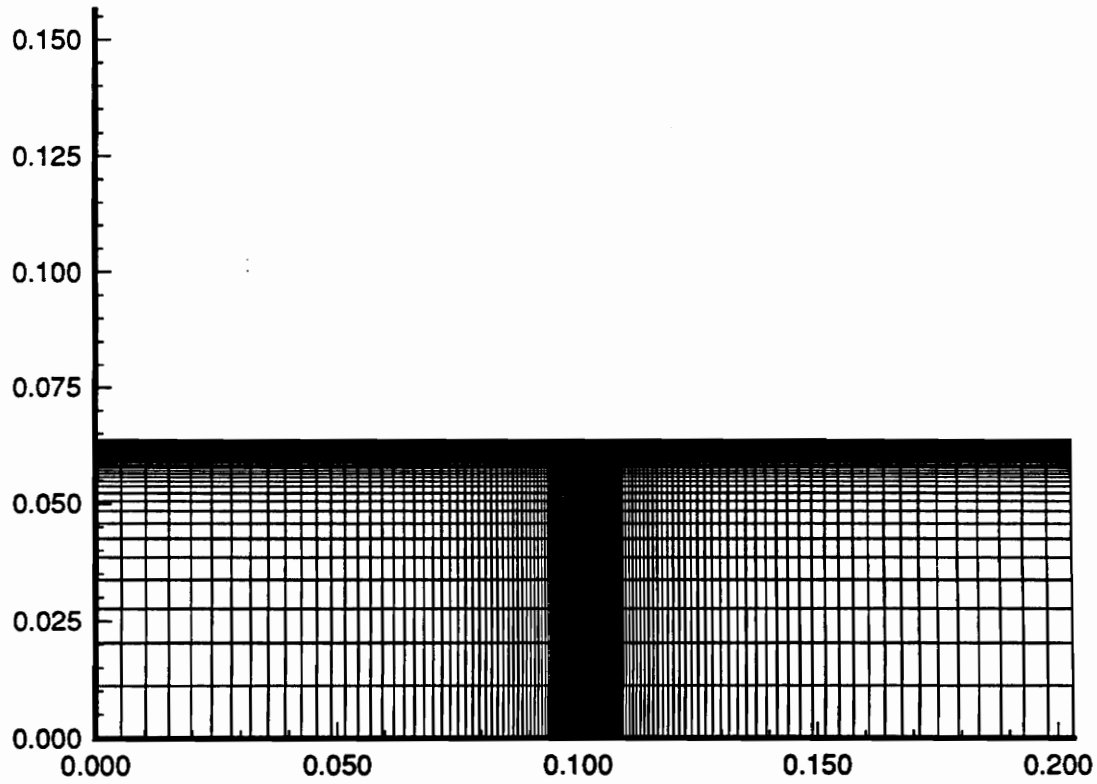

Figure 3.4 : The Computational Mesh

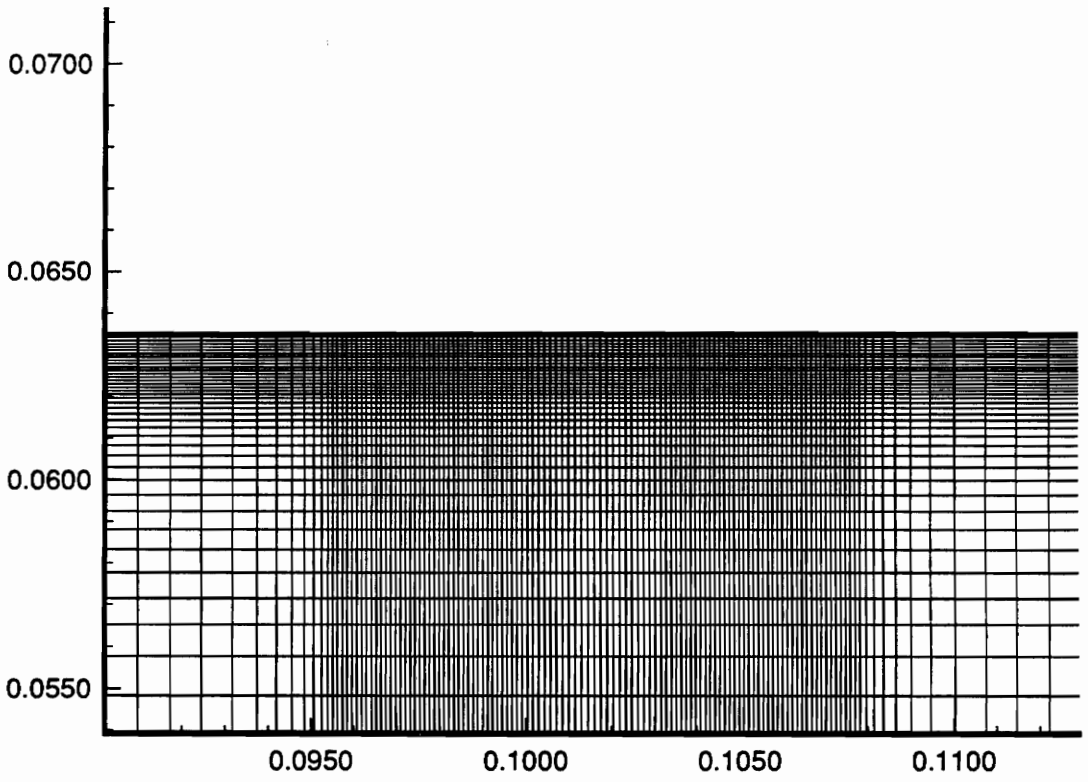

Figure 3.5 : The Computational Mesh Enlarged View

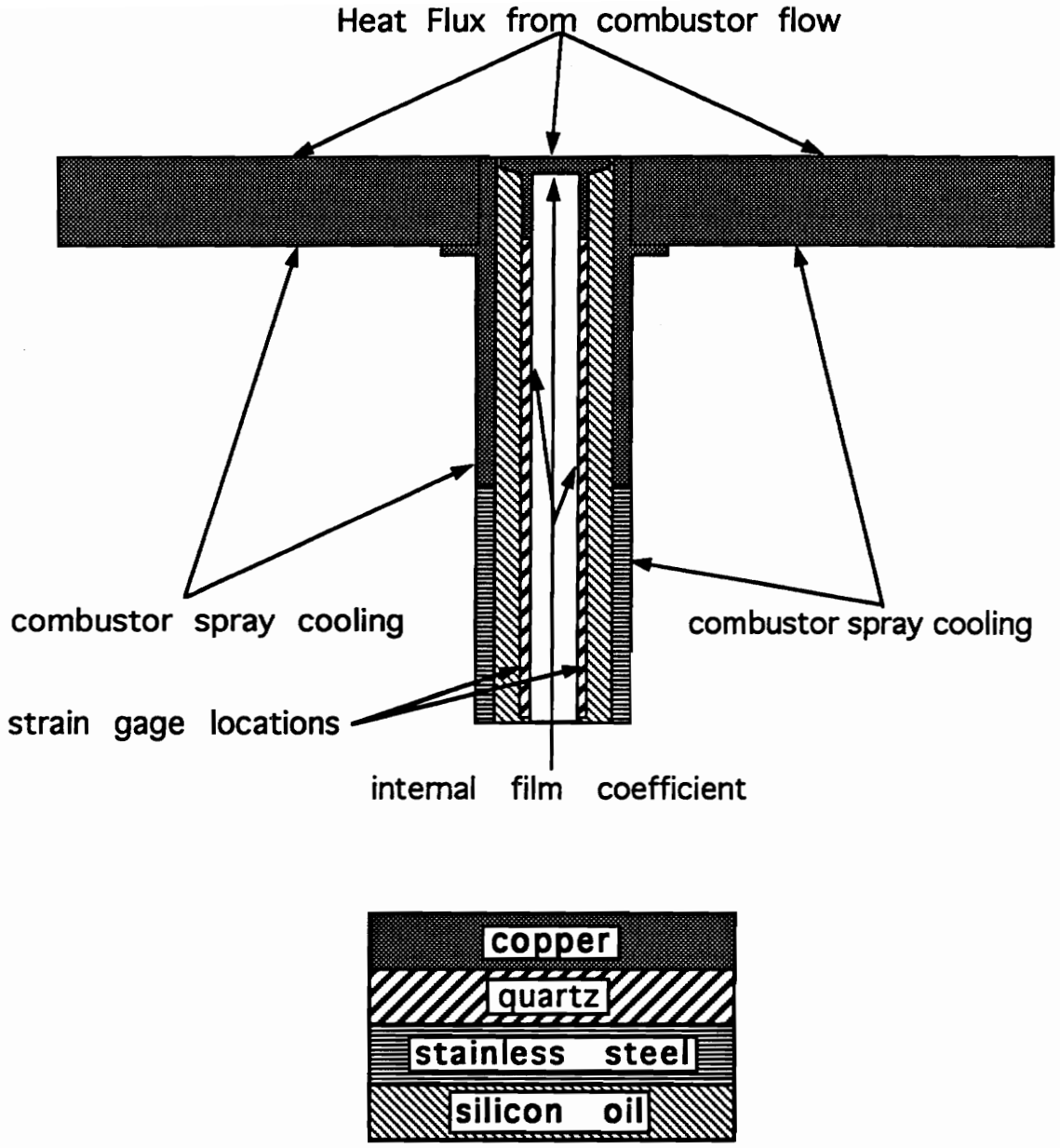

Figure 3.6 : Skin Friction Balance Heat Transfer Geometry

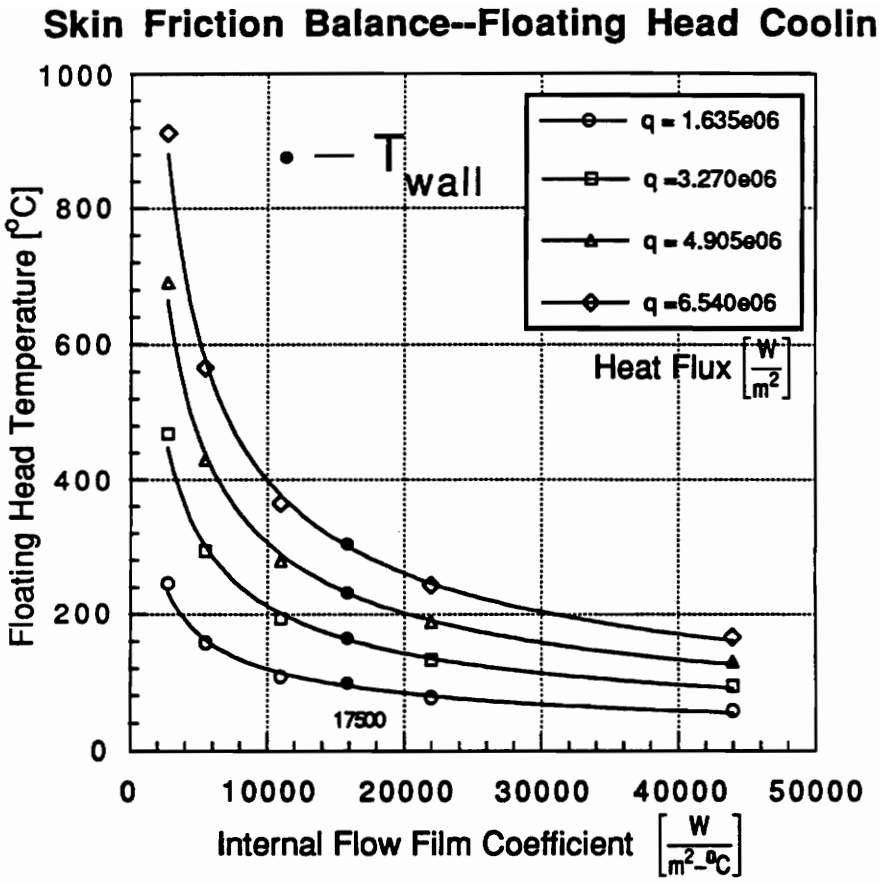

Figure 3.7 : Floating Head Cooling Effectivness

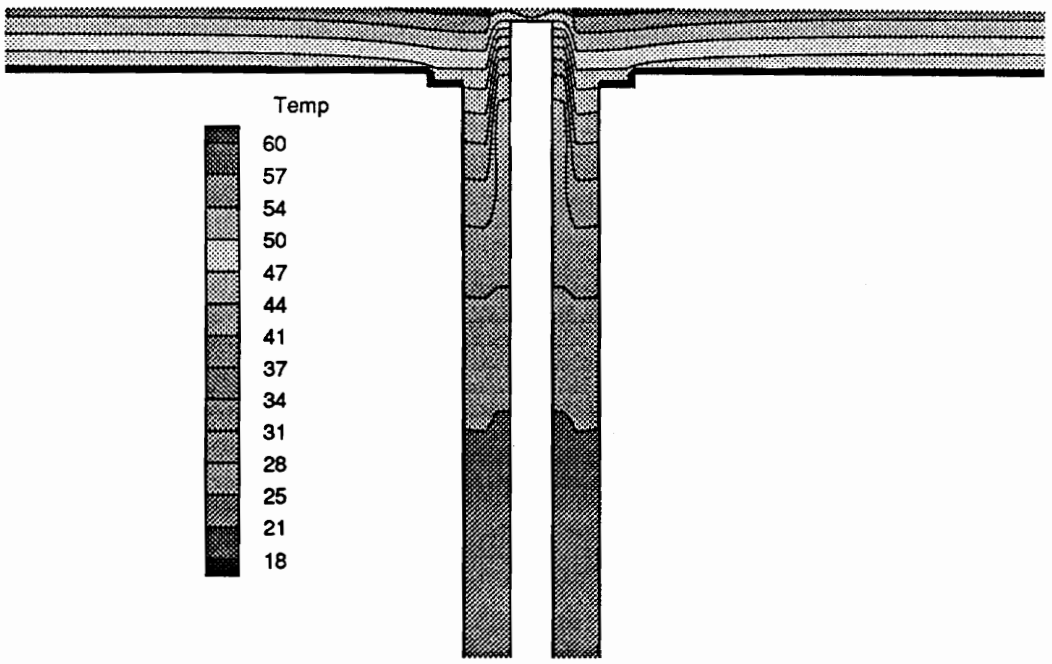

Figure 3.8 : Temperature Contours, q = 0.5 BTU/in^2/sec

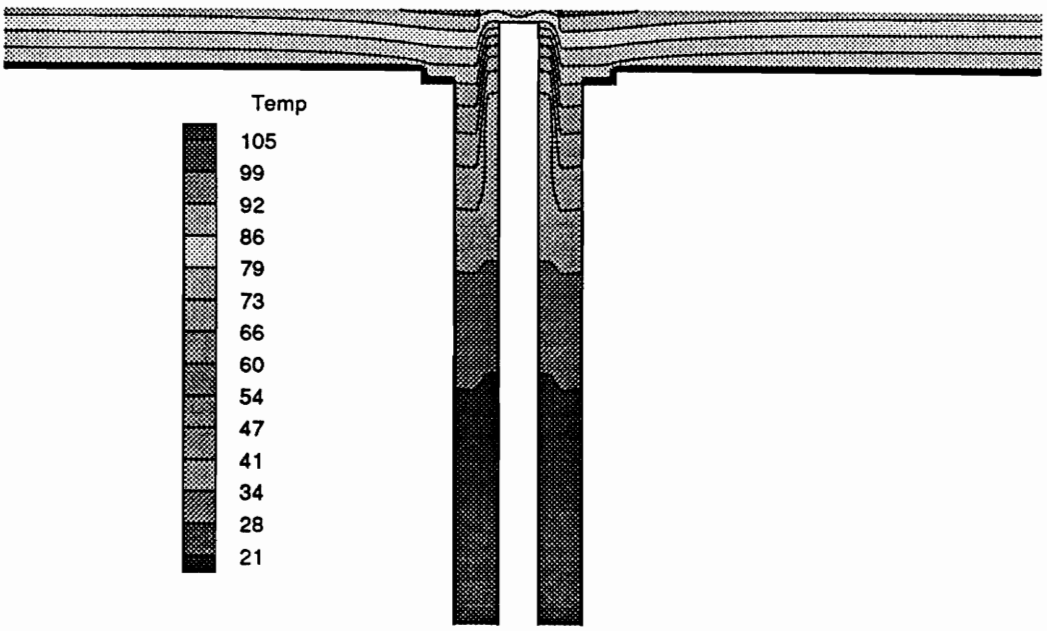

Figure 3.9 : Temperature Contours, q = 1.0 BTU/in^2/sec

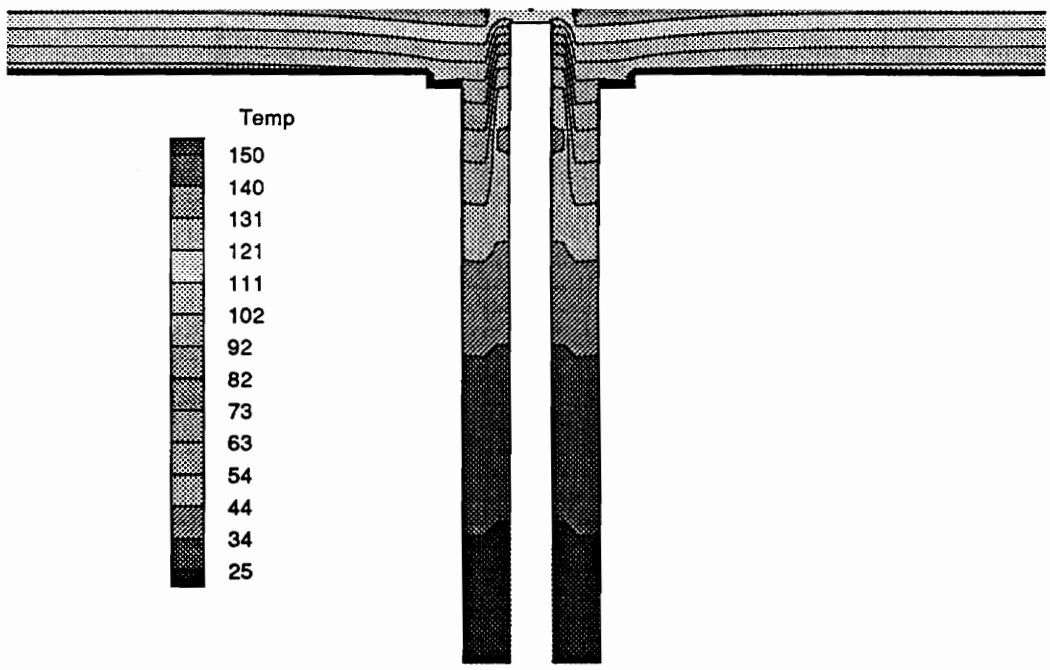

Figure 3.10 : Temperature Contours, q = 1.5 BTU/in^2/sec

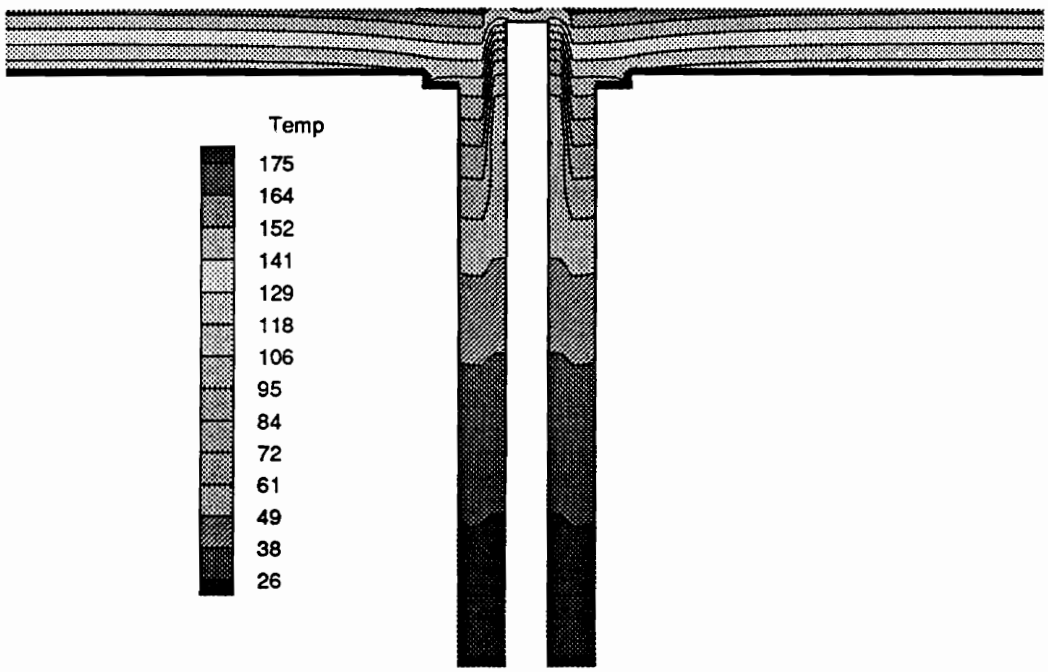

Figure 3.11 : Temperature Contours, q = 2.0 BTU/in^2/sec

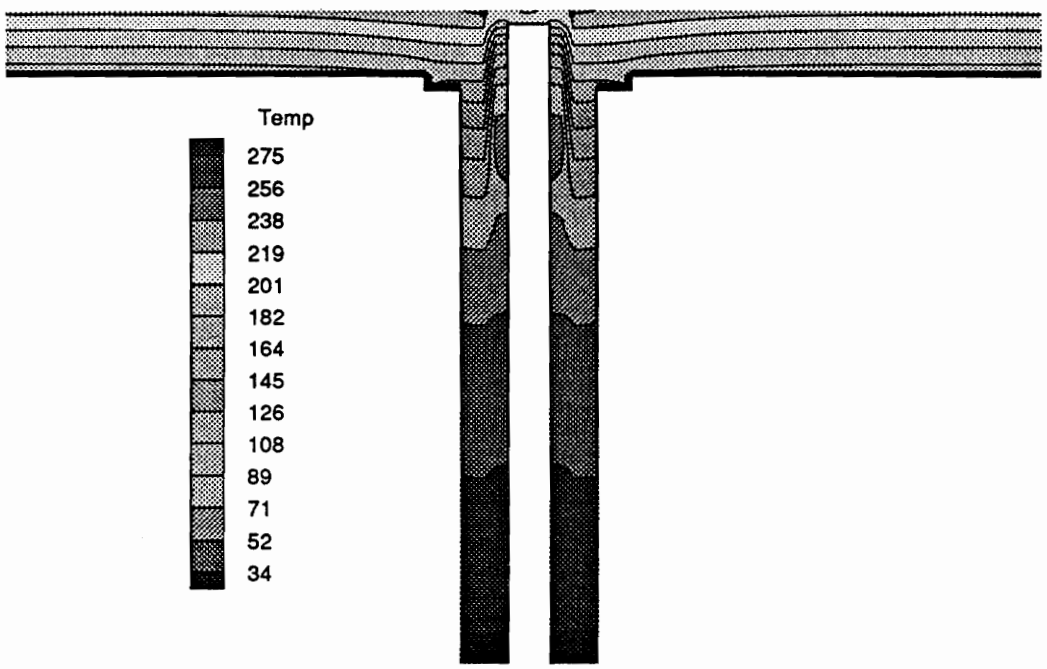

Figure 3.12 : Temperature Contours, q = 3.0 BTU/in^2/sec

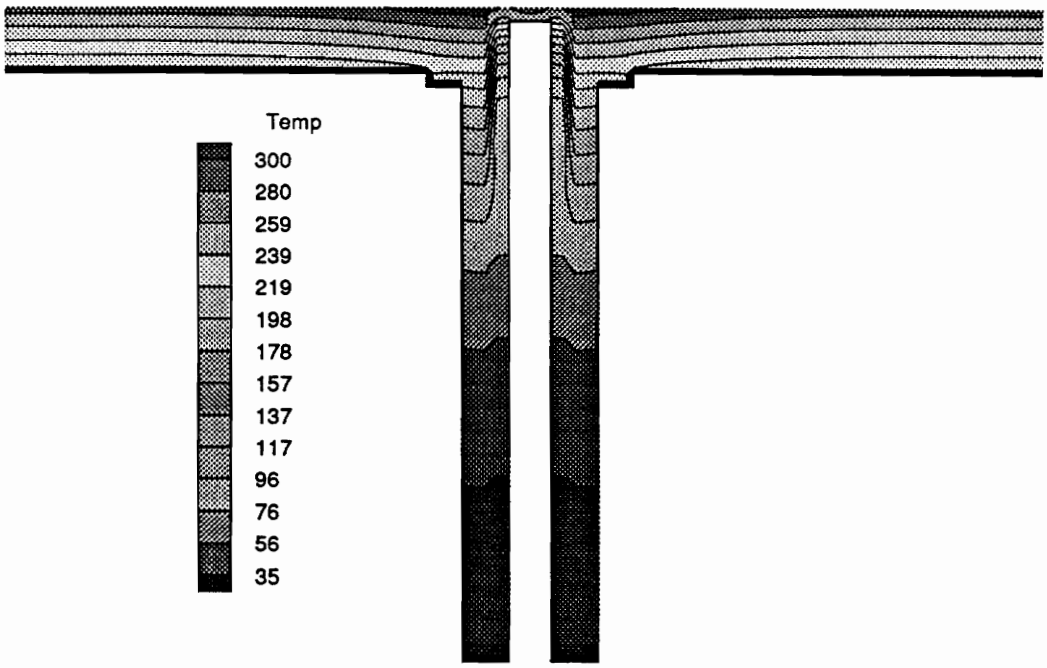

Figure 3.13 : Temperature Contours, q = 4.0 BTU/in^2/sec

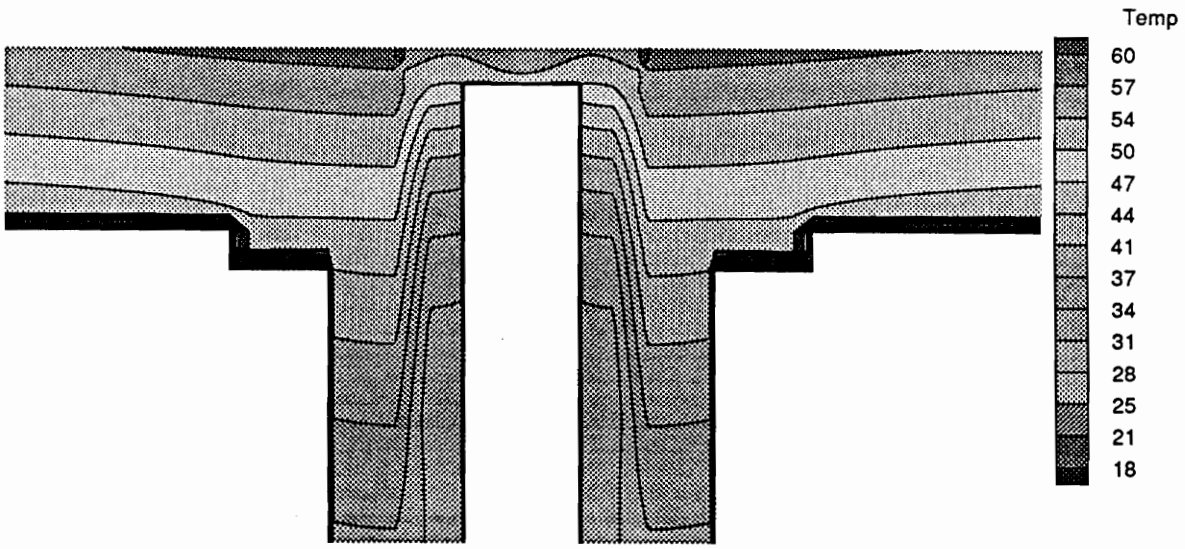

Figure 3.14 : Temperature Contours, q = 0.5 BTU/in^2/sec, Floating Head

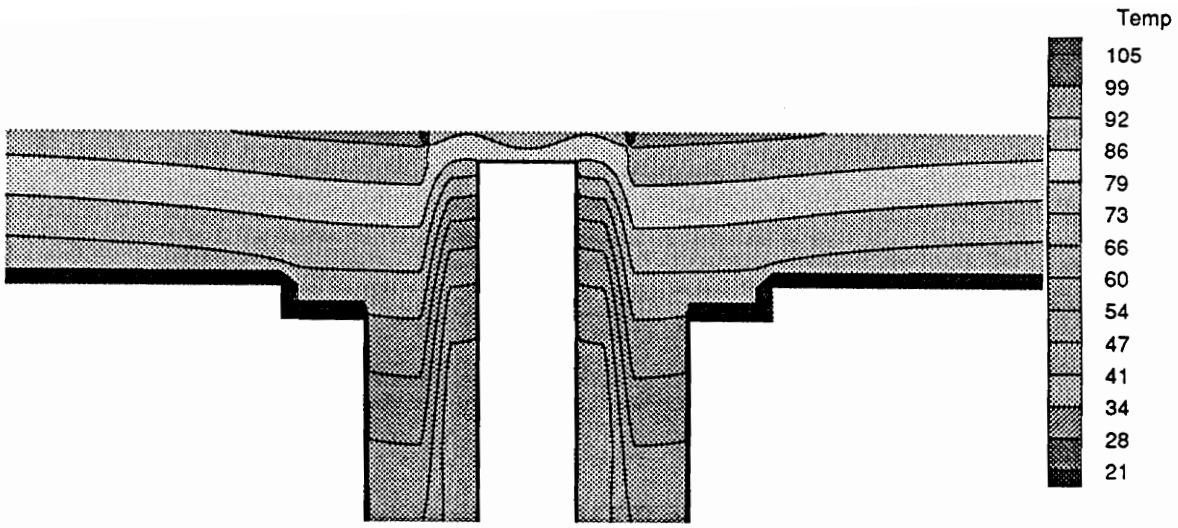

Figure 3.15 : Temperature Contours, q = 1.0 BTU/in^2/sec, Floating Head

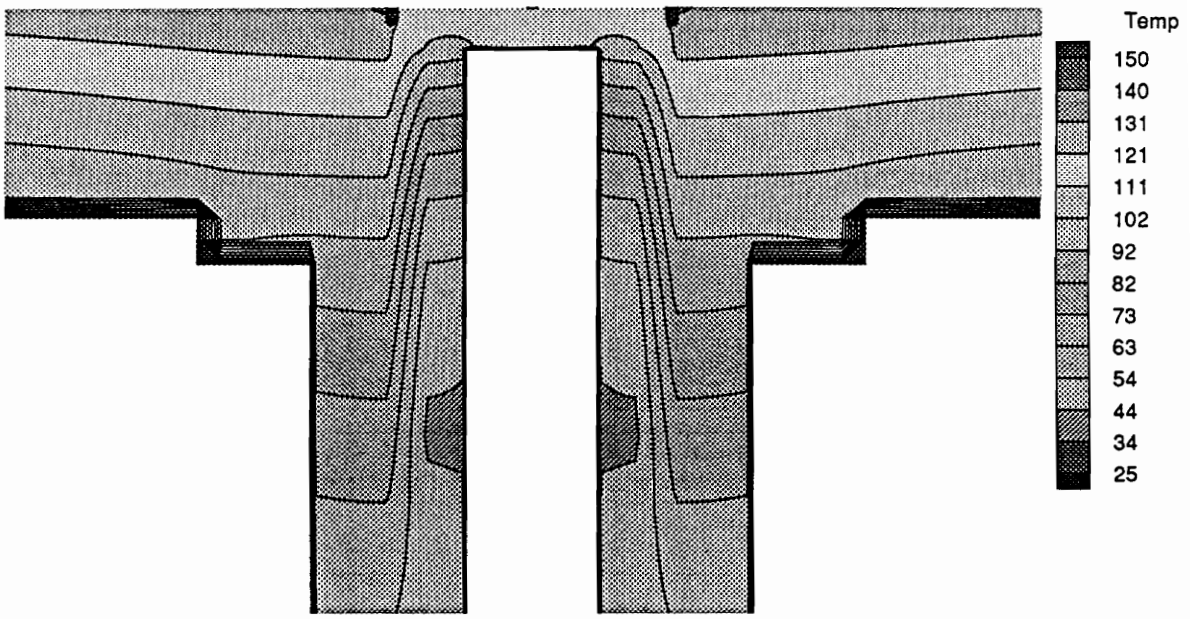

Figure 3.16 : Temperature Contours, q = 1.5 BTU/in^2/sec, Floating Head

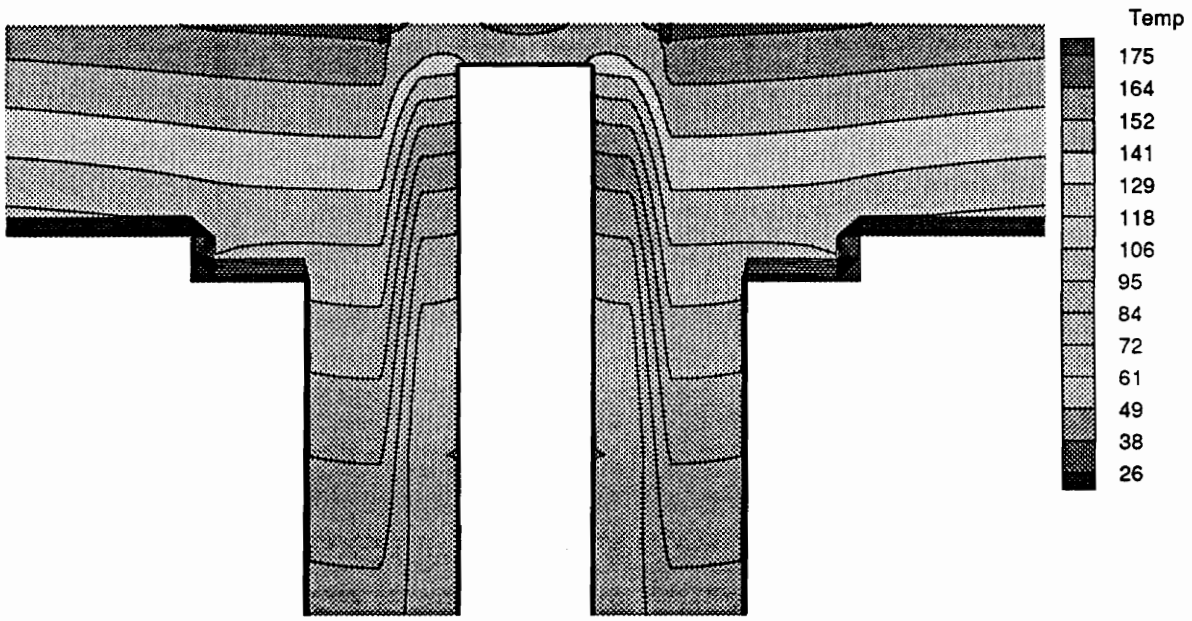

Figure 3.17 : Temperature Contours, q = 2.0 BTU/in^2/sec, Floating Head

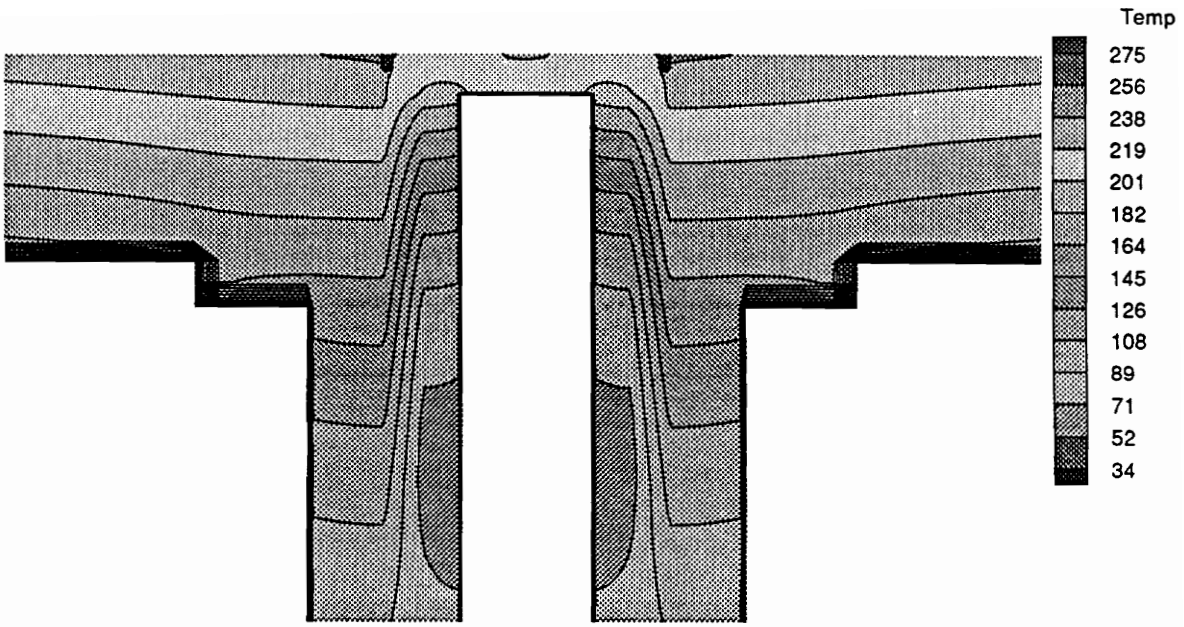

Figure 3.18 : Temperature Contours, q = 3.0 BTU/in^2/sec, Floating Head

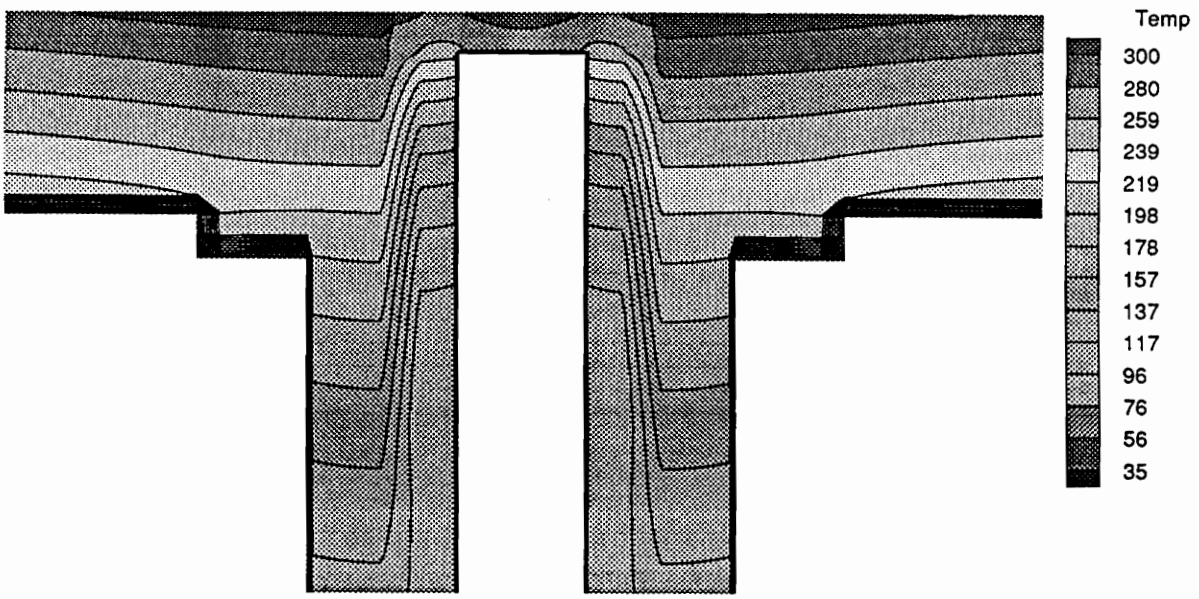

Figure 3.19 : Temperature Contours, q = 4.0 BTU/in^2/sec, Floating Head

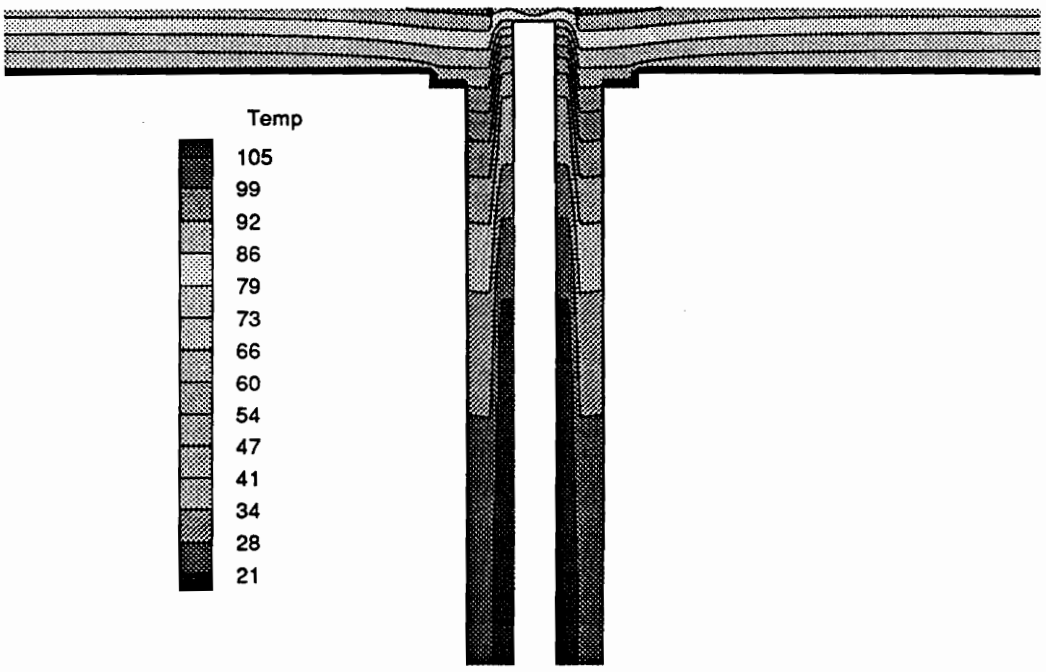

Figure 3.20 : Temperature Contours, q = 1.0 BTU/in^2/sec, No oil

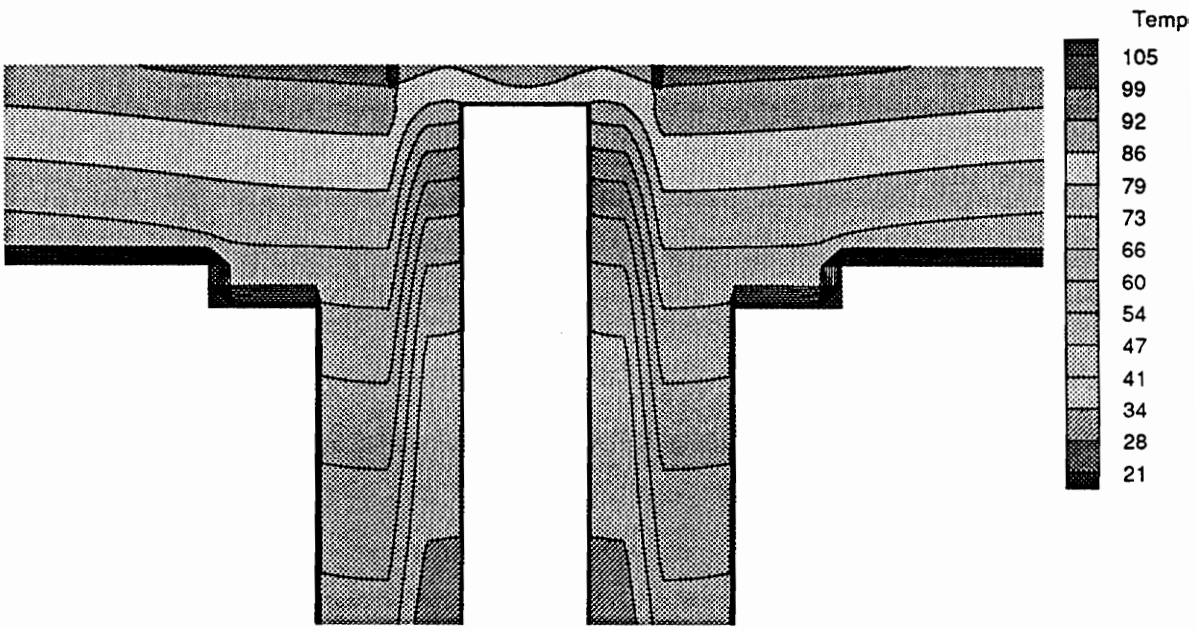

Figure 3.21 : Temperature Contours, q = 1.0 BTU/in^2/sec, No oil, Floating Head

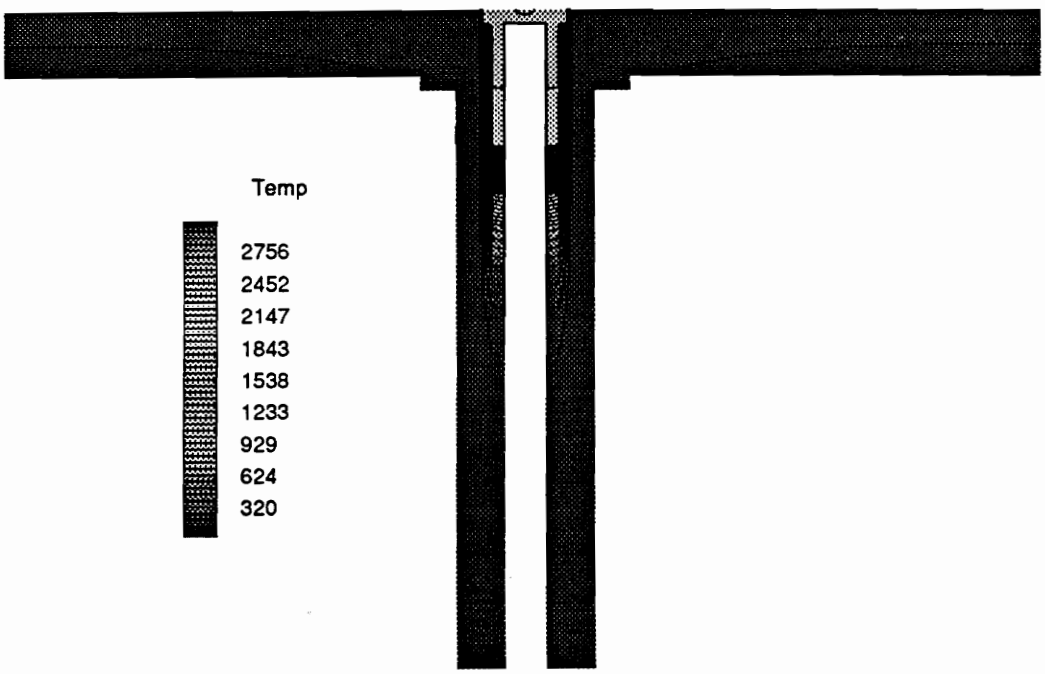

Figure 3.22 : Temperature Contours, q = 1.0 BTU/in^2/sec, No Internal Cooling

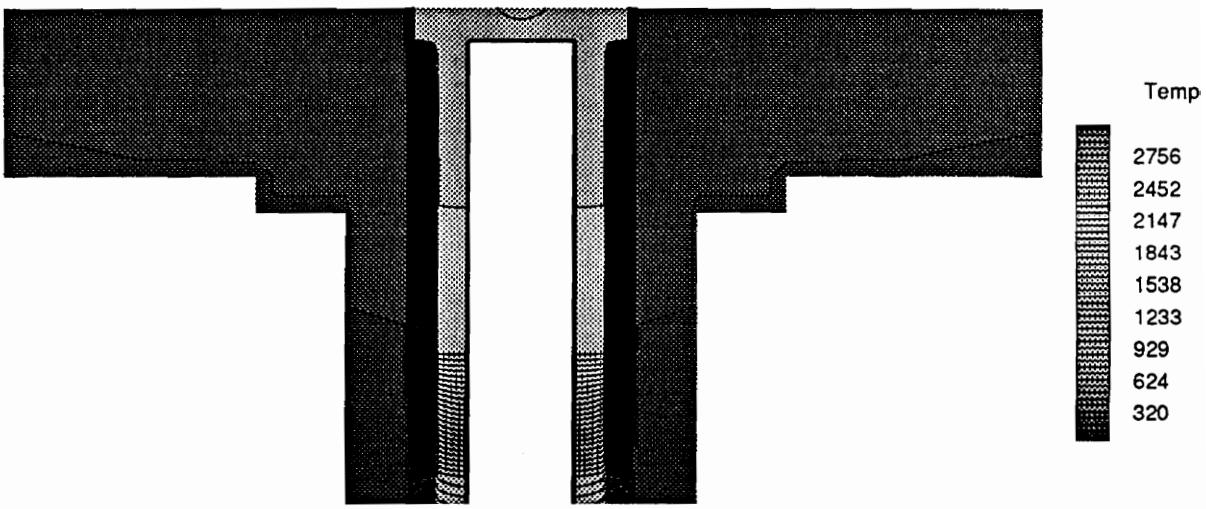

Figure 3.23 : Temperature Contours, q = 1.0 BTU/in^2/sec, No Internal Cooling, Floating Head

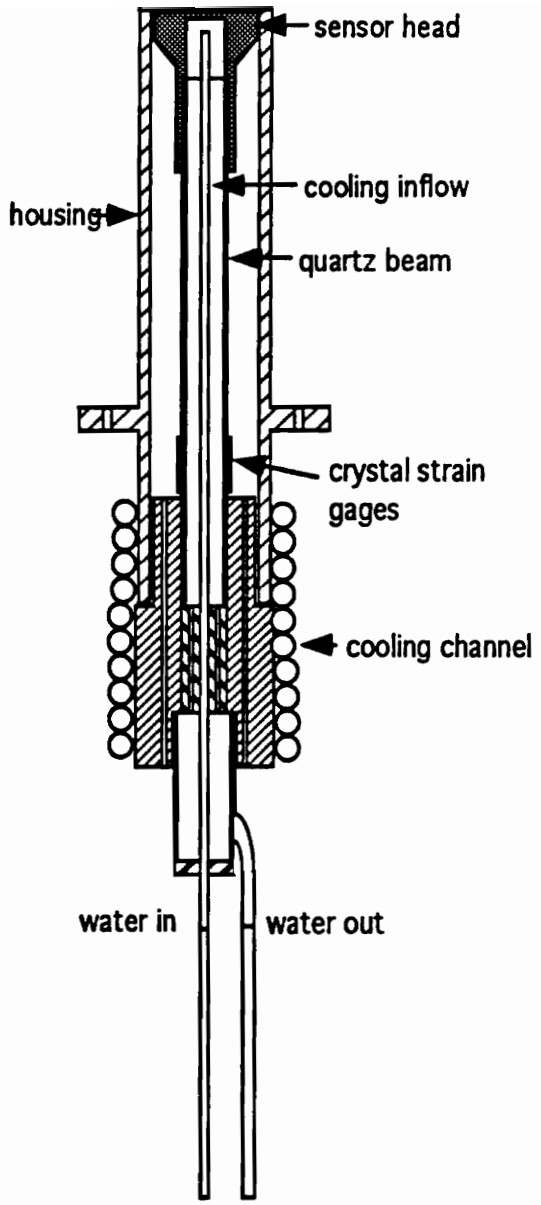

Figure 4.1 : Skin Friction Balance, GASL Test Design

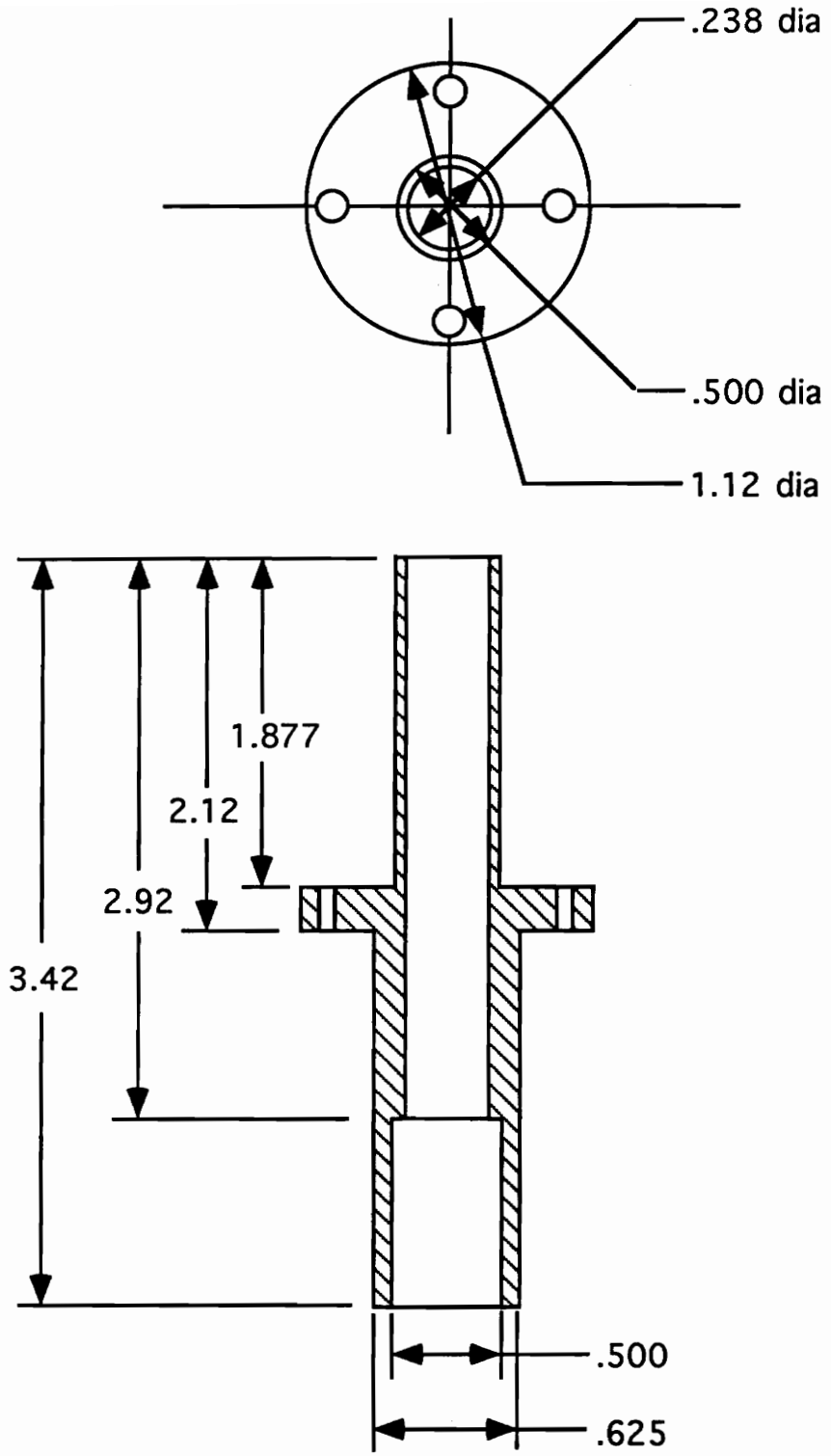

Figure 4.2 : Housing for GASL Skin Friction Balance

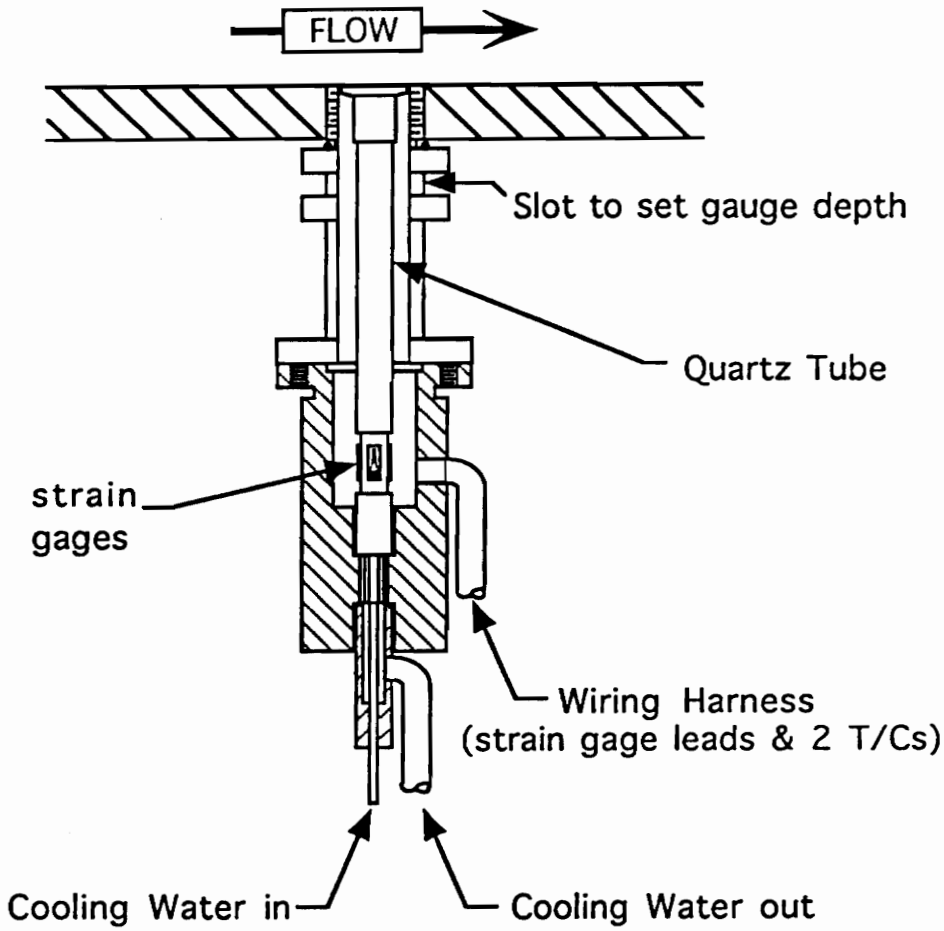

Figure 4.3 : Skin Friction Balance, DCAF 1st Entry Design

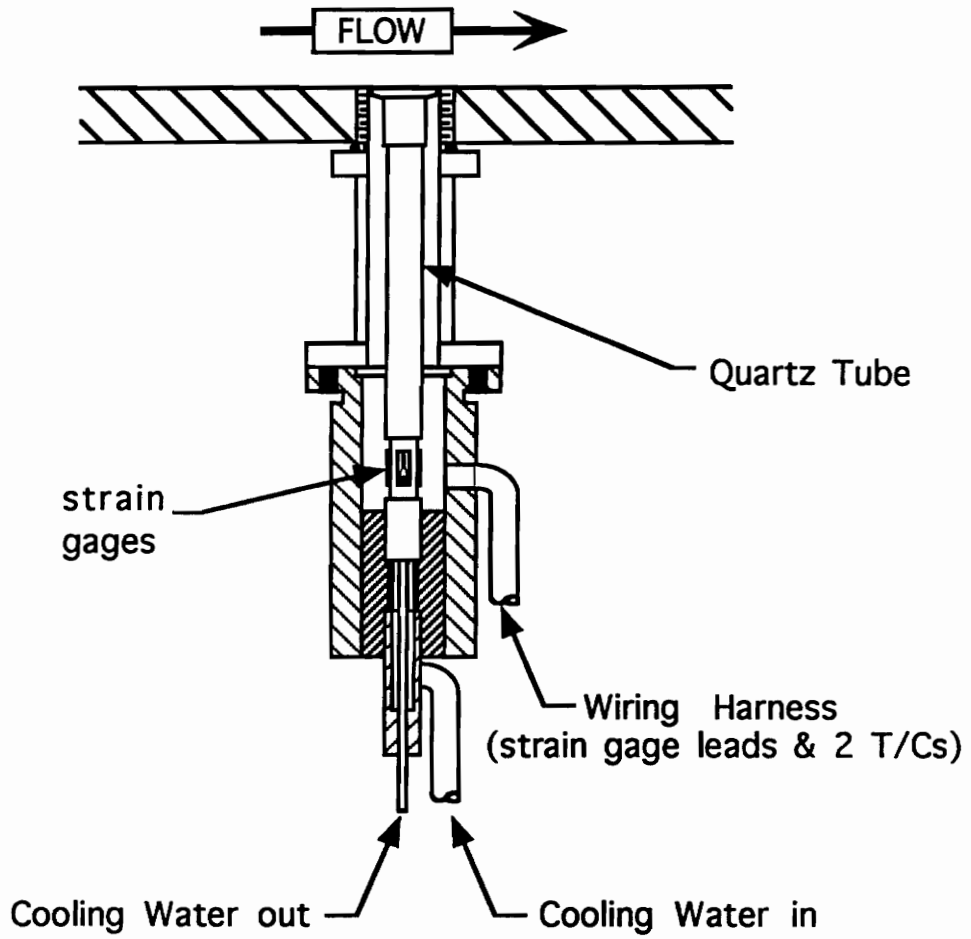

Figure 4.4 : Skin Friction Balance, DCAF 2^{cd} DCAF Entry Design

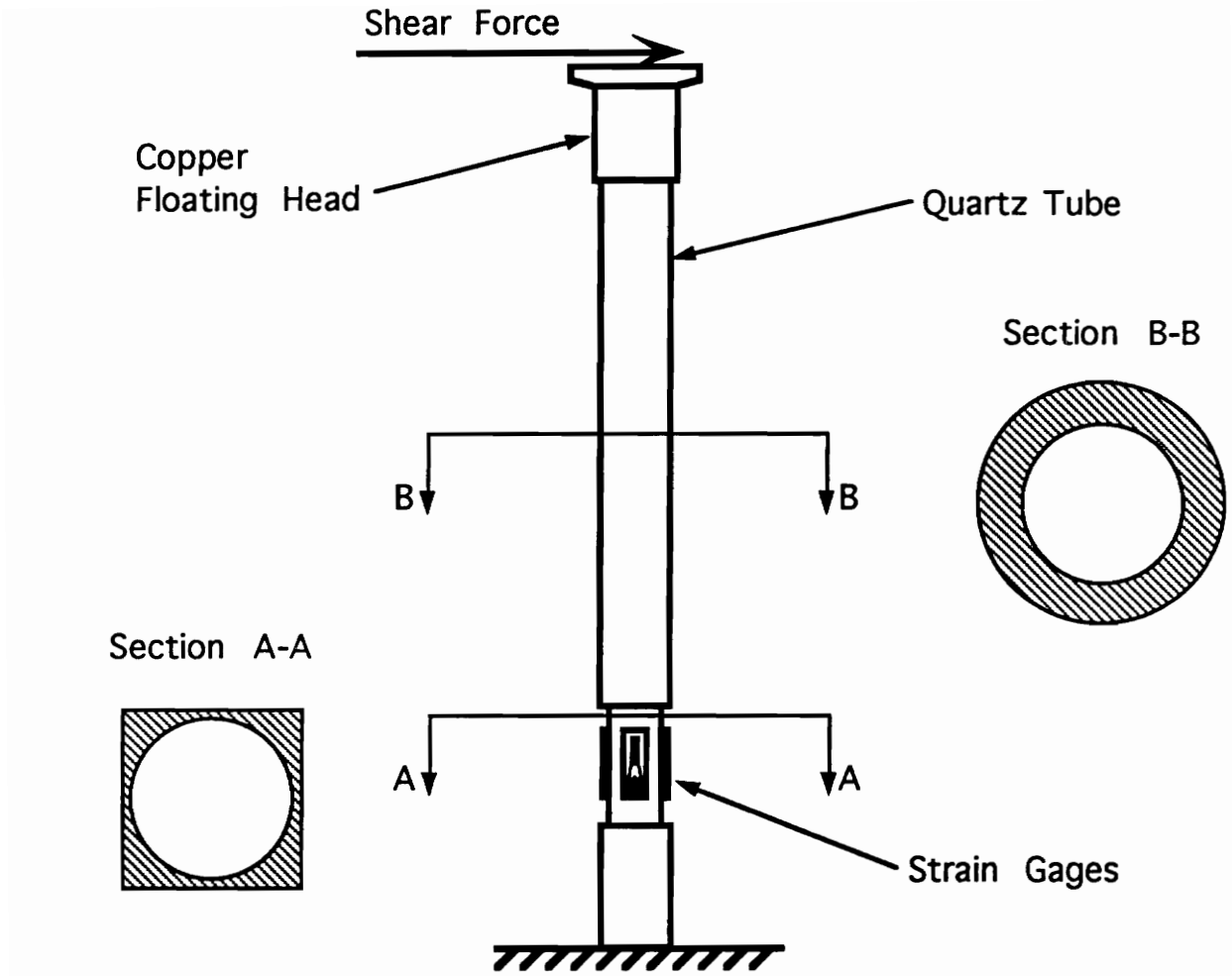

Figure 4.5 : Cantilever Beam Schematic with Strain Gages

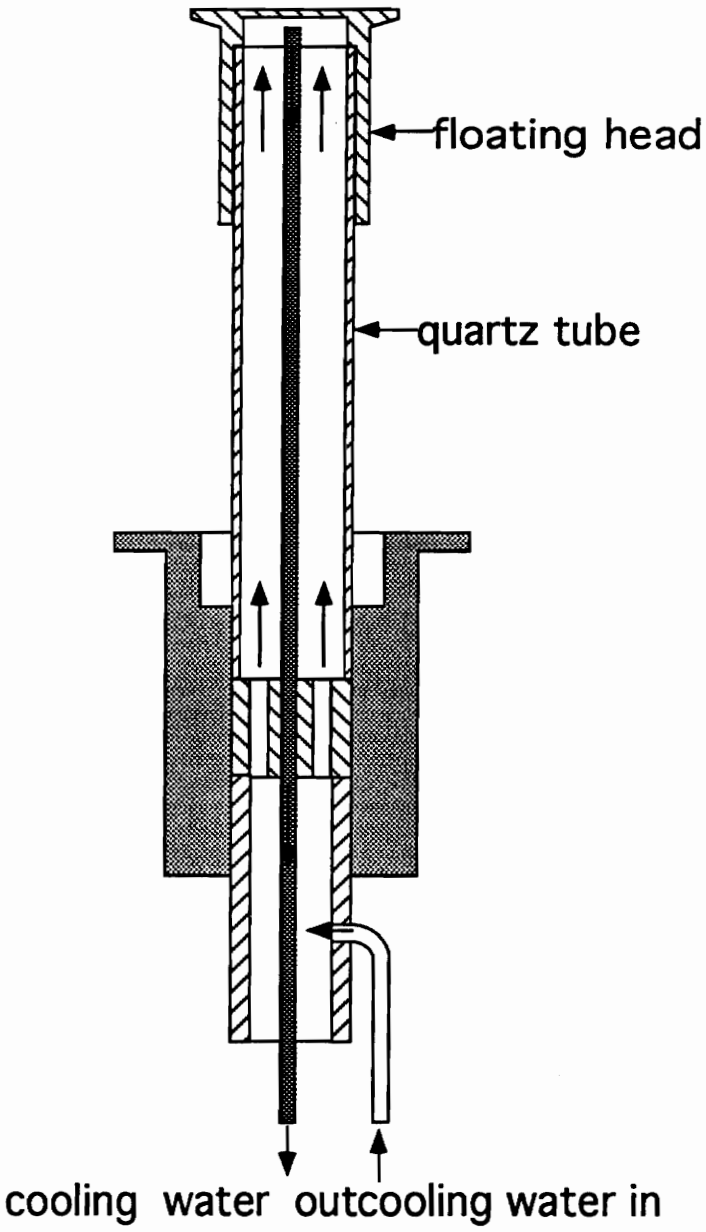

Figure 4.6 : Internal Floating Head Cooling Path, NASA ARC DCAF Design

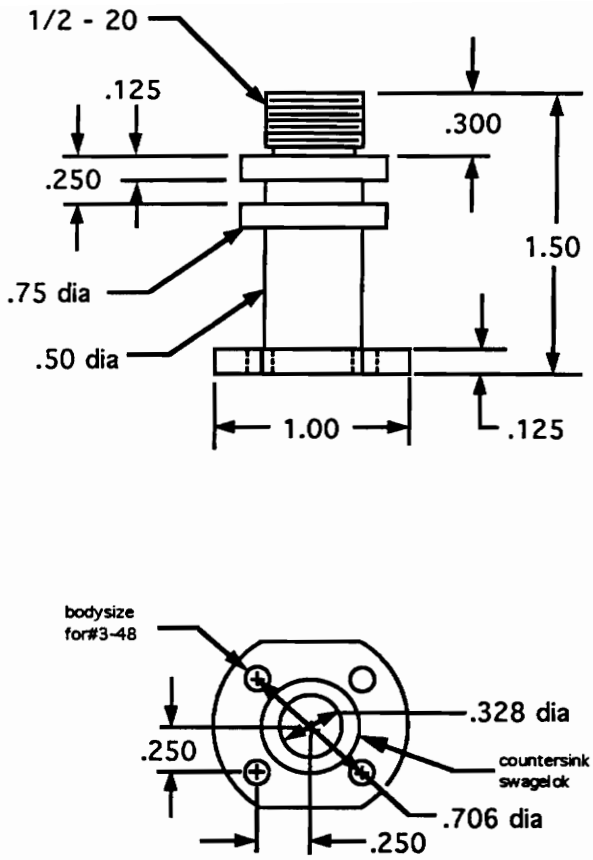

Figure 4.7 : Skin Friction Balance Upper Zirconium-Copper Housing

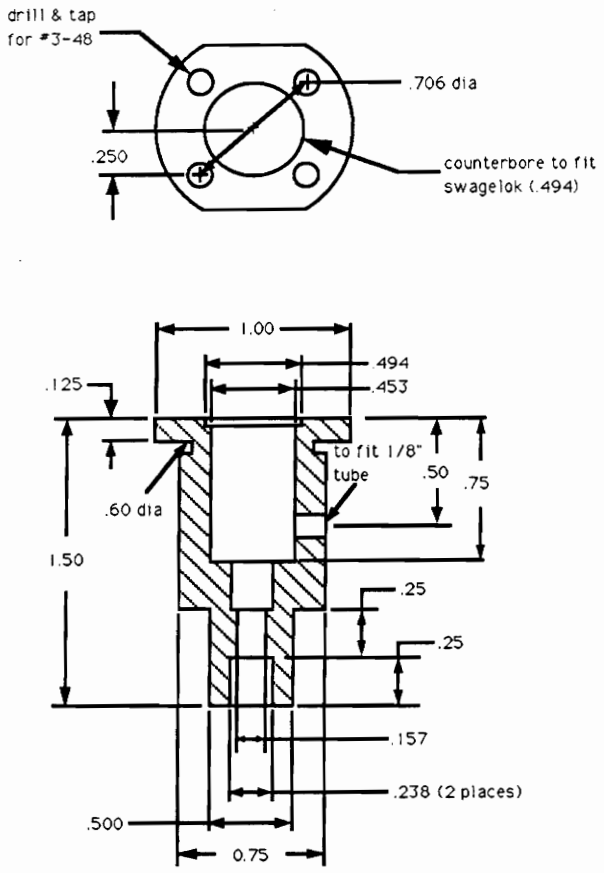

Figure 4.8 : Skin Friction Balance Stainless Steel Housing, 1st DCAF Entry

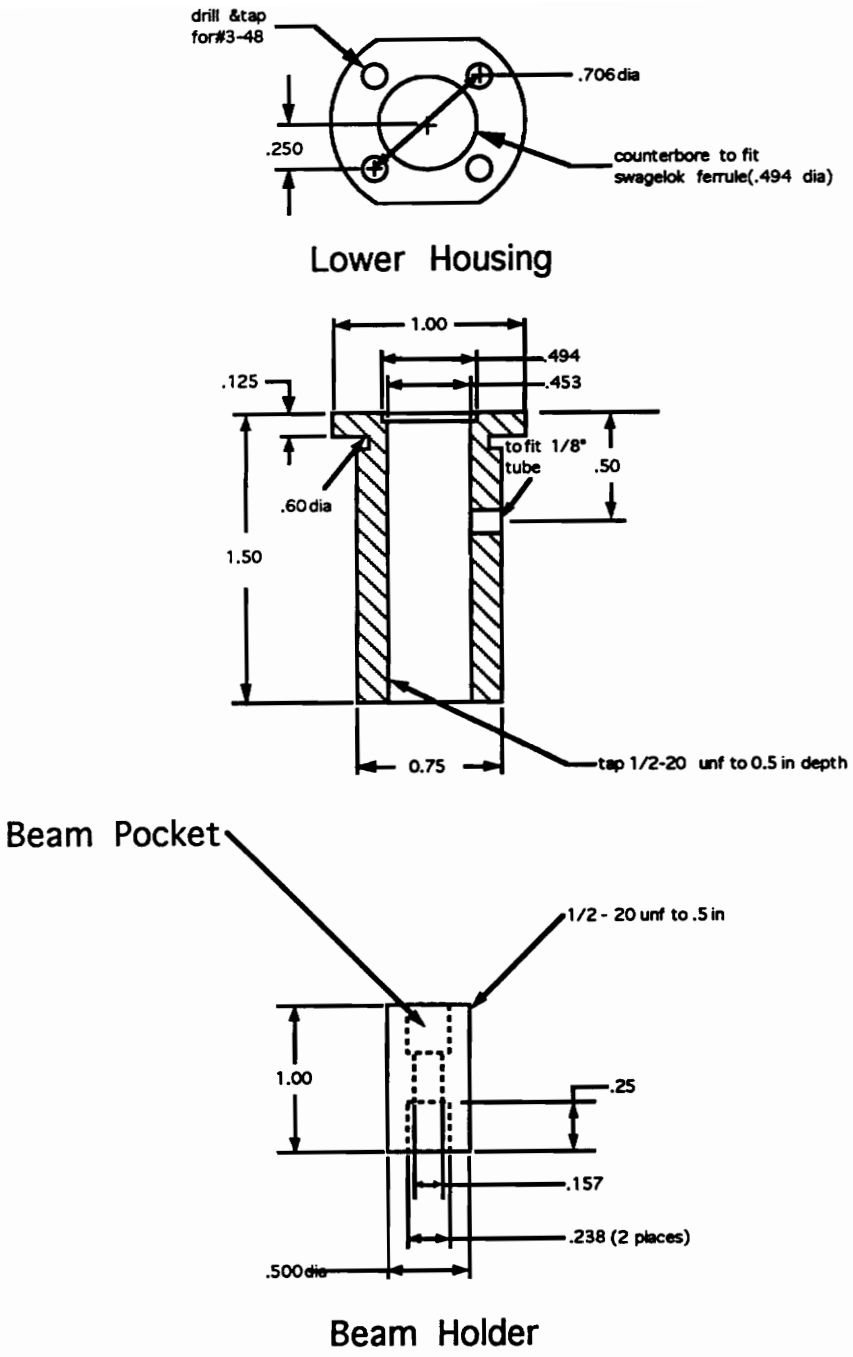

Figure 4.9 : Skin Friction Balance Stainless Steel Housing, 2^{cd} DCAF Entry

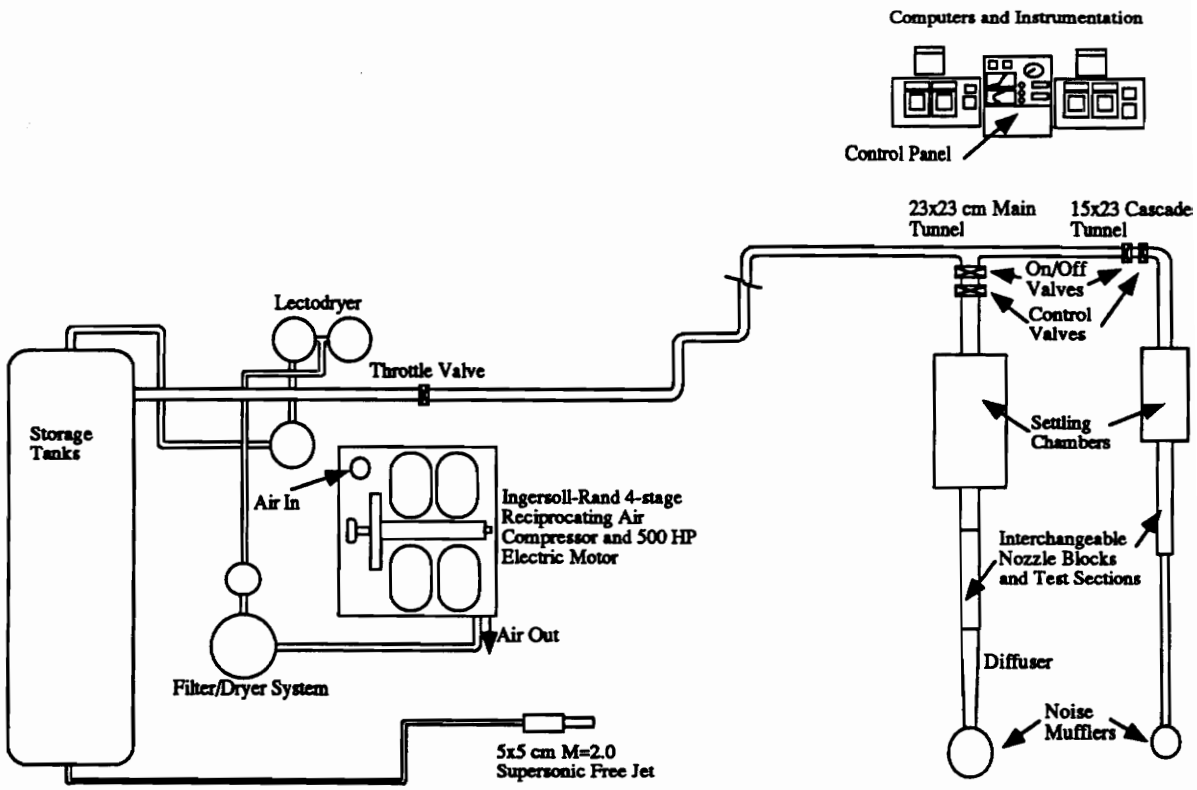

Figure 5.1 : Virginia Tech Supersonic Wind Tunnel Facilities

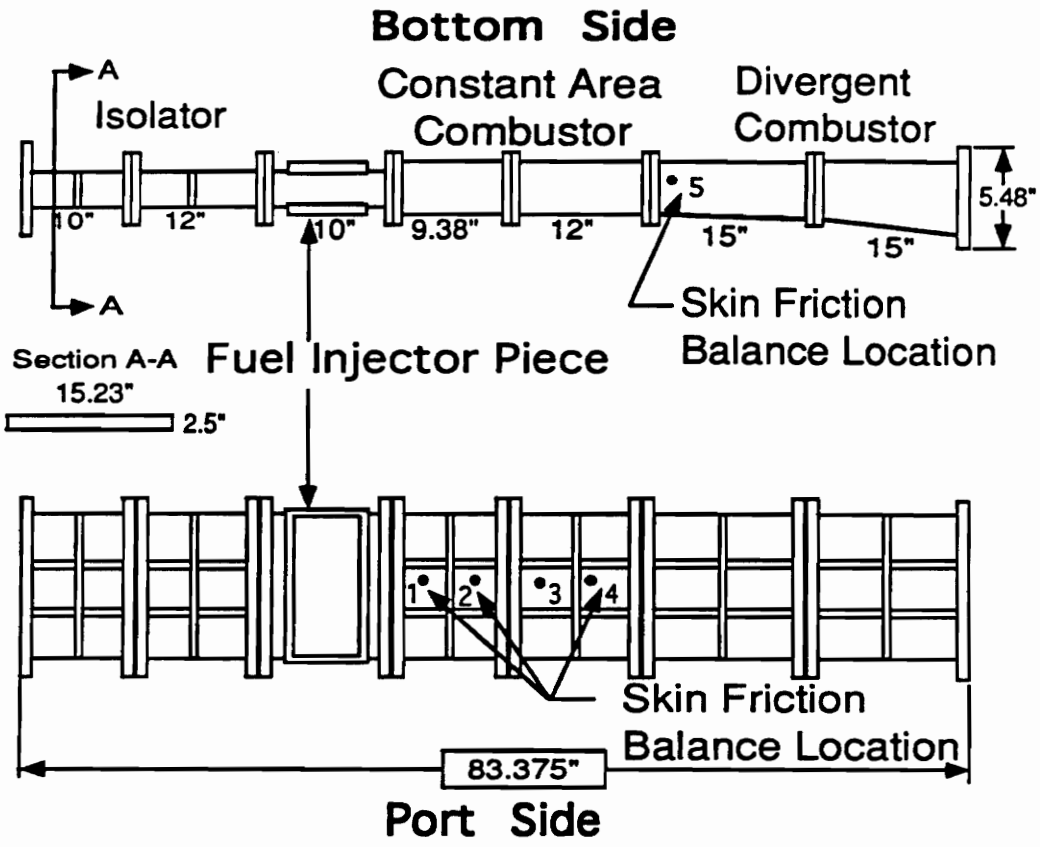

Figure 5.2 : Direct Connect Arcjet Facility Combustor Duct

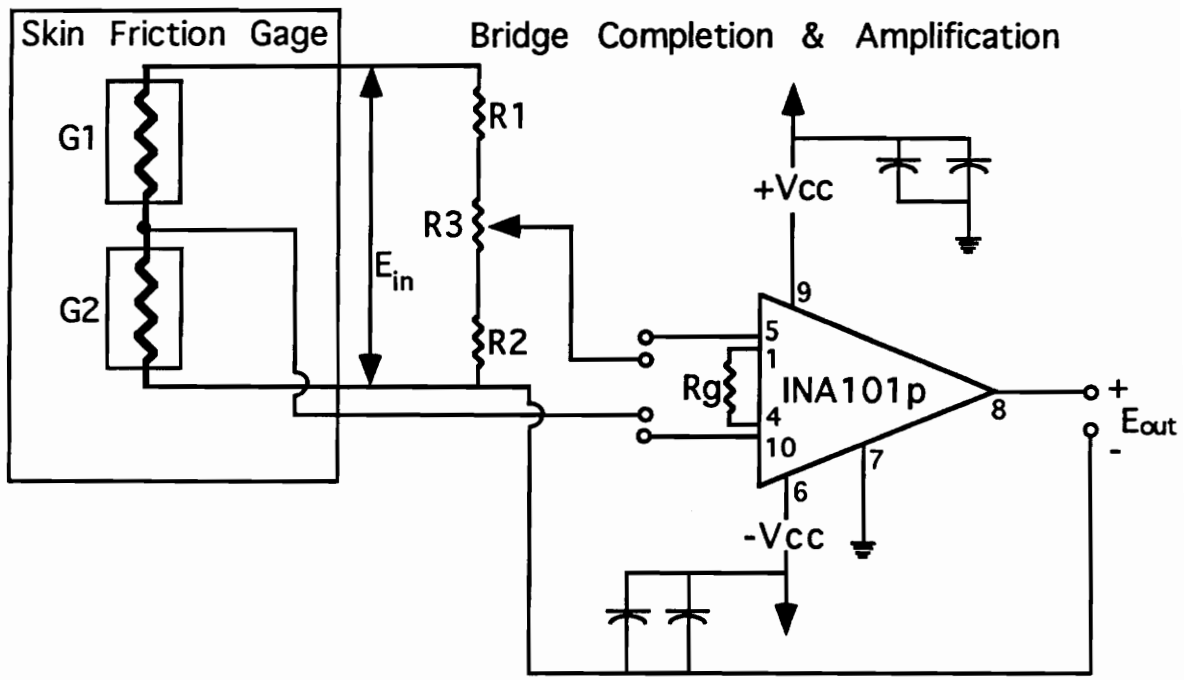

Note: G1, G2, R1, R2 = 750 ohms ; R3 = 500 ohms
Input voltage = 5 volts

Figure 5.3 : Amplifier and Bridge Completion Circuit Diagram

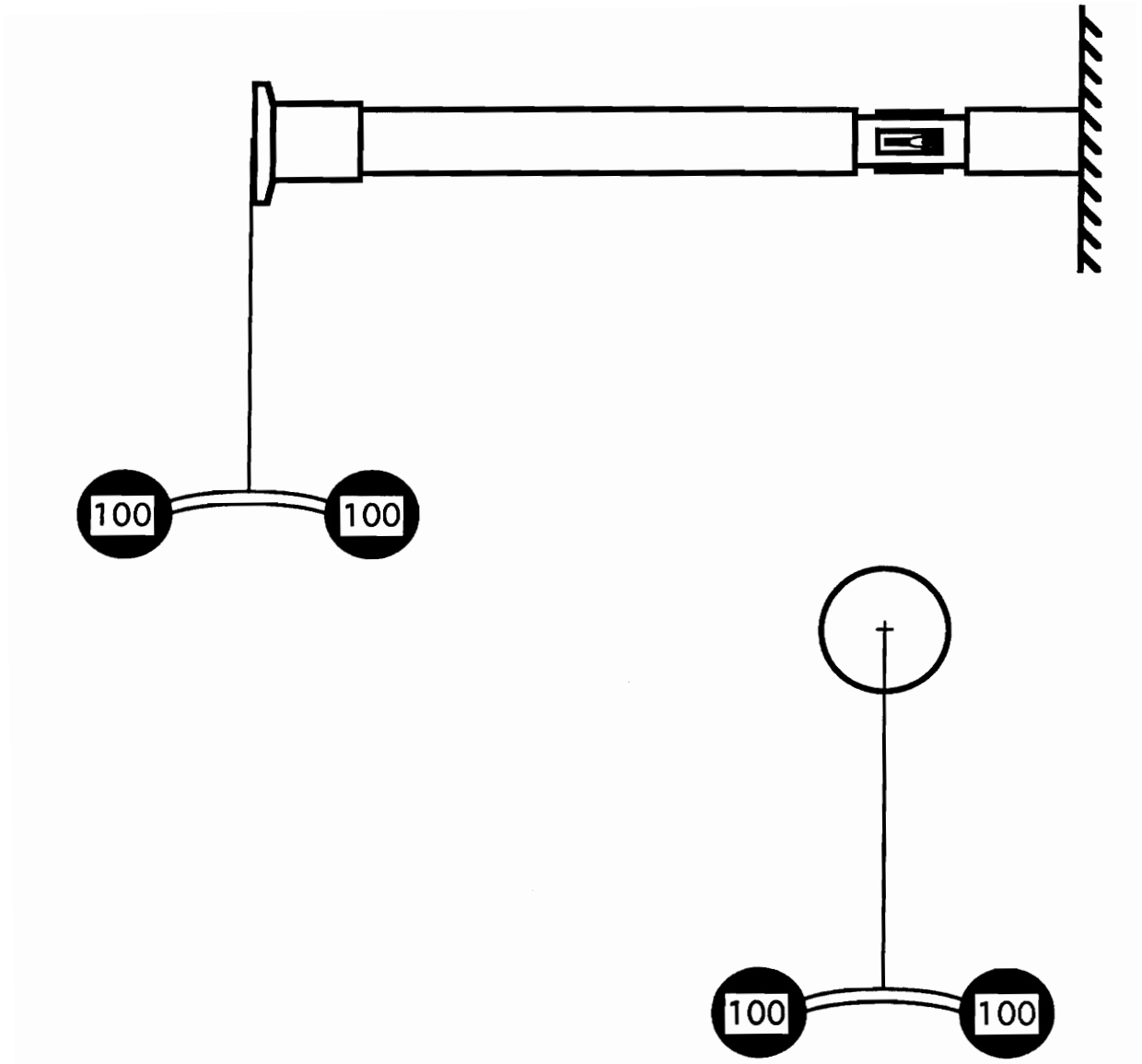

Figure 5.4 : Skin Friction Balance Calibration Technique

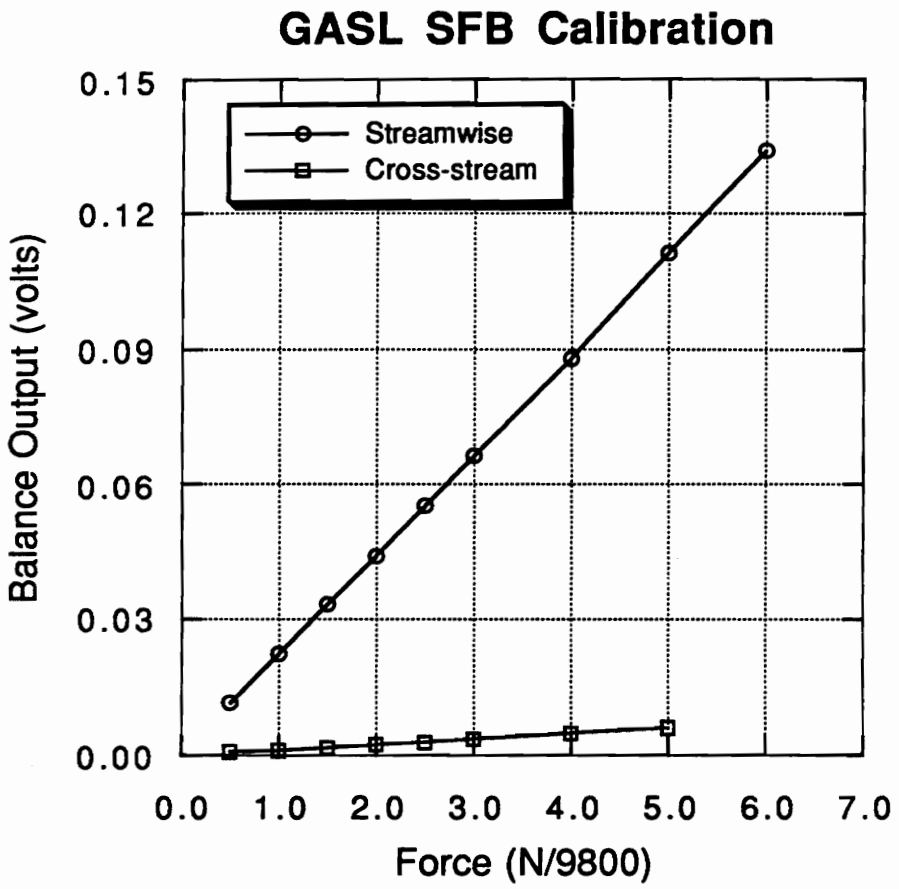

Figure 5.5 : Skin Friction Balance Calibration, GASL Design

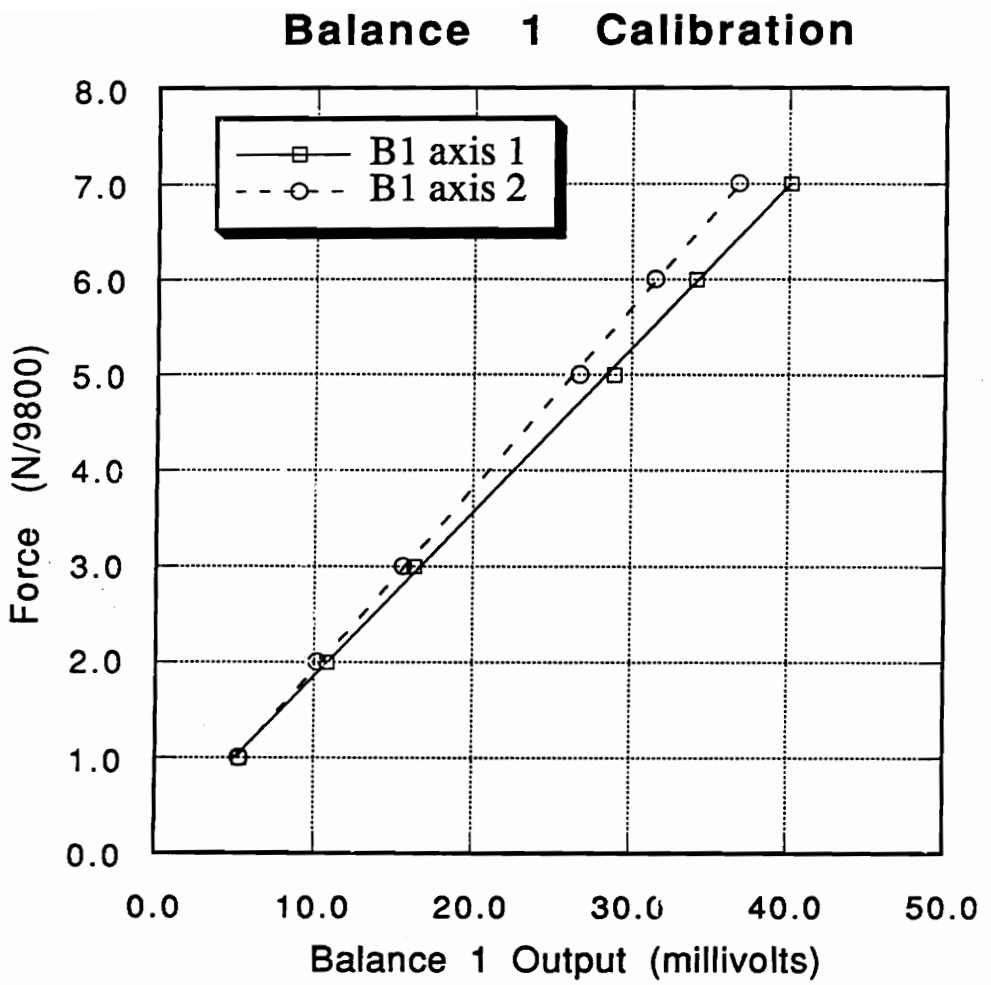

Figure 5.6 : Skin Friction Balance 1 Calibration, DCAF Design

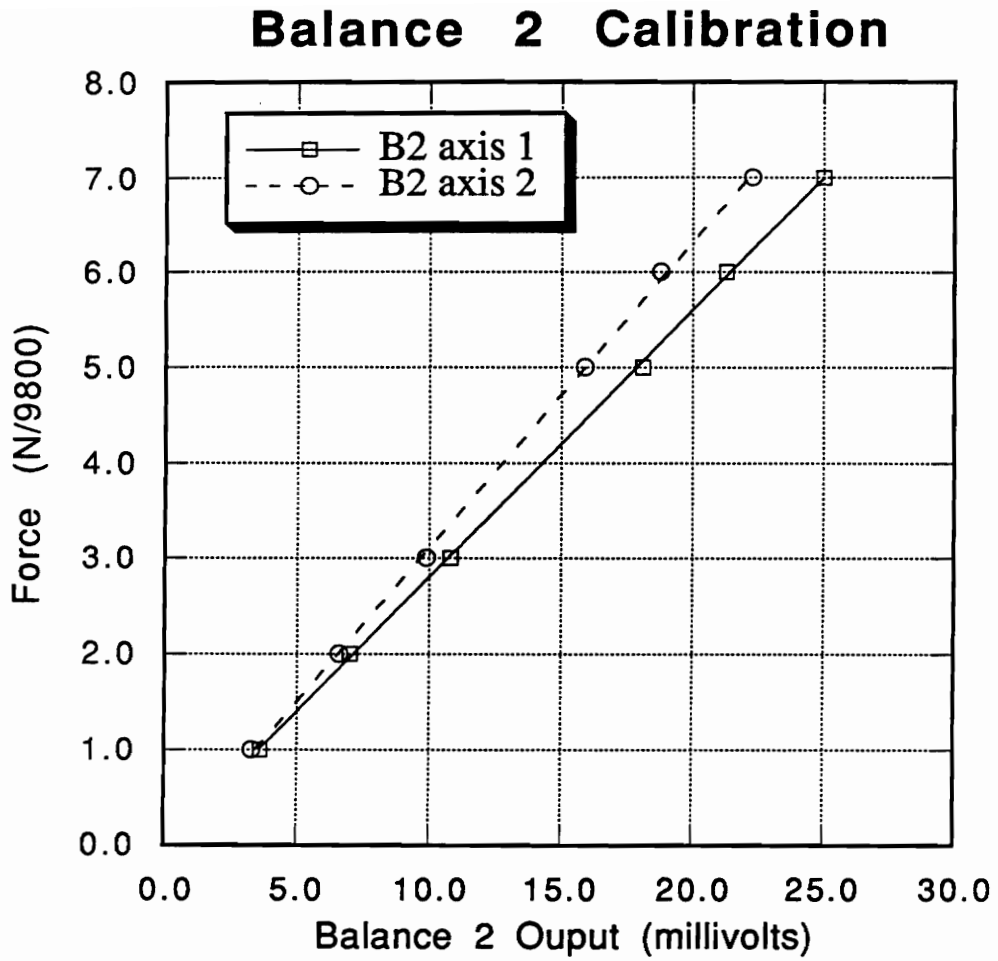

Figure 5.7 : Skin friction Balance 2 Calibration, DCAF Design

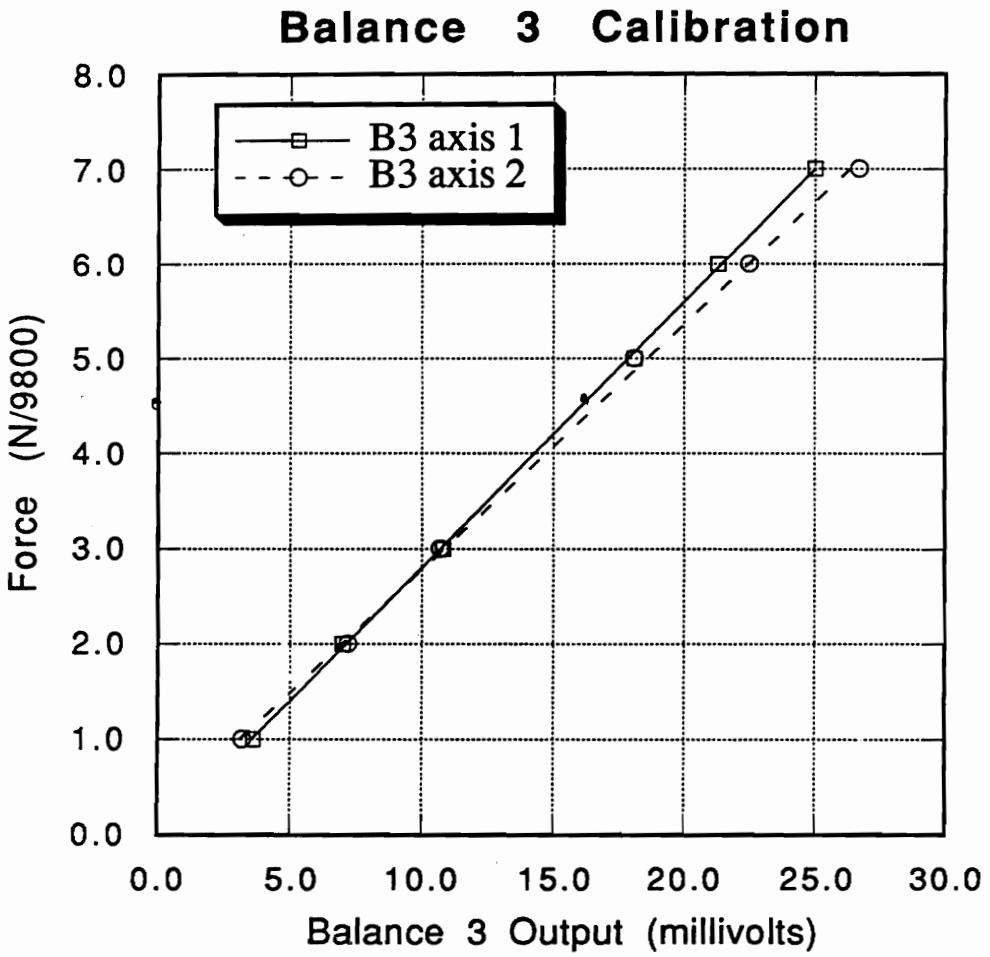

Figure 5.8 : Skin Friction Balance 3 Calibration, DCAF Design

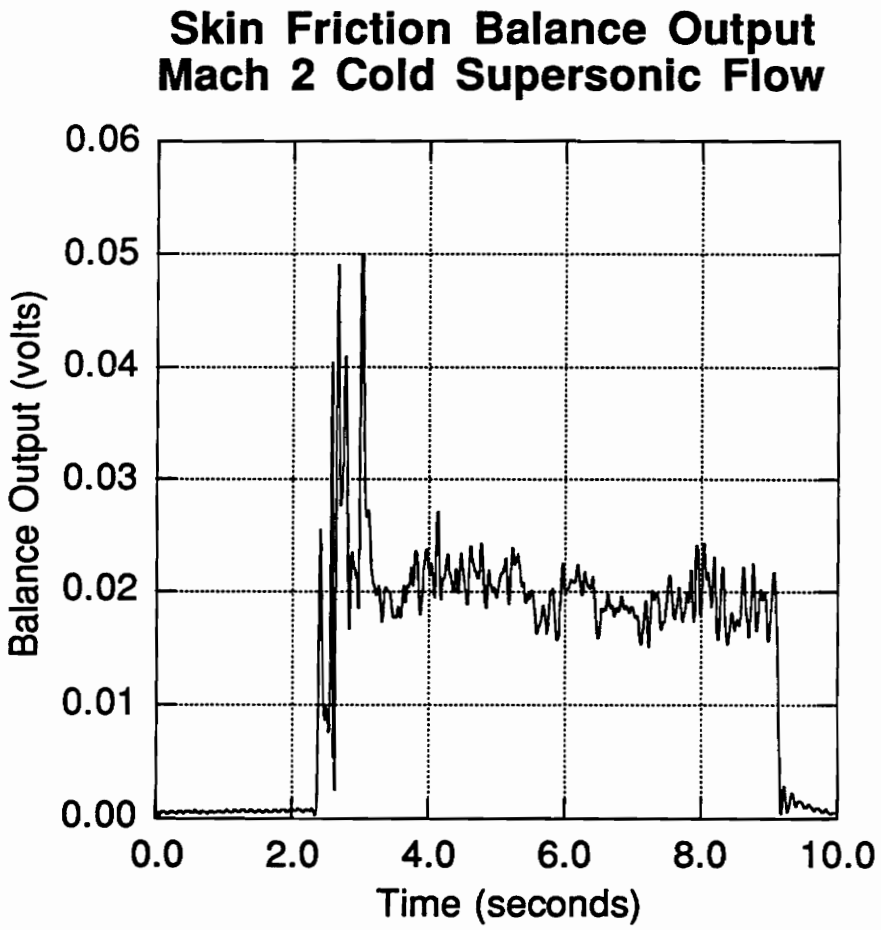

Figure 6.1 : Skin Friction Balance Output, Mach 3.0 Cold Supersonic Flow

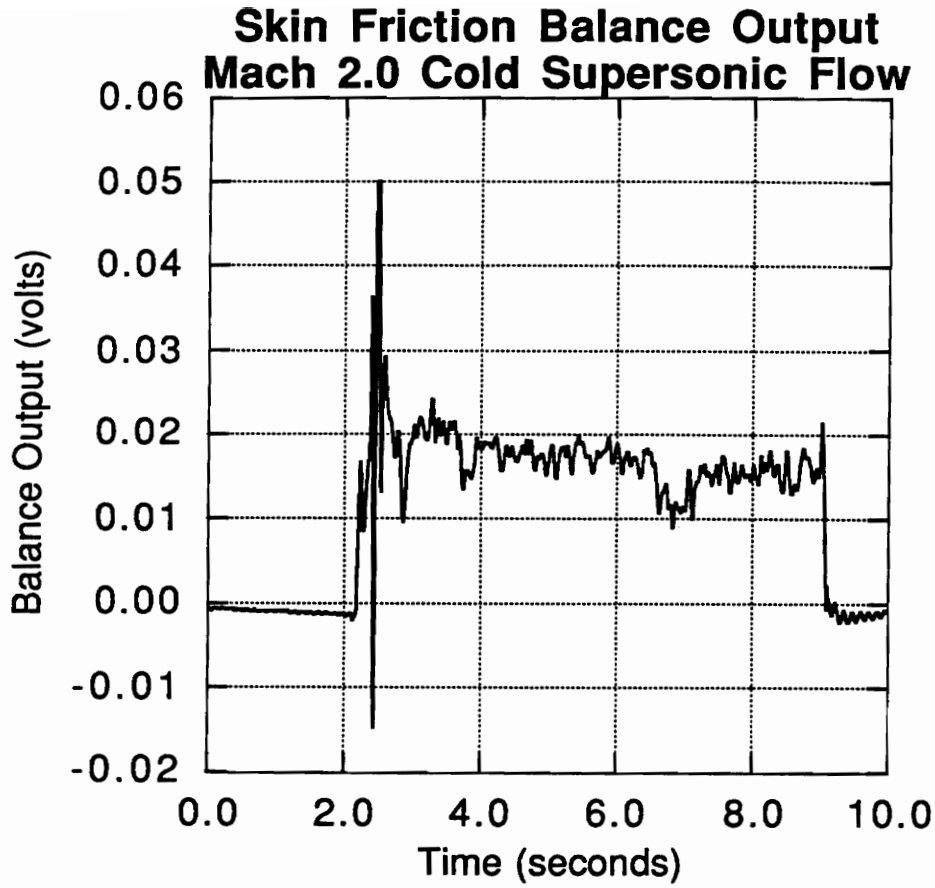

Figure 6.2 : Skin Friction Balance Output, Mach 2.0 Cold Supersonic Flow

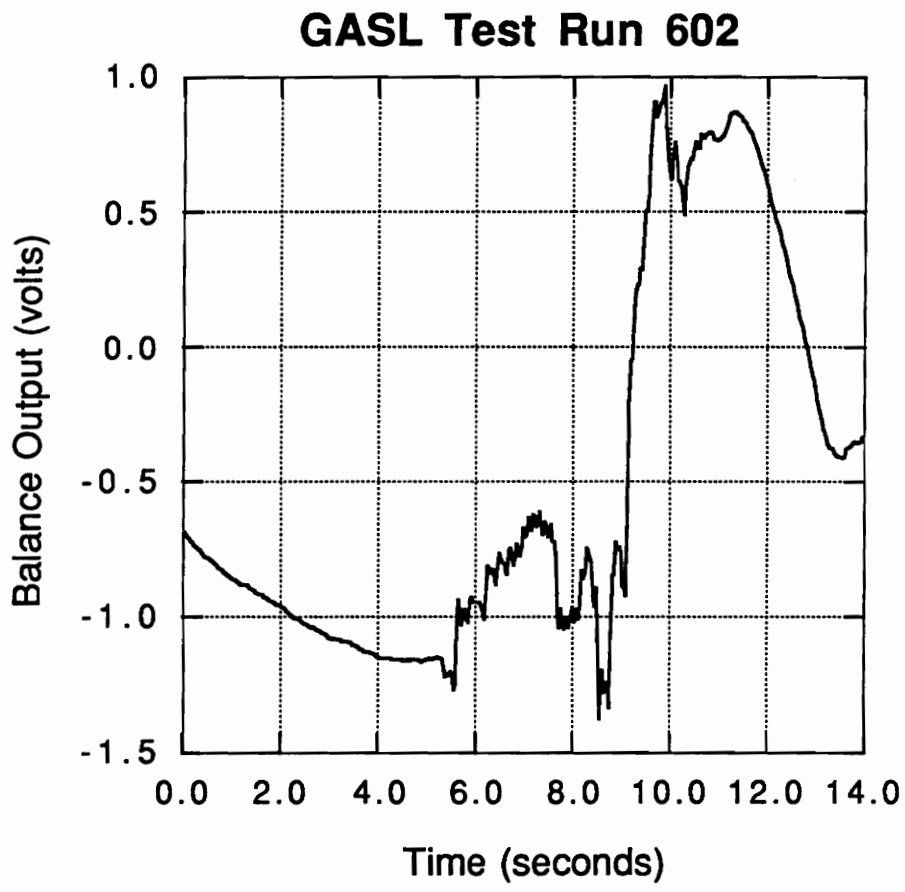

Figure 6.3 : Skin Friction Balance Output, GASL Test Series

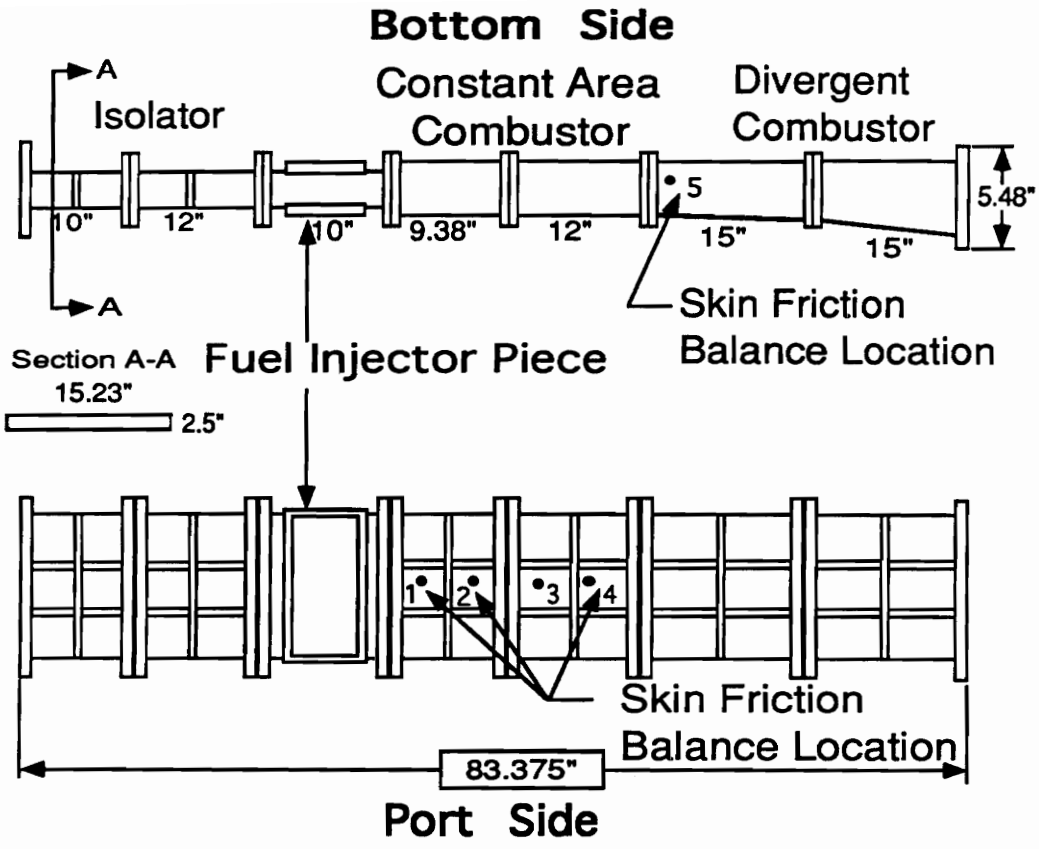

Figure 6.4 : Skin Friction Balance Locations, DCAF Combustor

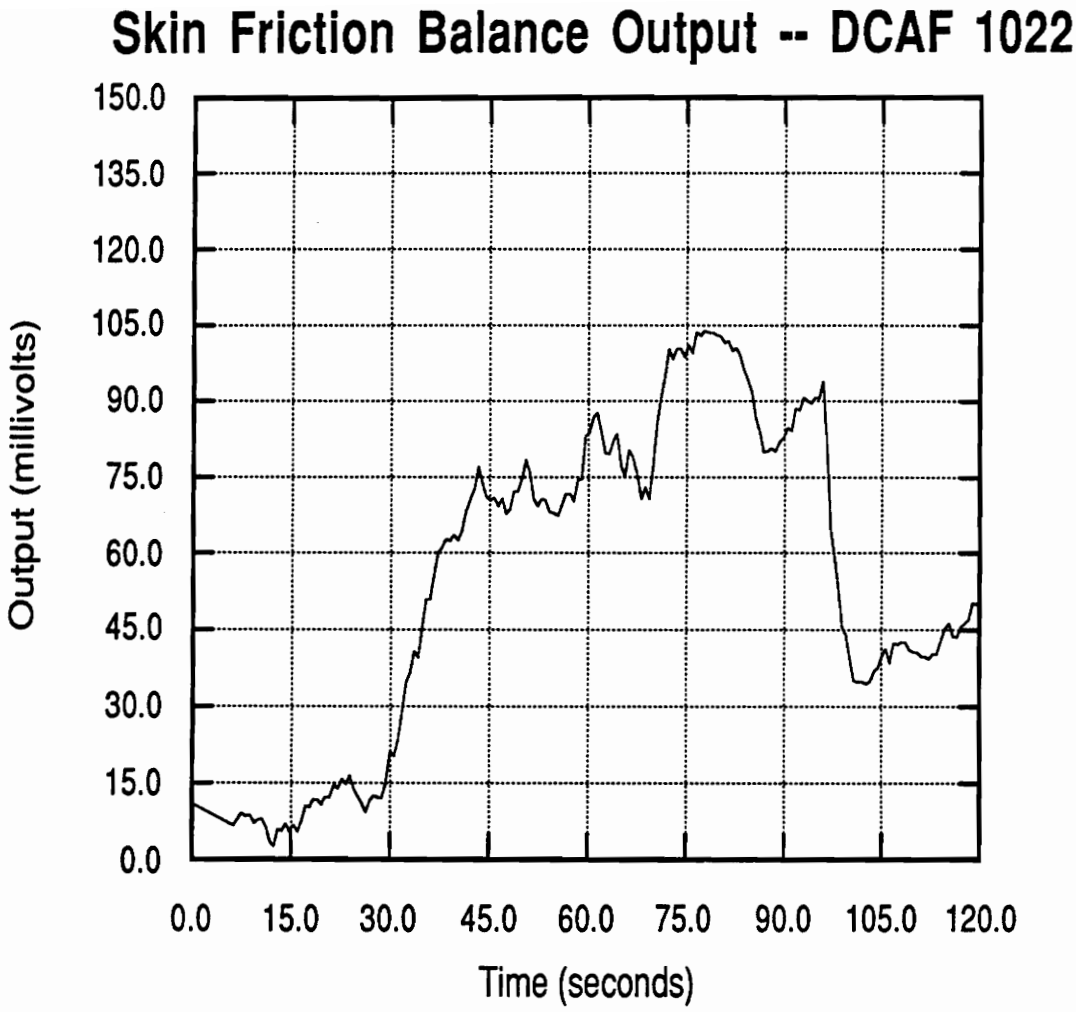

Figure 6.5 : Skin Friction Balance Output, DCAF 1022

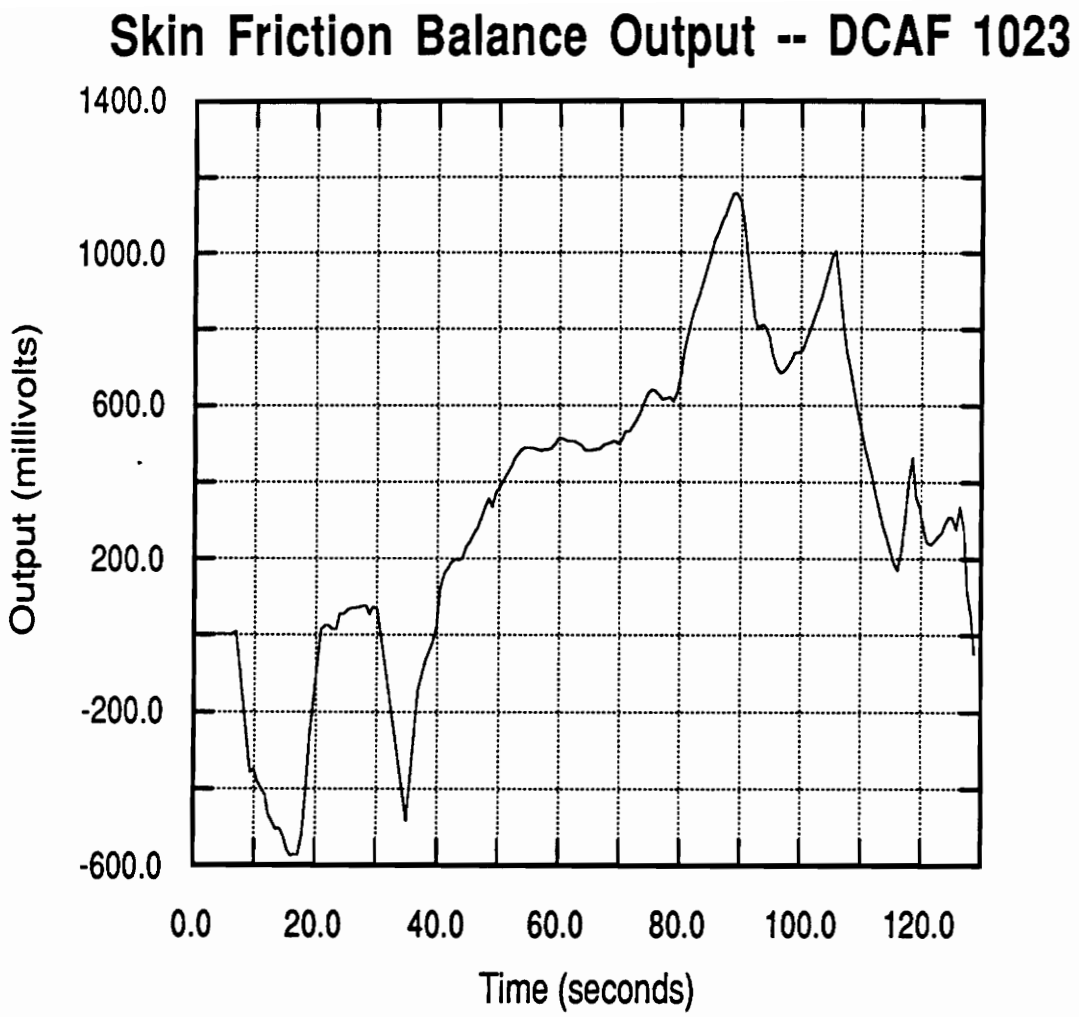

Figure 6.6 : Skin Friction Balance Output, DCAF 1023

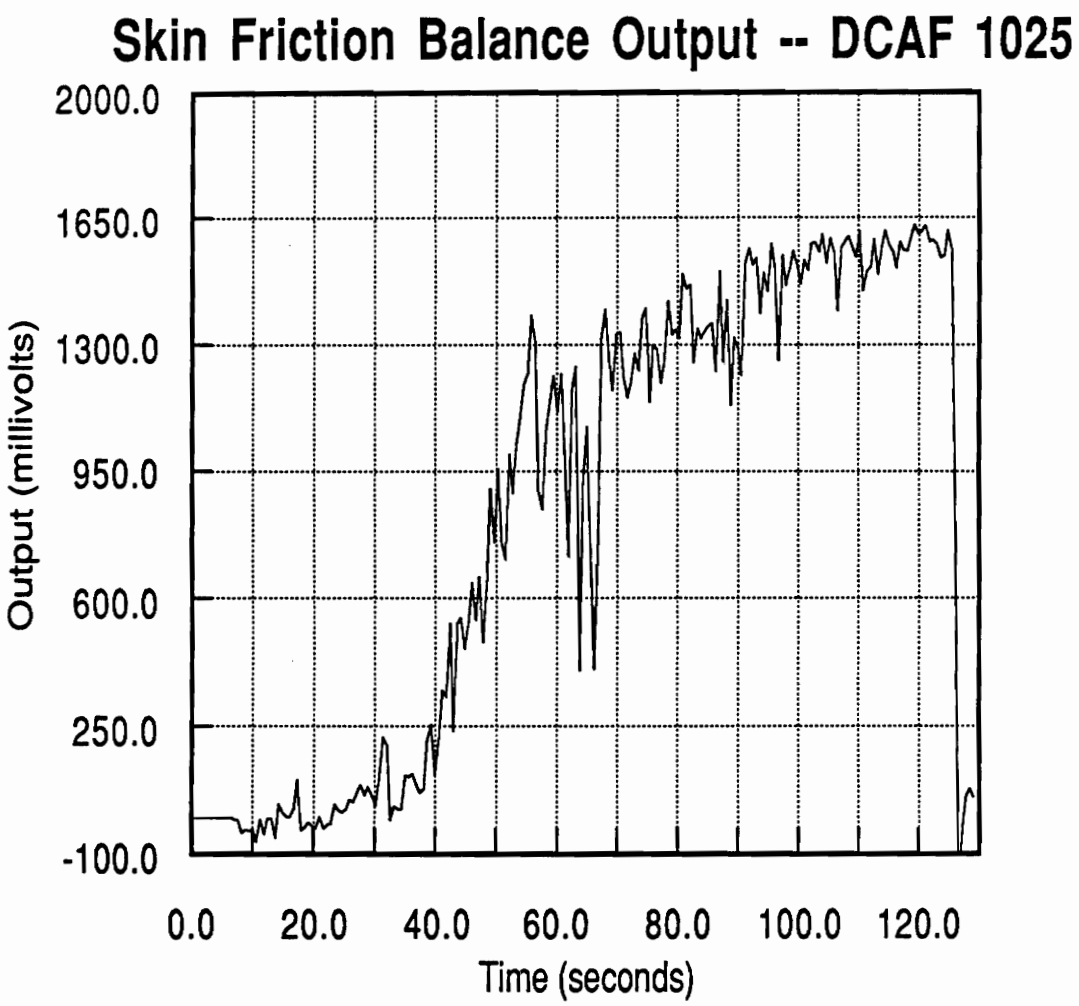

Figure 6.7 : Skin Friction Balance Output, DCAF 1025

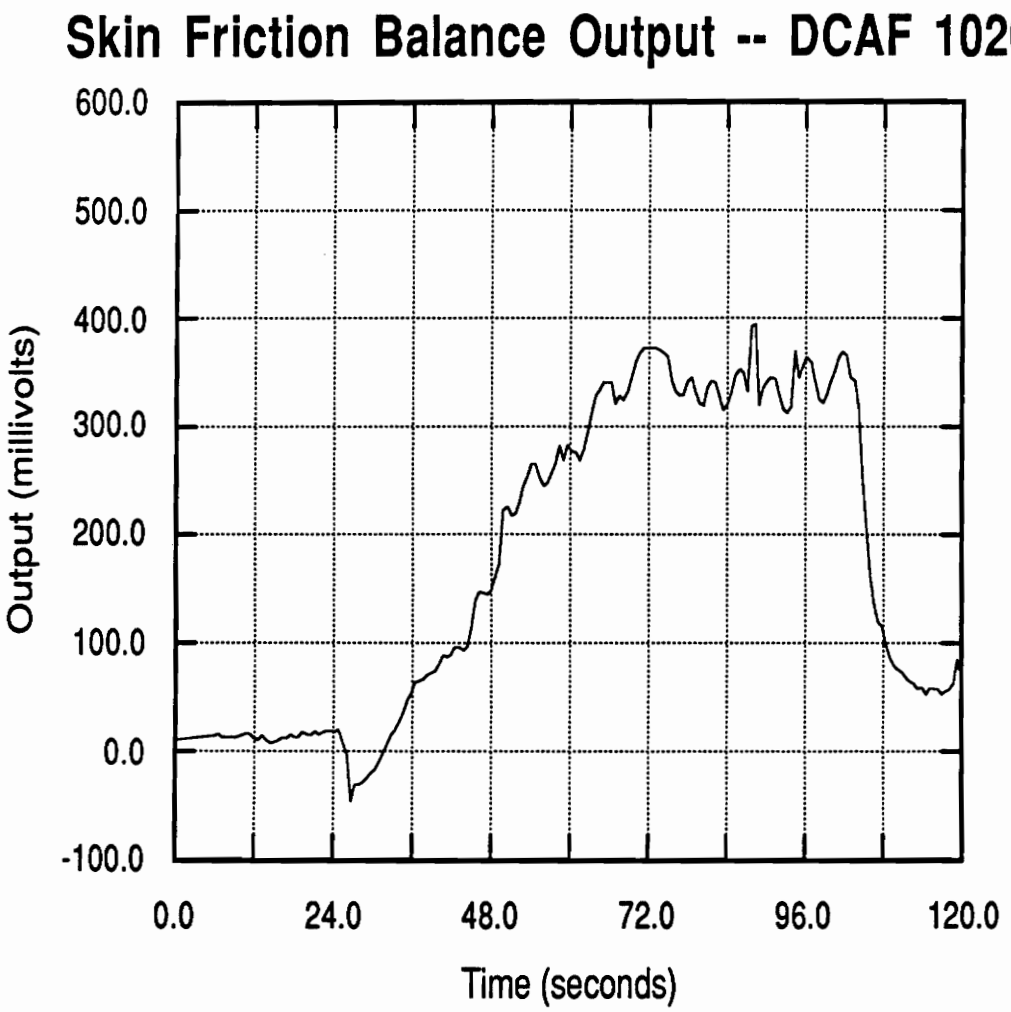

Figure 6.8 : Skin Friction Balance Output, DCAF 1026-3

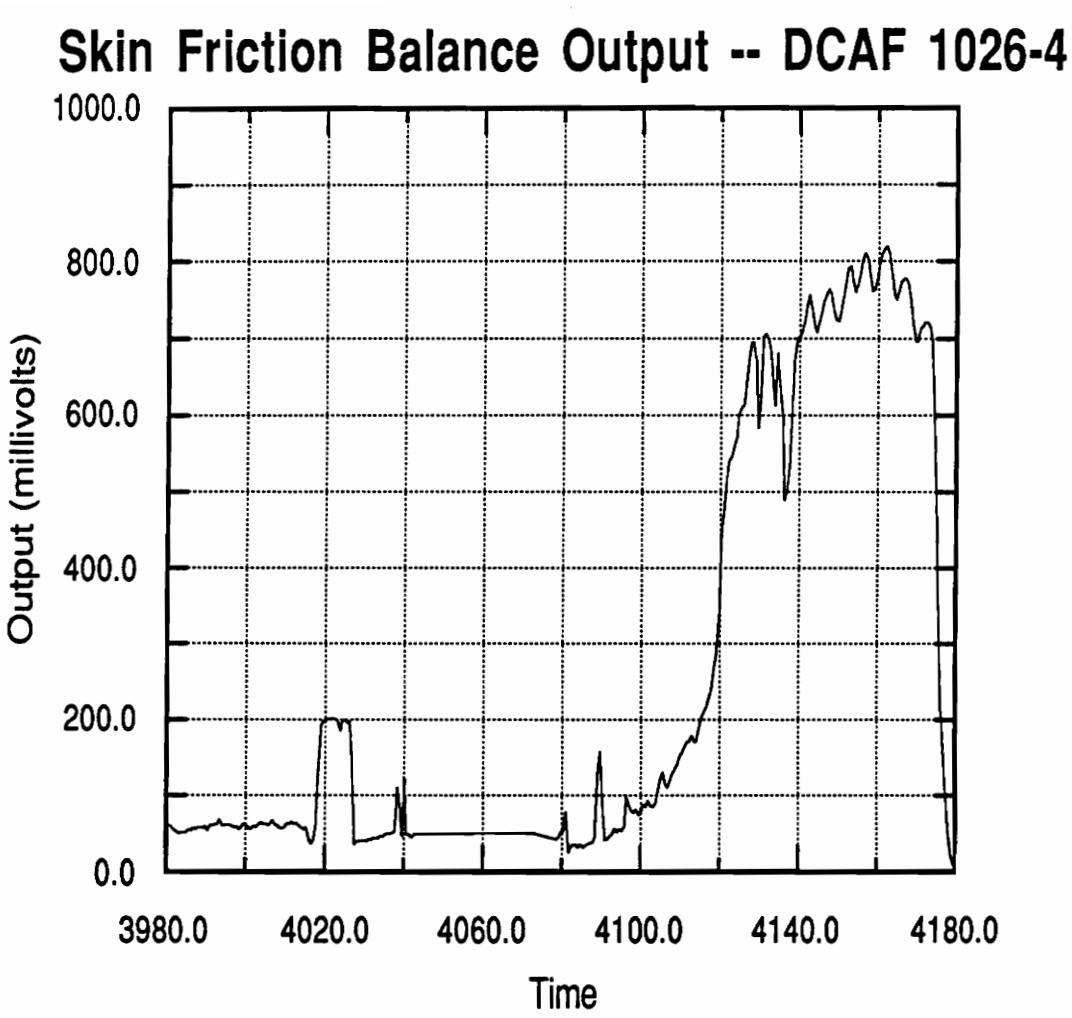

Figure 6.9 : Skin Friction Balance Output, DCAF 1026-4

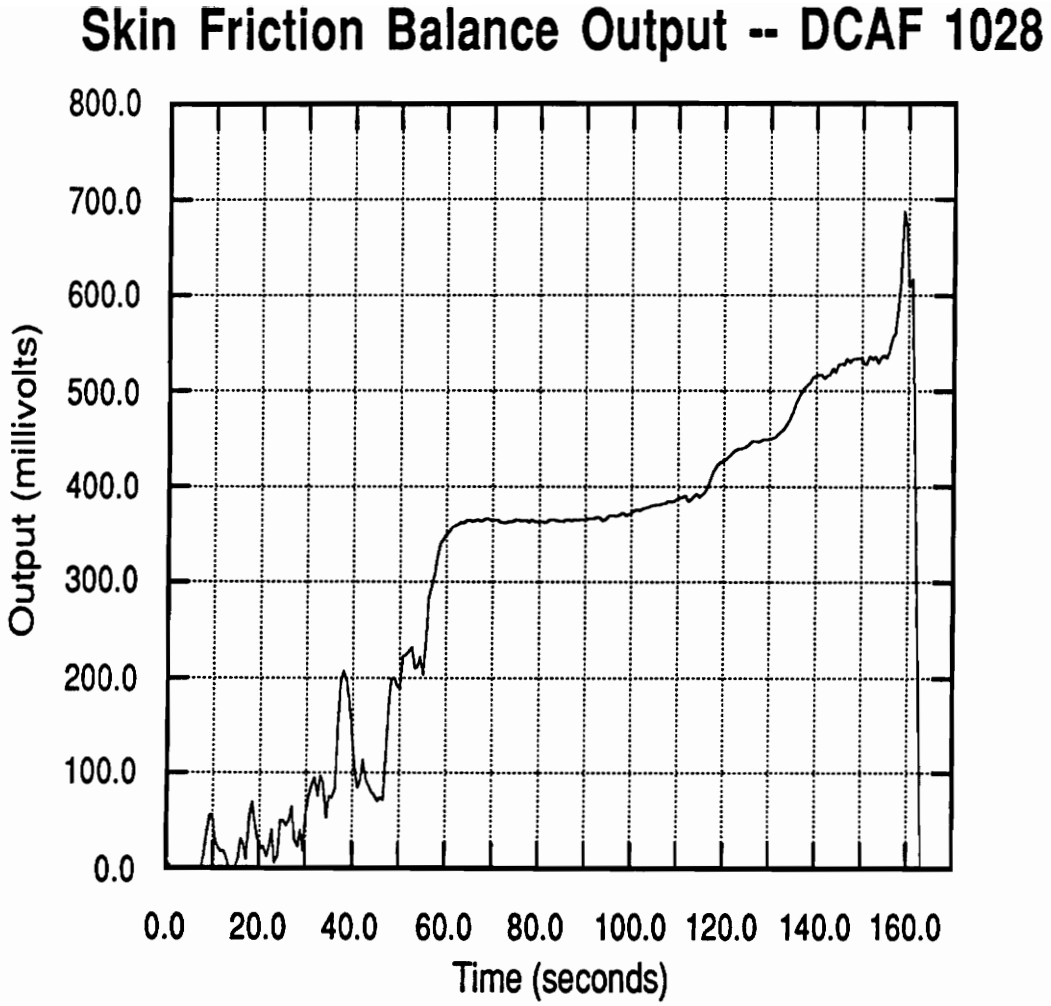

Figure 6.10 : Skin Friction Balance Output, DCAF 1028

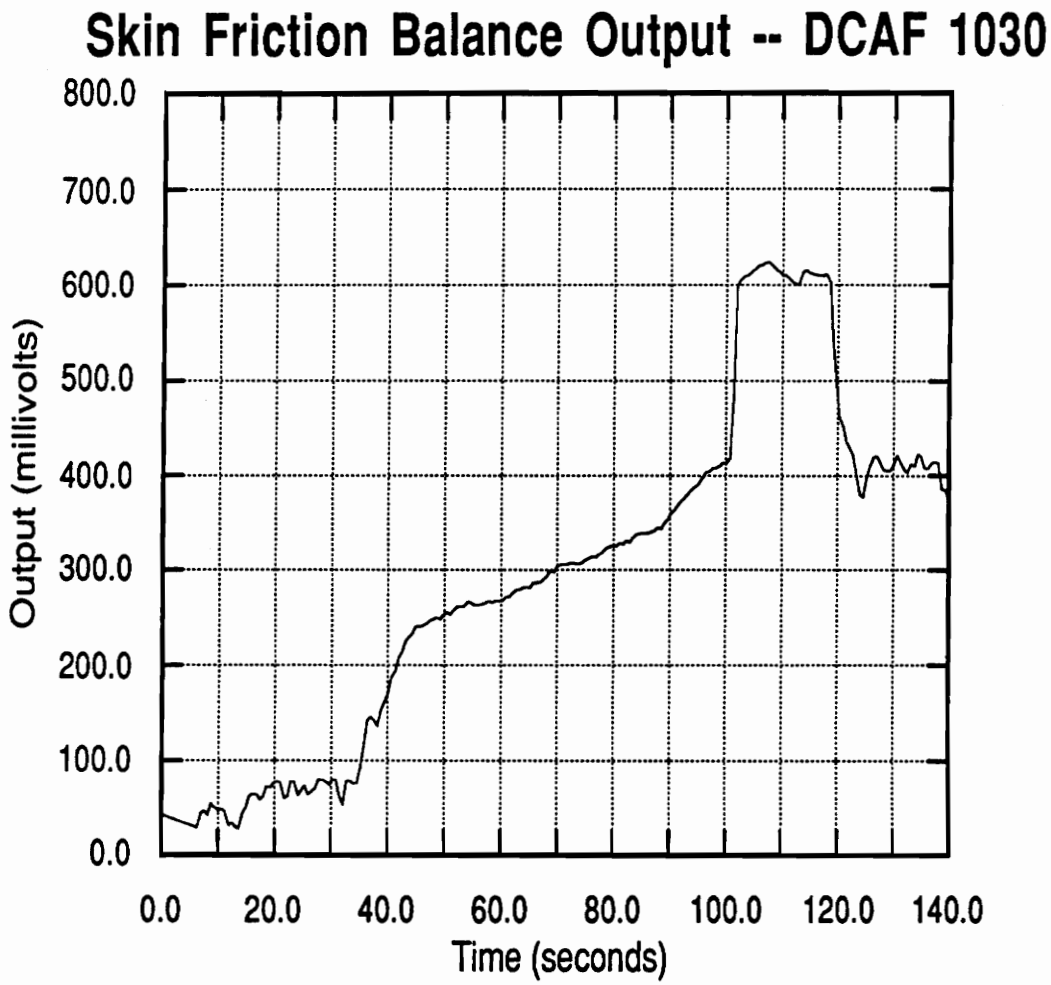

Figure 6.11 : Skin Friction Balance Output, DCAF 1030

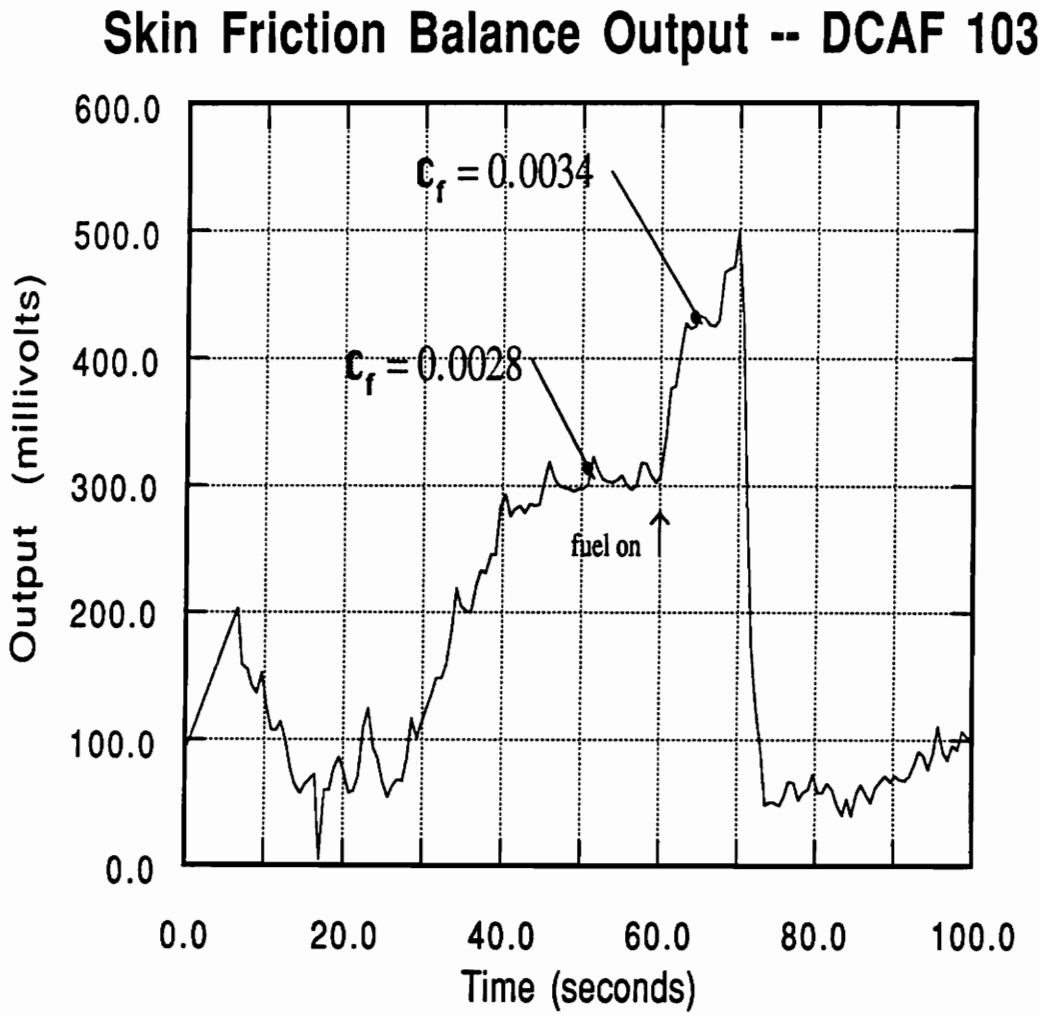

Figure 6.12 : Skin Friction Balance Output, DCAF 1031

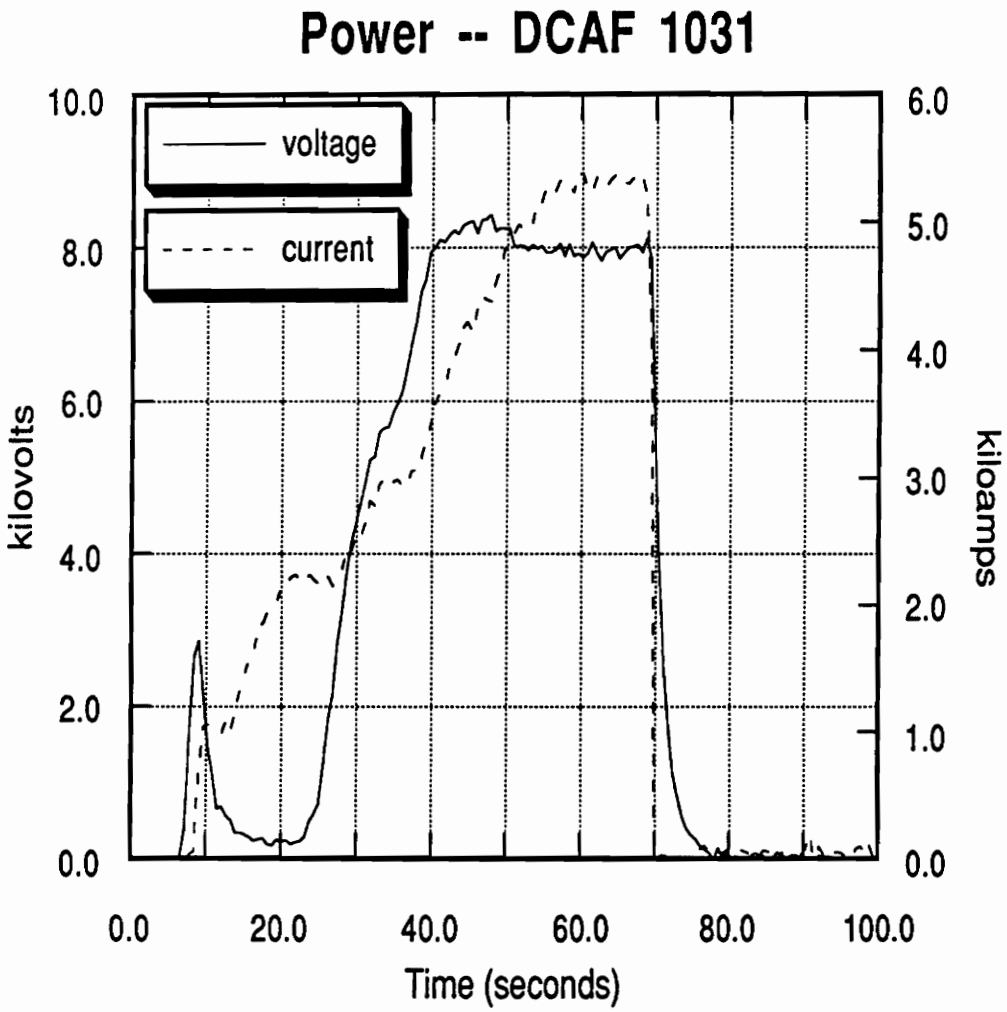

Figure 6.13 : Arc Heater Power, DCAF 1031

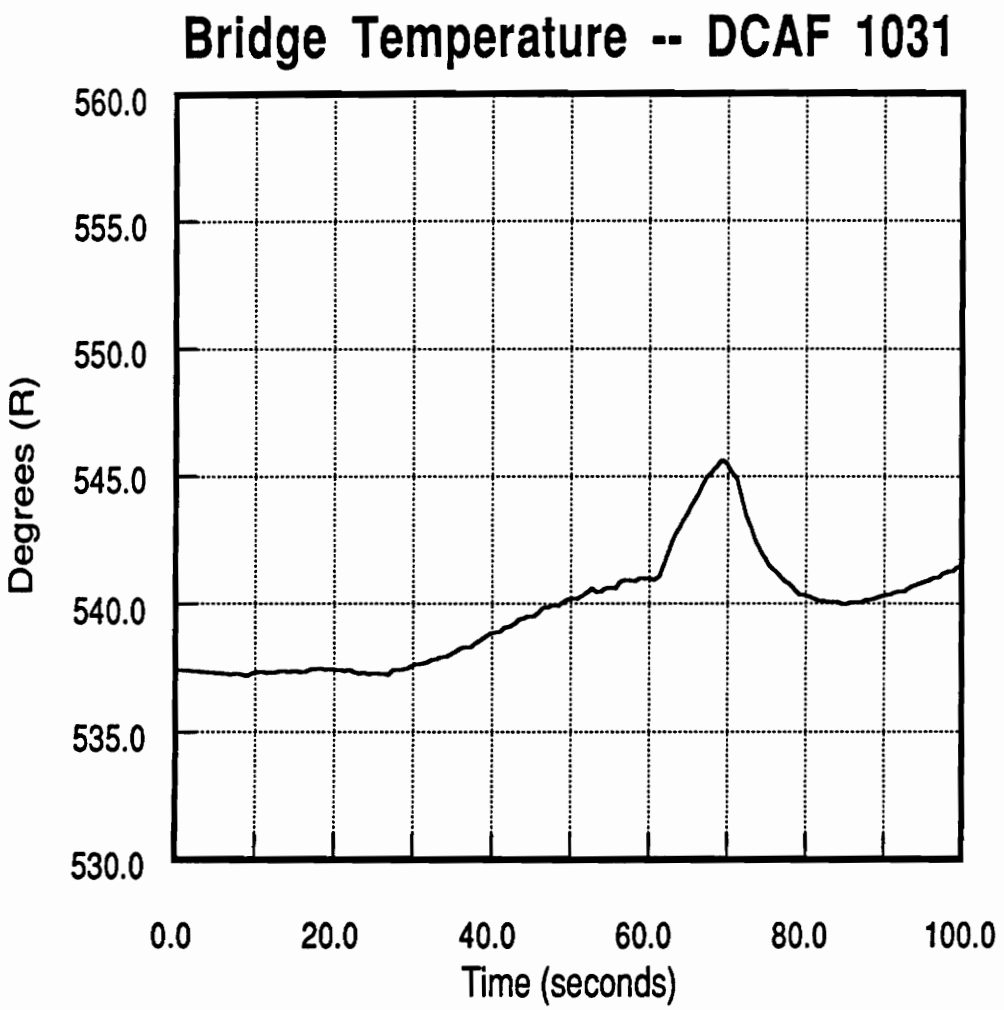

Figure 6.14 : Strain Gage Temperature, DCAF 1031

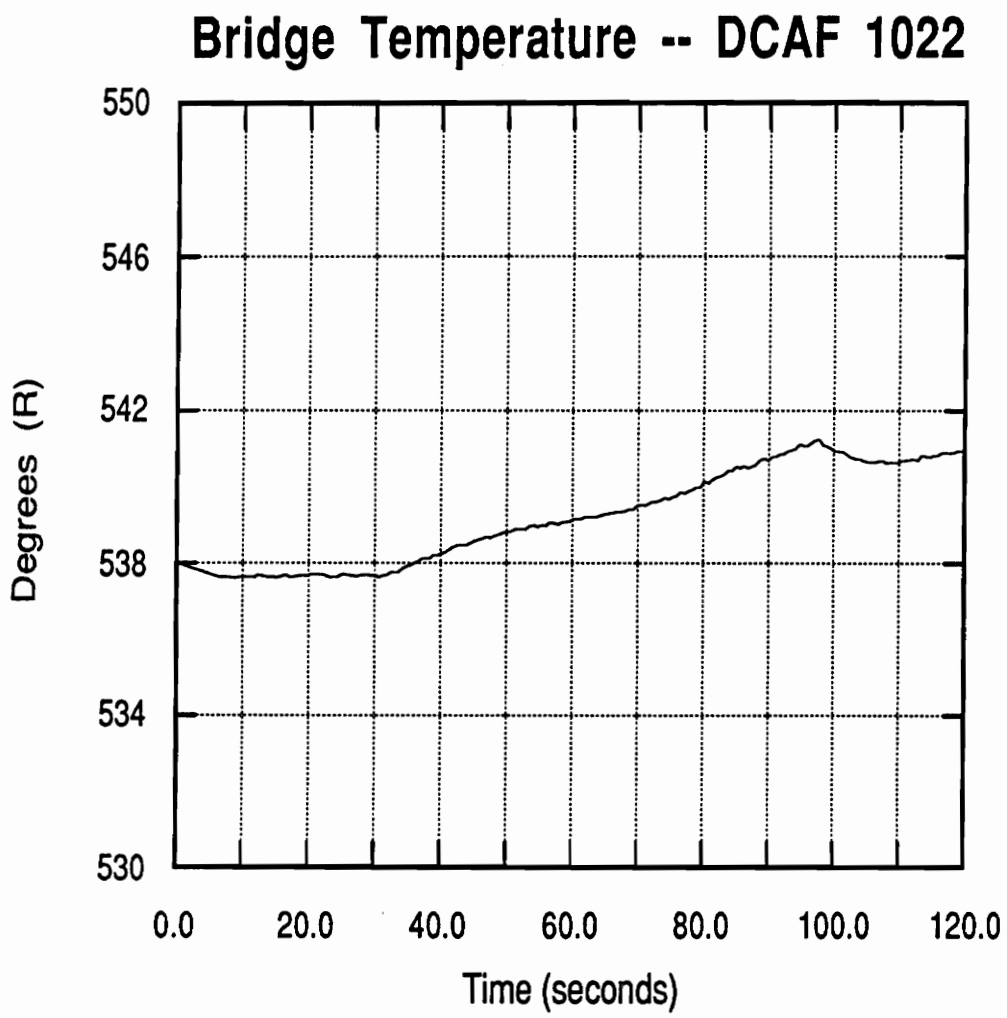

Figure 6.15 : Strain Gage Temperature, DCAF 1022

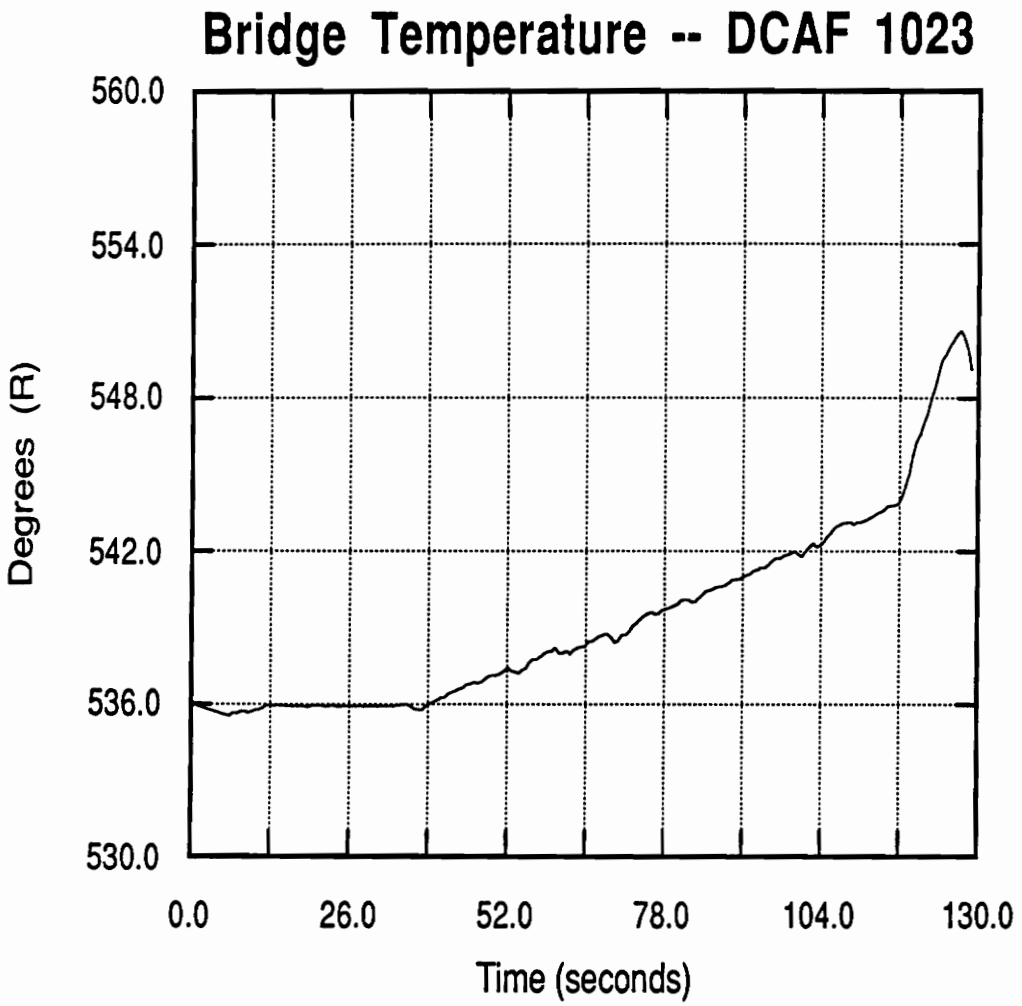

Figure 6.16 : Strain Gage Temperature, DCAF 1023

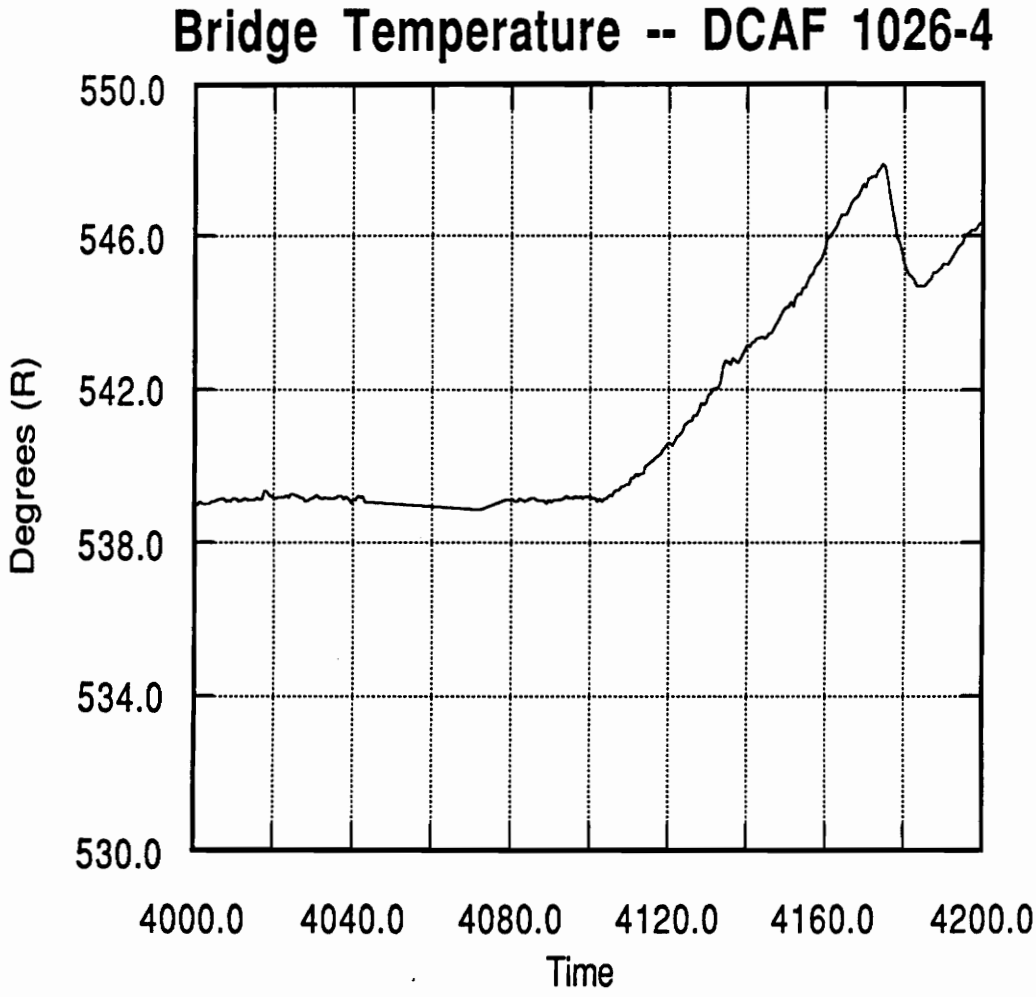

Figure 6.17 : Strain Gage Temperature, DCAF 1026-4

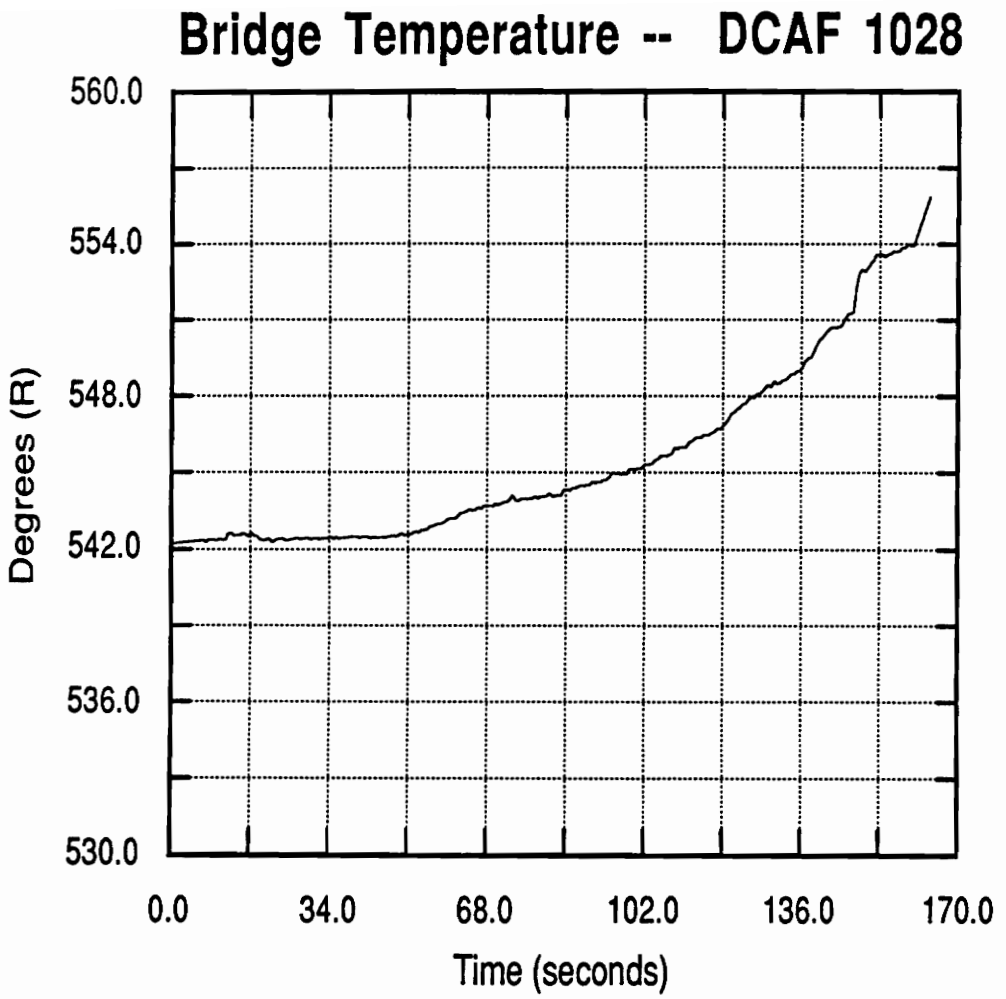

Figure 6.18 : Strain Gage Temperature, DCAF 1028

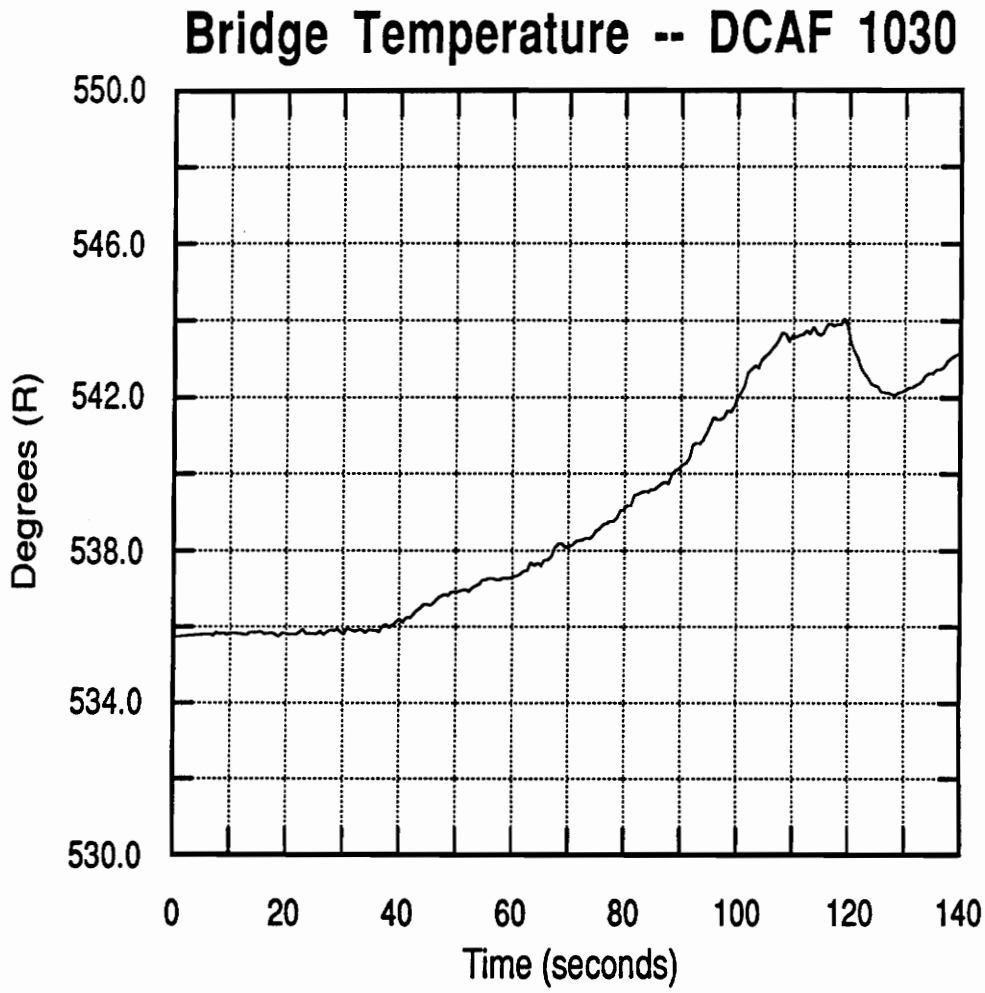

Figure 6.19 : Strain Gage Temperature, DCAF 1030

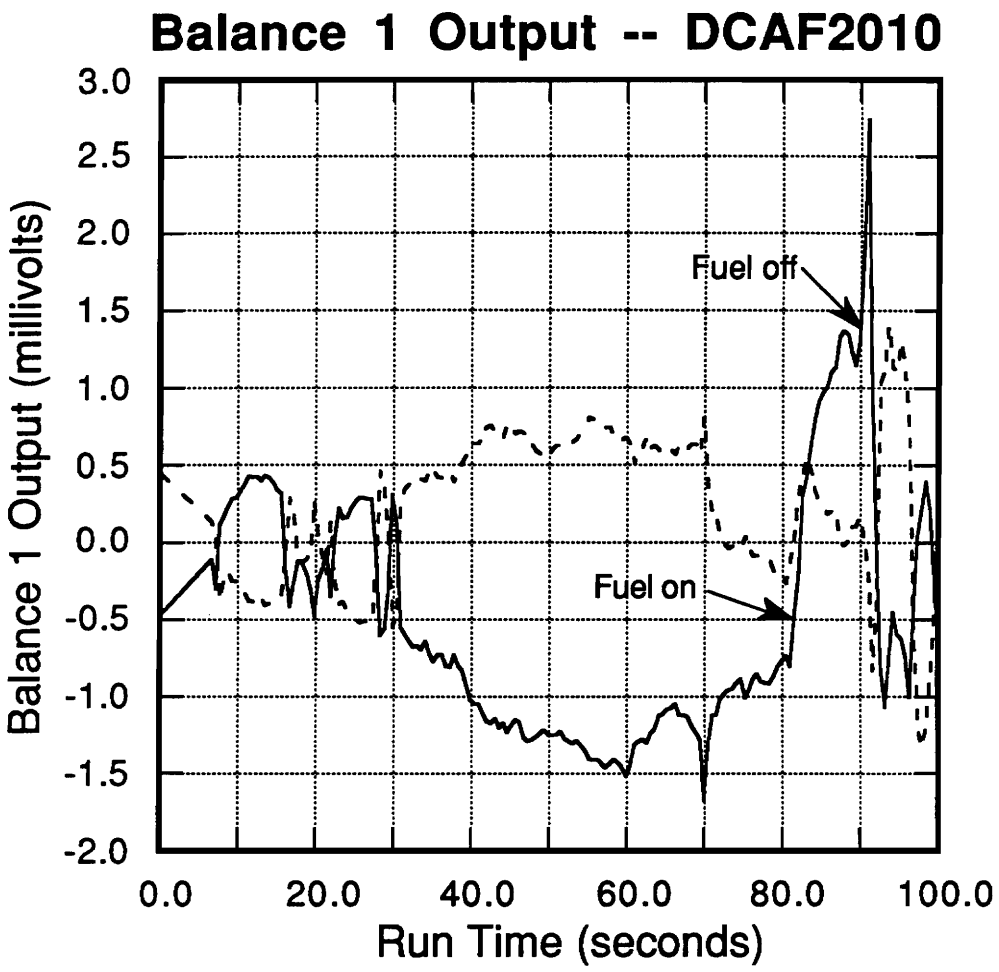

Figure 6.20 : Skin Friction Balance Output, DCAF 2010, Balance 1

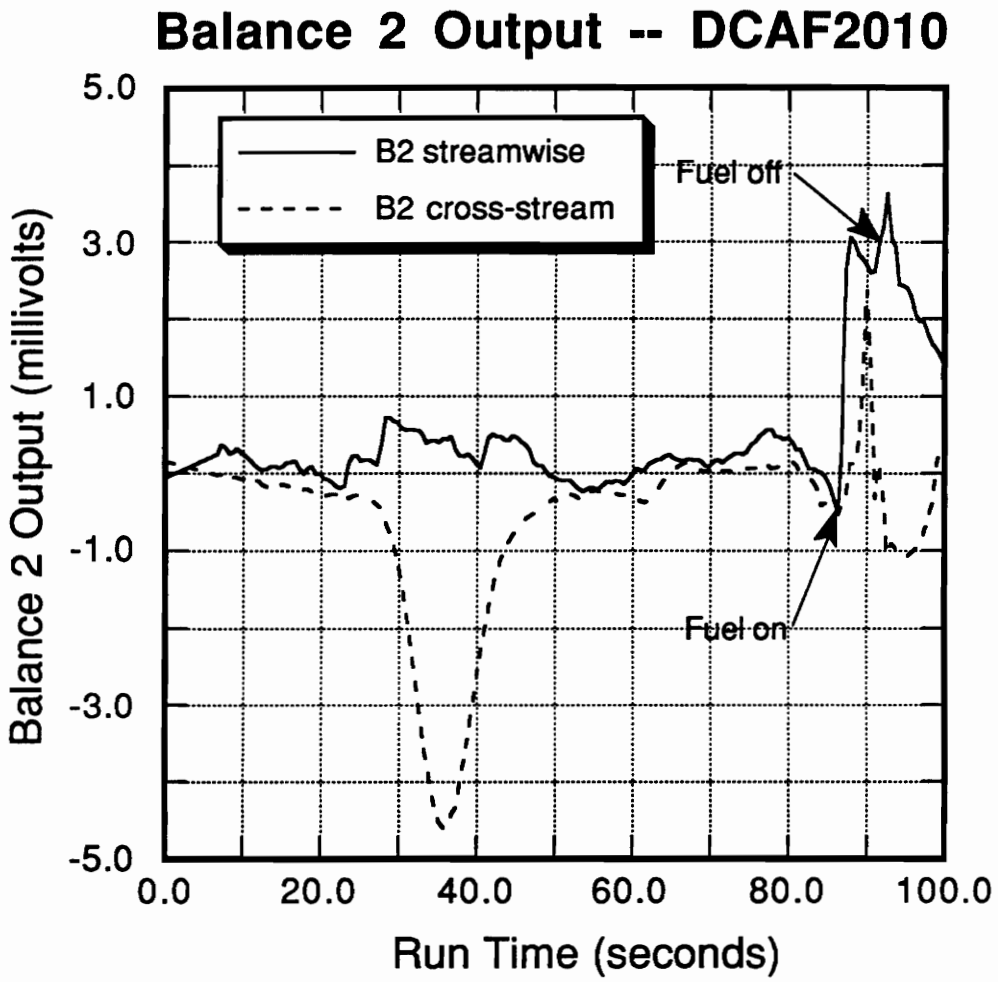

Figure 6.21 : Skin Friction Balance Output, DCAF 2010, Balance 2

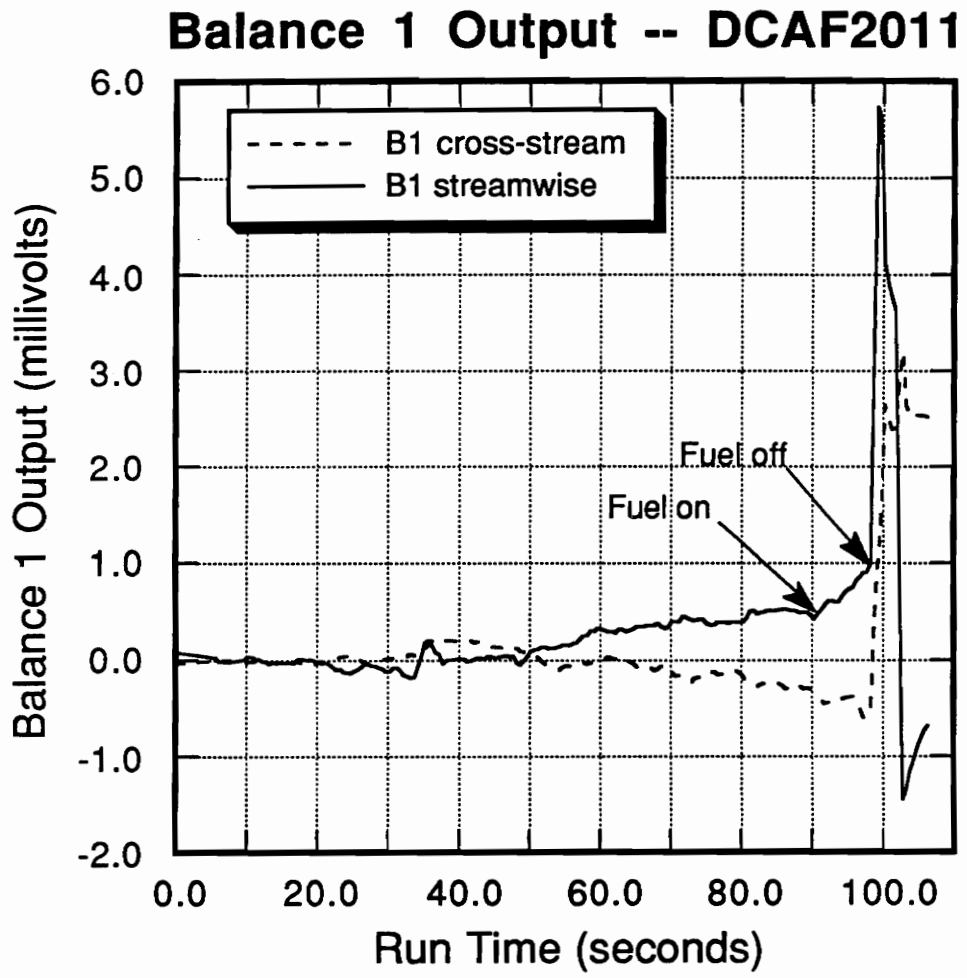

Figure 6.22 : Skin Friction Balance Output, DCAF 2011, Balance 1

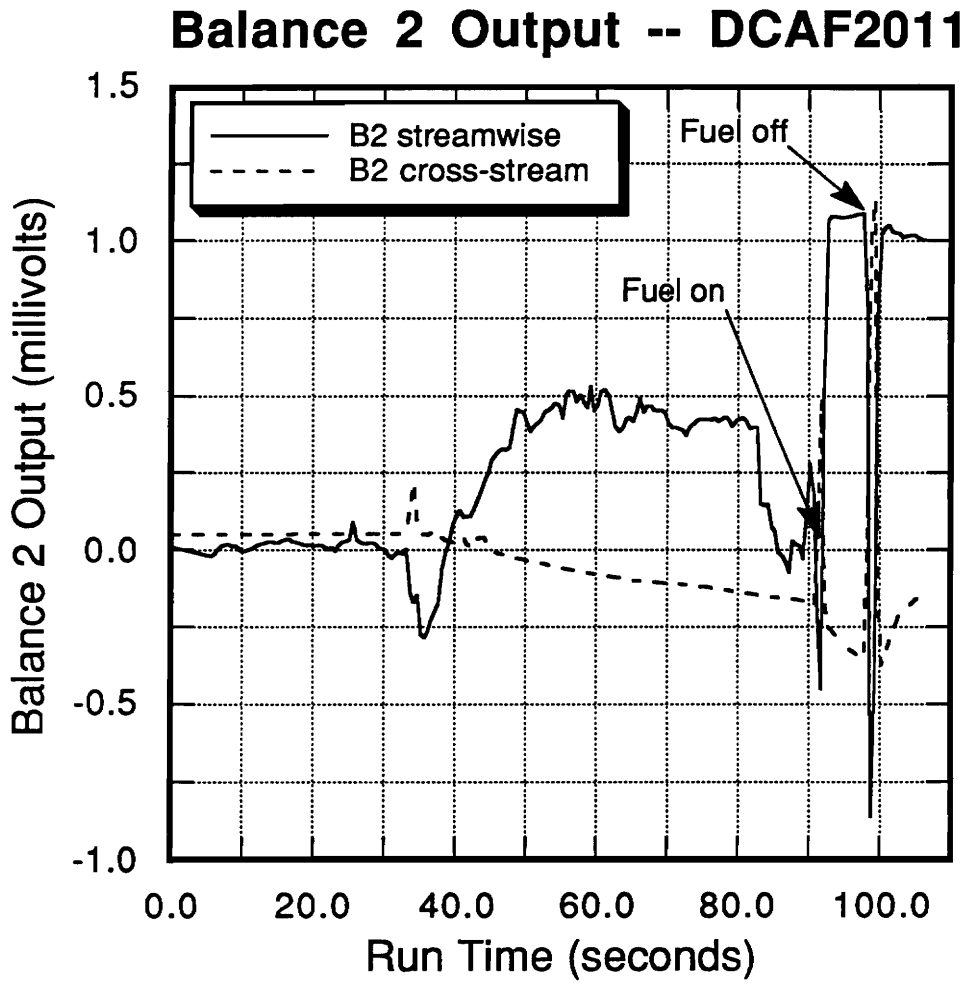

Figure 6.23 : Skin Friction Balance Output, DCAF 2011, Balance 2

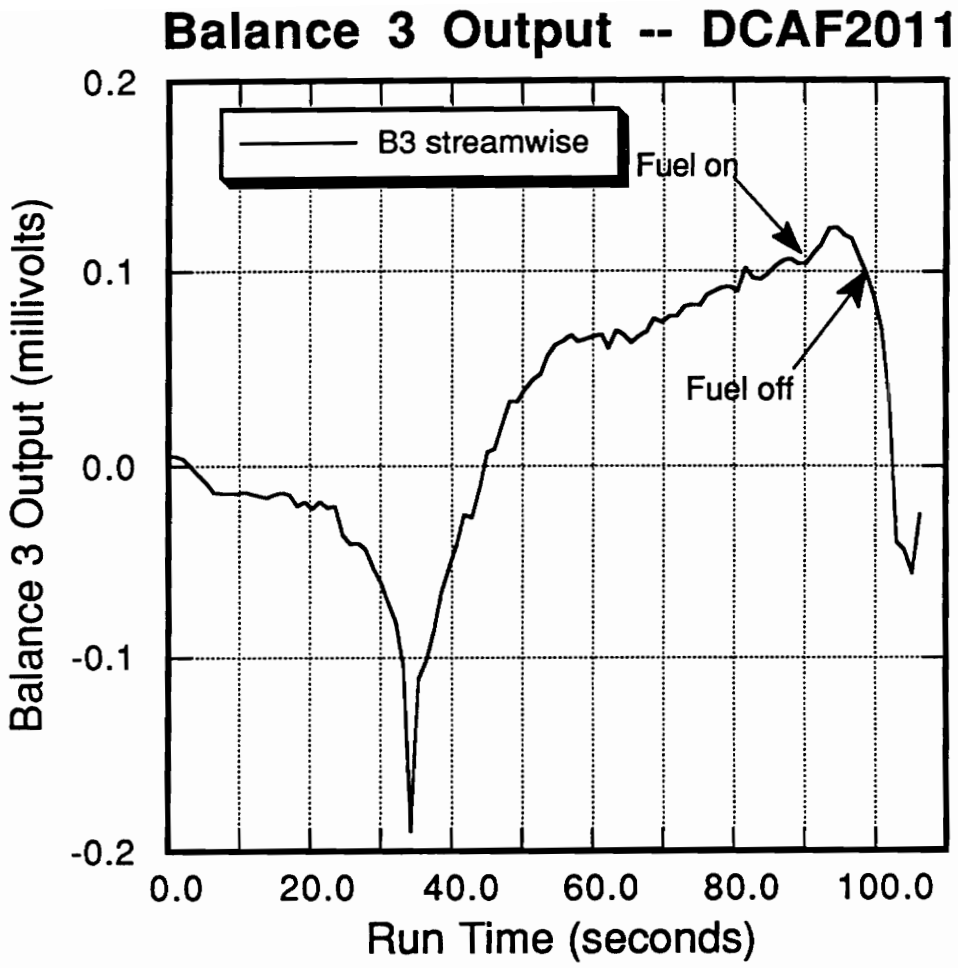

Figure 6.24 : Skin Friction Balance Output, DCAF 2011, Balance 3

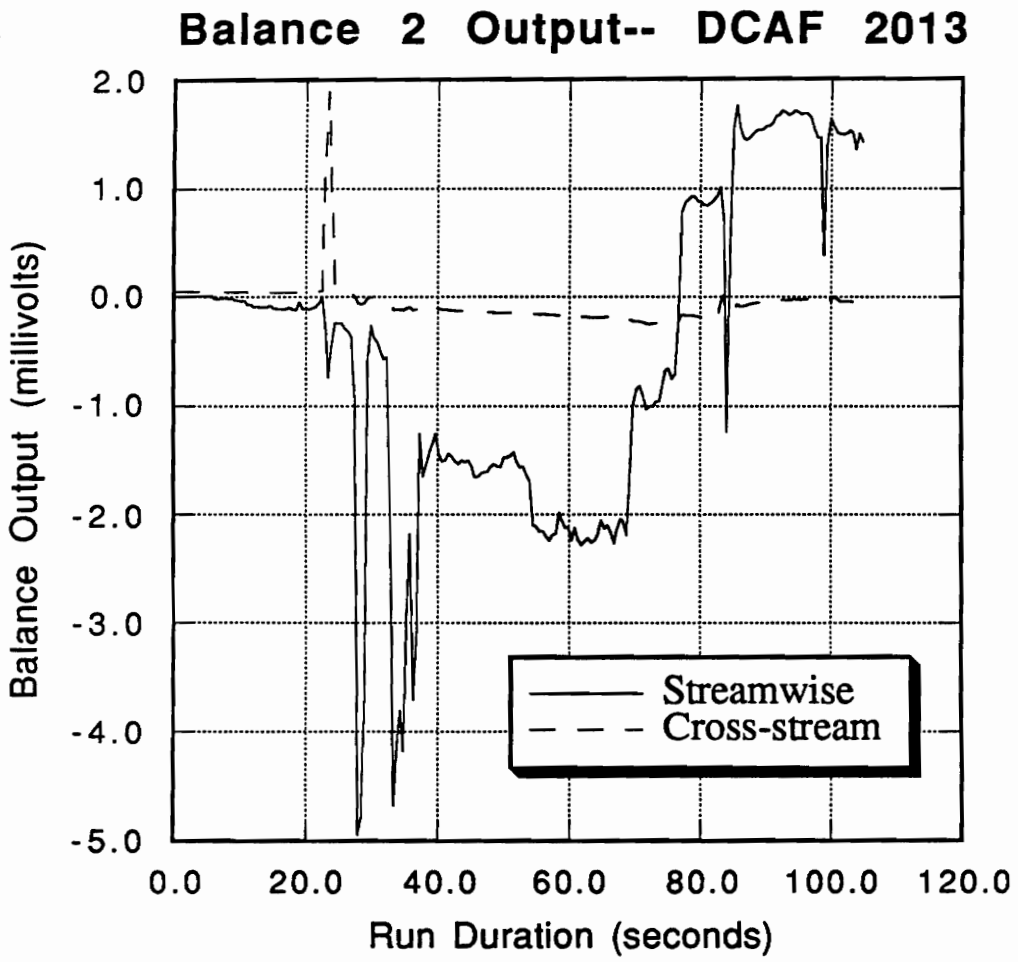

Figure 6.25 : Skin Friction Balance Output, DCAF 2013, Balance 2

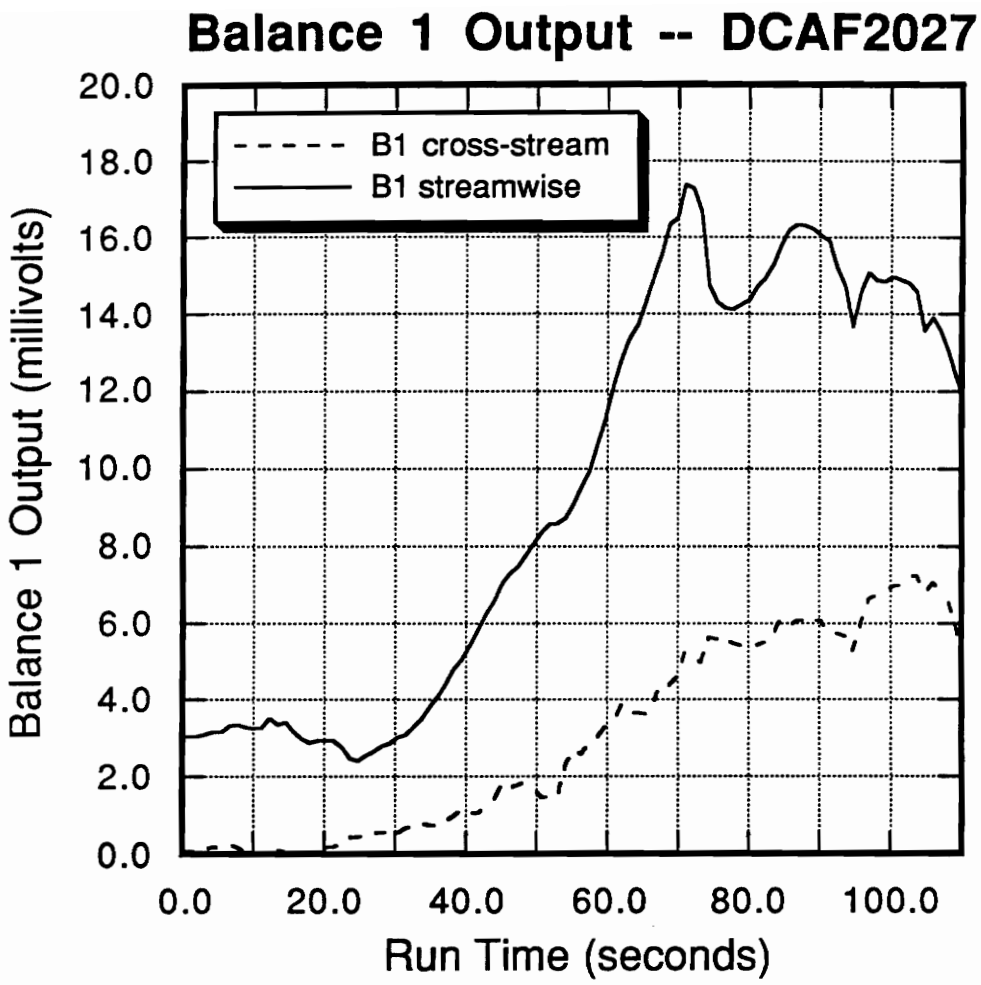

Figure 6.26 : Skin Friction Balance Output, DCAF 2027, Balance 1

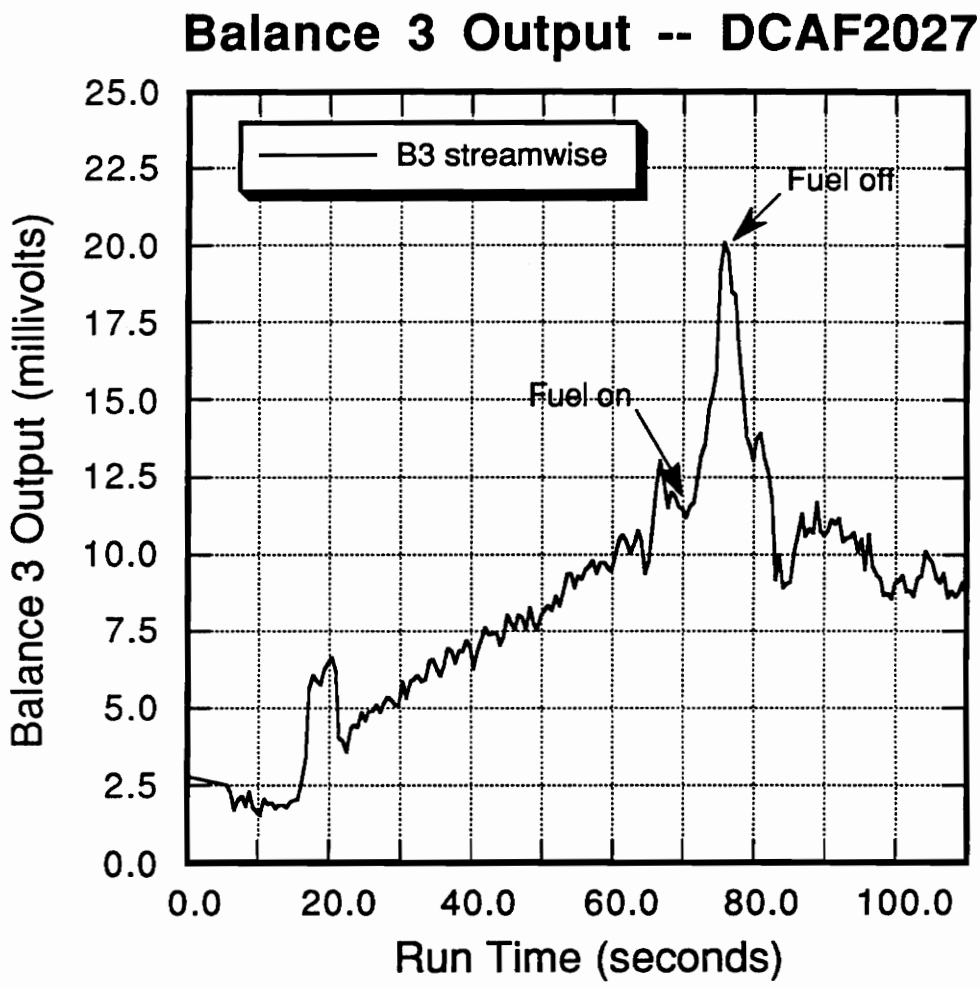

Figure 6.27 : Skin Friction Balance Output, DCAF 2027, Balance 3

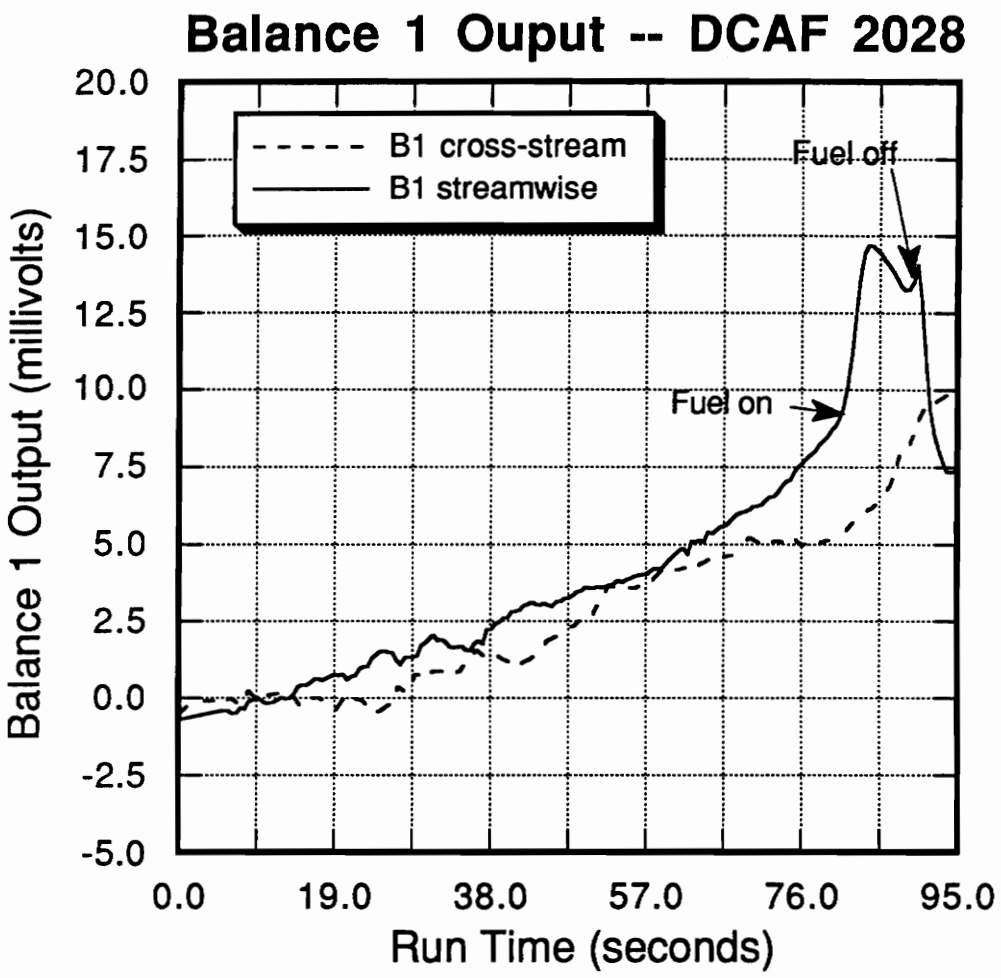

Figure 6.28 : Skin Friction Balance Output, DCAF 2028, Balance 1

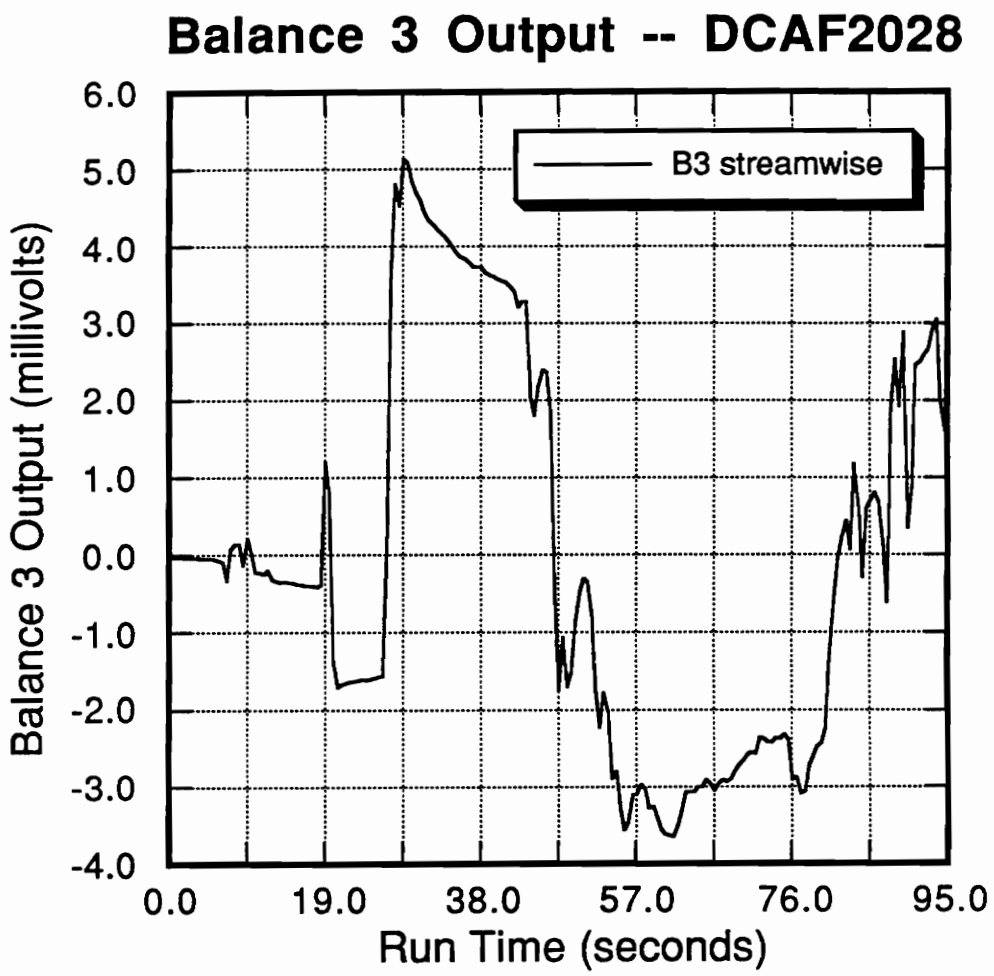

Figure 6.29 : Skin Friction Balance Output, DCAF 2028, Balance 3

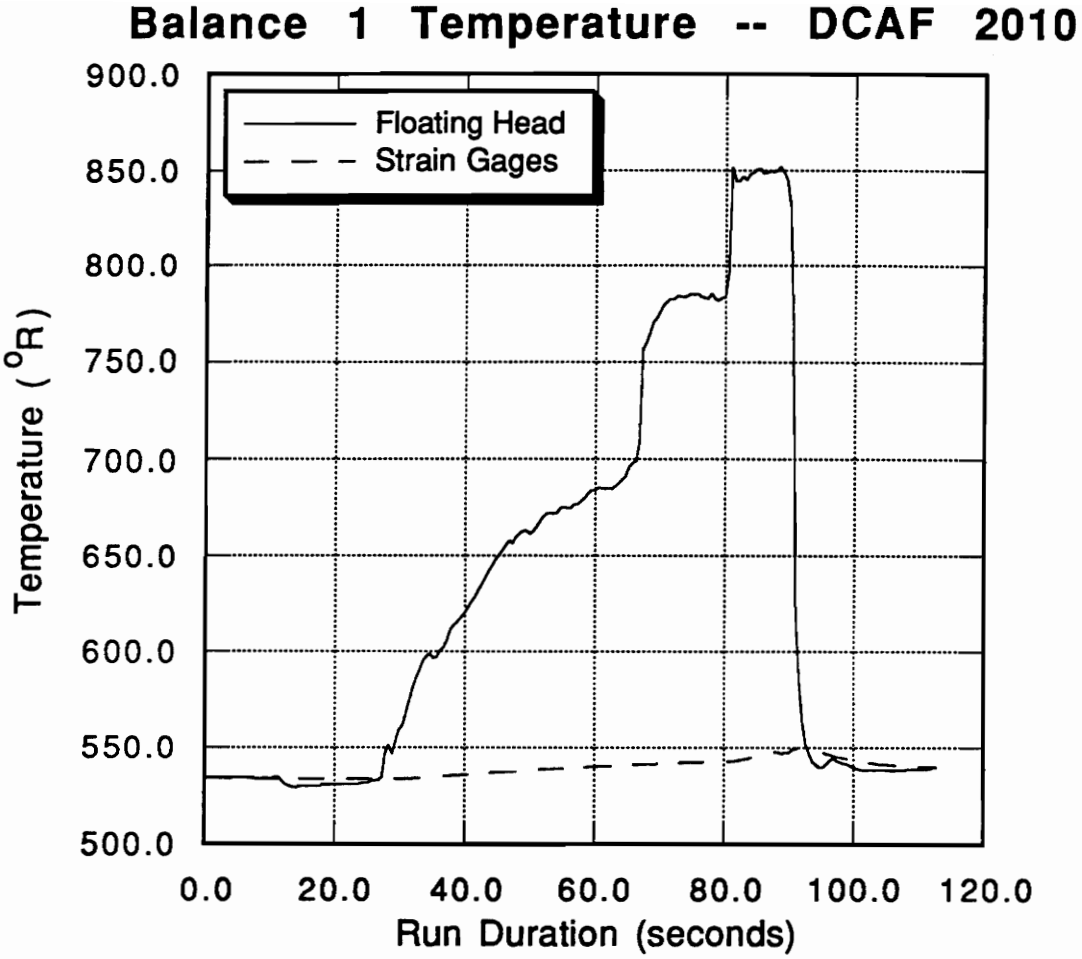

Figure 6.30 : Skin Friction Balance 1 Temperatures, DCAF 2010

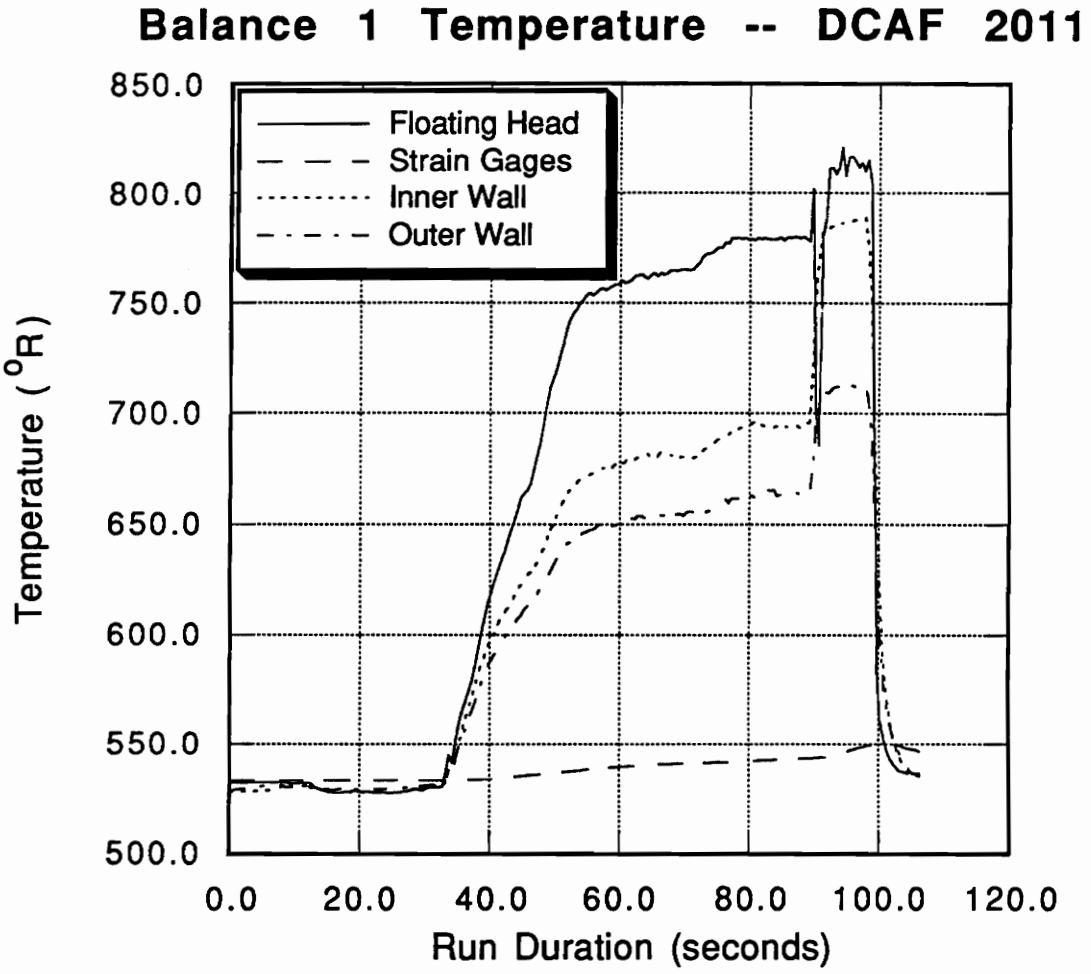

Figure 6.31 : Skin Friction Balance 1 Temperatures, DCAF 2011

VITA

The author was born in Malden, Massachusetts on October 5, 1961. He was raised and received his elementary education in neighboring New Hampshire. He entered the Mechanical Engineering program at Northeastern University of Boston Massachusetts in 1982 and received his Bachelor of Science Degree in 1987. In the fall of 1987 the author entered graduate school in the Aerospace Engineering Department at Virginia Tech. He received his Master of Science Degree in October 1990 and his Ph. D. in December 1992.